Non-coding RNA genes lost in Prader-Willi Syndrome stabilize target RNAs

Matthew Afshin Kocher

Dissertation submitted to the faculty of the Virginia Polytechnic Institute and State University in partial fulfillment of the requirements for the degree of

Doctor of Philosophy

In

Translational Biology, Medicine and Health

Deborah J. Good, Chair

Robert W. Grange

Christopher K. Thompson

Shihoko Kojima

Fenix W. Huang

March 2021

Blacksburg, Virginia

Keywords: Prader-Willi Syndrome, non-coding RNA, neuroendocrinology, Snord116, Nhlh2

© 2021
Matthew Afshin Kocher
All rights reserved

Non-coding RNA genes lost in Prader-Willi Syndrome stabilize target RNAs

Matthew A. Kocher

ABSTRACT

Prader-Willi Syndrome (PWS) is a genetic disease that results in abnormal hormone levels, developmental delay, intellectual disability, hypogonadism, and excessive appetite. The disease is caused by a *de novo* genetic deletion in chromosome 15. While many of the deleted genes have been identified, there is little known about their molecular function. There is evidence that a cluster of non-coding RNA genes in the deleted region known as the *SNORD116* genes may be the most critical genes deleted in Prader-Willi Syndrome. It is unknown what the *SNORD116* genes do at the molecular level, but recent evidence suggests they regulate the expression of other genes involved in the neuroendocrine system. Specifically, the *SNORD116* gene is implicated in regulation of *NHLH2,* a transcription factor gene which plays a key role in development, hormonal regulation, and body weight. In this study we identify phylogenetically conserved regions of *SNORD116* and predict interactions with its potential downstream RNA targets. We show that mouse *Snord116* post-transcriptionally increases *Nhlh2* RNA levels dependent on its 3'UTR and protects it from degradation within 45 minutes of its transcription. Additionally, a single nucleotide variant within *Nhlh2* at the predicted *Snord116* interaction site may disrupt *Snord116*'s protective effect. This is the first observation of a molecular mechanism for *Snord116,* identifying its role in RNA stability, and leads us closer to understanding Prader-Willi Syndrome and finding a possible treatment. However, *Snord116 in vitro* knockdown or paternally inherited *in vivo* deletion fail to detect differential expression of *Nhlh2*, likely due to missing the key timepoint of *Snord116* regulatory effects on *Nhlh2* RNA soon after its transcriptional stimulation, and dependent on leptin signals. Furthermore, the hypothalamic mRNA expression profile of PWS mouse models fed a nutraceutical dietary supplement of conjugated linoleic acid reveals minimal overall changes, while the effect of diet may be stronger than genotype and potentially changes gene expression of metabolic molecular pathways.

Non-coding RNA genes lost in Prader-Willi Syndrome stabilize target RNAs

Matthew A. Kocher

GENERAL AUDIENCE ABSTRACT

Prader-Willi Syndrome is a genetic disease that results in abnormal hormone levels, slow development, intellectual disability, gonad deficiency, and excessive appetite. The disease is caused by a genetic deletion in chromosome 15 that is almost always a spontaneous mutation not inherited from the parents. While many of the deleted genes have been identified, there is little known about what their molecular function is. There is evidence that a cluster of genes in the deleted region known as the *SNORD116* genes may be the most critical genes deleted in Prader-Willi Syndrome. It is unknown what the *SNORD116* genes do at the molecular level, but recent evidence suggests that it regulates other genes involved in the hormone system. Specifically, the *SNORD116* gene is implicated to regulate the levels of *NHLH2,* a gene which plays a key role in development, hormonal regulation, and body weight. In this study we identify key regions of *SNORD116* and predict interactions with its potential downstream targets. We show that *SNORD116* increases *NHLH2* levels and slows its degradation at the RNA transcript level. This is the first observation of a molecular mechanism for *SNORD116* and leads us closer to understanding Prader-Willi Syndrome and finding a possible treatment. However, other mouse models of *Snord116* deletion fail to find differences in *Nhlh2*. This is likely due to missing a brief key timepoint and hormonal signal when *Nhlh2* is most subject to *Snord116*'s effects. Furthermore, PWS mouse models fed a supplement intended for weight loss leads to mild overall gene expression changes in the hypothalamus, a brain region that regulates many hormonal signals including appetite and energy balance. The effect of diet may be stronger than genotype in this brain region, with diet potentially changing the activity of metabolic molecular pathways.

Dedication

To whoever actually reads this.

Acknowledgements

This work was supported by the Foundation for Prader-Willi Research, the Virginia Tech Adaptive Brain and Behavior Destination Area, and Sigma-Xi Scientific Research Honor Society. I would like to thank the Translational Biology, Medicine and Health Graduate Program for their support. I would like to thank Erin Le for helping create molecular constructs used in the study, Fenix W. Huang (University of Virginia) for assistance with RNA interaction prediction and RNA folding used in the study, Stephan Stamm (University of Kentucky) for the generous gifts of molecular constructs used in the study, Joe Grieco for assistance with Western blots. I would also like to thank my committee for their valuable insights, and all the characters of Blacksburg, Roanoke, Virginia Tech, and the Integrated Life Science Building that supported me and added flavor to my life.

Finally, I would like to thank Deborah J. Good for mentorship. It goes without saying that “mentorship” means so much more than a single word can describe. Thank you.

Contents

List of Figures

List of Tables

List of Abbreviations

PWS – Prader-Willi Syndrome

Chr15 – chromosome 15

RNA – Ribonucleic acid

DNA – deoxyribonucleic acid

ncRNA – non-coding RNA

snoRNA – Small Nucleolar RNA

lncRNA – long non-coding RNA

rRNA – ribosomal RNA

snRNA – Small Nuclear RNA

SNORD – Small Nucleolar RNA with C/D box motifs

snoRNP – Small Nucleolar RNA RiboNucleoProtein complex

miRNA – micro RNA

piRNA – Piwi-interacting RNA

siRNA - Small interfering RNA

SNORD116 – gene; Small Nucleolar RNA with C/D box motifs #116

SNORD116@ - gene cluster of all the homologs of individual SNORD116 genes

116HG – SNORD116 host gene

Sno-lncRNA – long non-coding RNA with snoRNA “caps” on the 5’ and 3’ ends

SPA-lncRNA – 5’ snoRNA capped and 3’polyadenylated long non-coding RNA

SNRPN – gene; Small Nuclear Ribonucleoprotein Polypeptide N

SNURF – gene; SNRPN Upstream Rreading Frame

SNHG14 – gene; Small Nucleolar RNA Host Gene 14

ASD – autism spectrum disorder

UPD – uniparental disomy

mUPD15 – maternal uniparental disomy of chromosome 15

kb – kilobases = 1,000 bases

Mb – megabases = 1,000,000 bases

nt – nucleotides

bp – base pairs

LD1 – large deletion 1

LD2 – large deletion 2

IC – imprinting center

PWS-IC – Prader-Willi Syndrome imprinting center

AS-IC – Angelman Syndrome imprinting center

PWS-MDR – Prader-Willi Syndrome Minimal Deletion Region

iPSC – induced pluripotent stem cell

ESC – embryonic stem cell

hESC – human embryonic stem cell

mESC – mouse embryonic stem cell

NPC – neural progenitor cell

siRNA – short/small interfering RNA

RNAi – RNA interference

ASO – anti-sense oligonucleotide

H3K9me3 - histone-3 lysine-9 trimethylation

H3K4 – histone-3 lysine-4

GH – growth hormone

IGF1 – insulin-like growth factor 1

NPY – gene; neuropeptide Y

AGRP – gene; Agouti-related peptide

POMC – gene; pro-opiomelanocortin

HCRT – gene; hypocretin neuropeptide precursor / orexin

PMCH – gene; pro-melanin concentrating hormone

GHRH – gene; growth hormone releasing hormone

GnRH – gonadotropic releasing hormone

PCSK1 – gene; Proprotein Convertase Subtilisin/Kexin Type 1

PCSK2 – gene; Proprotein Convertase Subtilisin/Kexin Type 2

PC1 – prohormone convertase 1, product of PCSK1 gene

PC2 – prohormone convertase 2, product of PCSK2 gene

NHLH2 – gene; nescient helix-loop-helix 2

aMSH – alpha melanocyte stimulating hormone

ACTH – adrenocorticotropic hormone

MC4R – melanocortin 4 receptor

KBDy - kisspeptin/neurokinin B/dynorphin

TRH - thyrotropin releasing hormone

TSH – thyroid stimulating hormone

LH - luteinizing hormone

FSH - follicle-stimulating hormone

PWS iPSC-neurons - neurons differentiated from iPSCs of PWS patients

MAGE – melanoma antigen family

bHLH – basic helix-loop-helix

LepR - leptin receptor

JAK – janus kinase

STAT - signal transducer and activator of transcription

STAT3 – gene; signal transducer and activator of transcription 3

HNRNP-U – Heterogeneous nuclear ribonucleoprotein U

HEK293 – human embryonic kidney cell line

SNV – single nucleotide variant

3'UTR - 3' untranslated region

RNA-seq – RNA sequencing

scRNA-seq – single cell RNA sequencing

DEG – differentially expressed gene

CLA – conjugated linoleic acid

N2A – neuro2A mouse neuroblastoma cell line

RISC – RNA-induced silencing complex

RT-QPCR - reverse-transcriptase quantitative polymerase chain reaction

PVN - paraventricular nucleus of the hypothalamus

ARC - arcuate nucleus of the hypothalamus

VMH - ventromedial nucleus of the hypothalamus

DMH - dorsomedial nucleus of the hypothalamus

SCN – suprachiasmatic nucleus of the hypothalamus

Snord116$^{m+/p-}$ - Paternally inherited deletion of the *Snord116* gene cluster

*Snord116*del – deletion of the *Snord116* gene cluster

WT - wildtype

SOCS3 – gene; suppressor of cytokine signalling 3

Chapter 1. Introduction

Prader-Willi Syndrome (PWS) is a genetic disease characterized by slow development, hypotonia, hormone deficiency, intellectual disability, hypogonadism, and hyperphagia that often leads to obesity if not managed by a caregiver. The incidence of PWS is estimated between 1/10,000 – 1/30,000, and the genetic causation is a loss of function in the paternal chromosome 15q11 – q13.[1–8] While the region of chromosome 15q (Chr15q) has been identified as critical for PWS, the causative deletions are variable.

Some PWS causative deletions encompass a large stretch of 5-6 Mb.[1,6] However, some microdeletions in PWS patients have identified a minimal causative deletion in PWS of about 70kb which contains multiple non-coding RNA (ncRNA) genes.[9,10] This 70kb microdeletion region includes the *IPW* gene, and the *SNORD116* gene cluster of about 30 highly homologous paralogs of *SNORD116*.[9–14] The *SNORD116* gene cluster is the most well described of the 2 microdeletion genes, and most strongly implicated in the causation of PWS. *SNORD116* is a small nucleolar RNA (snoRNA) with C/D box motifs (SNORD). SNORDs are usually ncRNAs that target pre-ribosomal RNA (rRNA) for 2'O methylation, which is involved in the downstream processing and splicing of pre-rRNA to become functional rRNA.[15–25] SNORDs show high sequence complementarity to their targeted rRNA, and due to this, many SNORDs have predicted rRNA targets with high confidence. However, *SNORD116* shows no sequence complementarity to rRNA and has no predicted targets. This leaves *SNORD116* with an unknown molecular mechanism and further questions about the etiology of PWS.

PWS is a neurodevelopmental disorder, as there are many implications for hypothalamic dysregulation in PWS.[26–31] The hypothalamus is a critical brain region for the endocrine system as it regulates the pituitary gland and is involved in the autonomic nervous system and metabolic processes. *SNORD116* is also highly expressed in the hypothalamus. Recent observations suggest *SNORD116* may regulate the neuroendocrine related gene *NHLH2.*[32,33] This molecular link is an enticing hypothesis, as there is much crossover between *NHLH2* knockout mice, PWS symptoms, and PWS mouse models, which display hypogonadism, obesity, and developmental delay.[32] However, multiple studies were unable to find a link between *SNORD116* and *NHLH2* in RNA expression datasets.[27,34,35] The absence of consistent findings leads the PWS research community to question the hypothesis that

SNORD116 regulates *NHLH2*. Clarity on this subject will direct future PWS research, and the current study seeks to definitively determine if *SNORD116* regulates *NHLH2*.

The current study uses *in silico* analysis including RNA interaction prediction, *in vitro* studies using mouse neuronal cell culture with *Nhlh2* reporter constructs, and *in vivo* studies to observe RNA expression of PWS mouse model hypothalamus under various feeding conditions. These approaches were used to predict a potential Snord116-Nhlh2 RNA interaction, to test if this predicted interaction mediates Snord116-dependent changes on Nhlh2 RNA, and to test if Snord116-dependent changes on Nhlh2 RNA are observable in PWS mouse models. Some work shown here argues for a molecular relationship between *Snord116* and *Nhlh2* while others are inconclusive. Chapter 2 is a literature review of PWS, *SNORD116*, and *NHLH2*. Chapter 3 is *in silico* work describing a phylogenetic analysis of the *SNORD116* cluster. Chapter 4 shows that mouse *Snord116* post transcriptionally stabilizes *Nhlh2* mRNA dependent on its 3'UTR. Chapter 5 shows a lack of changes in *Nhlh2* RNA levels with an *in vitro* knockdown or an *in vivo* deletion of *Snord116*. Chapter 6 describes mRNA sequencing results from the PWS mouse model hypothalamus under a dietary supplement intervention.

References

1. Chung MS, Langouët M, Chamberlain SJ, Carmichael GG. Prader-Willi syndrome: reflections on seminal studies and future therapies. *Open Biol*. 2020;10(9):200195. doi:10.1098/rsob.200195
2. Butler MG, Miller JL, Forster JL. Prader-Willi Syndrome - Clinical Genetics, Diagnosis and Treatment Approaches: An Update. *Curr Pediatr Rev*. 2019;15(4):207-244. doi:10.2174/1573396315666190716120925
3. Butler MG, Hartin SN, Hossain WA, et al. Molecular genetic classification in Prader-Willi syndrome: a multisite cohort study. *J Med Genet*. 2019;56(3):149-153. doi:10.1136/jmedgenet-2018-105301
4. Vogels A, Van Den Ende J, Keymolen K, et al. Minimum prevalence, birth incidence and cause of death for Prader–Willi syndrome in Flanders. *Eur J Hum Genet*. 2004;12(3):238-240. doi:10.1038/sj.ejhg.5201135
5. Whittington JE, Holland AJ, Webb T, Butler J, Clarke D, Boer H. Population prevalence and estimated birth incidence and mortality rate for people with Prader-Willi syndrome in one UK Health Region. *J Med Genet*. 2001;38(11):792-798. doi:10.1136/jmg.38.11.792
6. Cassidy SB, Schwartz S, Miller JL, Driscoll DJ. Prader-Willi syndrome. *Genet Med*. 2012;14(1):10-26. doi:10.1038/gim.0b013e31822bead0

7. Butler MG, Thompson T. Prader-Willi Syndrome: Clinical and Genetic Findings. *The Endocrinologist*. 2000;10(4 Suppl 1):3S-16S.
8. Butler MG, Bittel DC, Kibiryeva N, Talebizadeh Z, Thompson T. Behavioral Differences Among Subjects With Prader-Willi Syndrome and Type I or Type II Deletion and Maternal Disomy. *Pediatrics*. 2004;113(3 Pt 1):565-573. doi:10.1542/peds.113.3.565
9. Bieth E, Eddiry S, Gaston V, et al. Highly restricted deletion of the SNORD116 region is implicated in Prader–Willi Syndrome. *Eur J Hum Genet*. 2015;23(2):252-255. doi:10.1038/ejhg.2014.103
10. Tan Q, Potter KJ, Burnett LC, et al. Prader–Willi-Like Phenotype Caused by an Atypical 15q11.2 Microdeletion. *Genes*. 2020;11(2). doi:10.3390/genes11020128
11. Sahoo T, del Gaudio D, German JR, et al. Prader-Willi phenotype caused by paternal deficiency for the HBII-85 C/D box small nucleolar RNA cluster. *Nat Genet*. 2008;40(6):719-721. doi:10.1038/ng.158
12. Duker AL, Ballif BC, Bawle EV, et al. Paternally inherited microdeletion at 15q11.2 confirms a significant role for the SNORD116 C/D box snoRNA cluster in Prader–Willi syndrome. *Eur J Hum Genet*. 2010;18(11):1196-1201. doi:10.1038/ejhg.2010.102
13. de Smith AJ, Purmann C, Walters RG, et al. A deletion of the HBII-85 class of small nucleolar RNAs (snoRNAs) is associated with hyperphagia, obesity and hypogonadism. *Hum Mol Genet*. 2009;18(17):3257-3265. doi:10.1093/hmg/ddp263
14. Fontana P, Grasso M, Acquaviva F, et al. SNORD116 deletions cause Prader-Willi syndrome with a mild phenotype and macrocephaly. *Clin Genet*. 2017;92(4):440-443. doi:https://doi.org/10.1111/cge.13005
15. Bachellerie J-P, Michot B, Nicoloso M, Balakin A, Ni J, Fournier MJ. Antisense snoRNAs: a family of nucleolar RNAs with long complementarities to rRNA. *Trends Biochem Sci*. 1995;20(7):261-264. doi:10.1016/S0968-0004(00)89039-8
16. Dunbar DA, Baserga SJ. The U14 snoRNA is required for 2'-O-methylation of the pre-18S rRNA in Xenopus oocytes. *RNA*. 1998;4(2):195-204.
17. Kiss-László Z, Henry Y, Kiss T. Sequence and structural elements of methylation guide snoRNAs essential for site-specific ribose methylation of pre-rRNA. *EMBO J*. 1998;17(3):797-807. doi:10.1093/emboj/17.3.797
18. Rebane A, Roomere H, Metspalu A. Locations of several novel 2'-O-methylated nucleotides in human 28S rRNA. *BMC Mol Biol*. 2002;3:1. doi:10.1186/1471-2199-3-1
19. Tycowski KT, Smith CM, Shu M-D, Steitz JA. A small nucleolar RNA requirement for site-specific ribose methylation of rRNA in Xenopus. *Proc Natl Acad Sci U S A*. 1996;93(25):14480-14485.
20. Falaleeva M, Pages A, Matuszek Z, et al. Dual function of C/D box small nucleolar RNAs in rRNA modification and alternative pre-mRNA splicing. *Proc Natl Acad Sci U S A*. 2016;113(12):E1625-E1634. doi:10.1073/pnas.1519292113
21. Tycowski KT, You Z-H, Graham PJ, Steitz JA. Modification of U6 Spliceosomal RNA Is Guided by Other Small RNAs. *Mol Cell*. 1998;2(5):629-638. doi:10.1016/S1097-2765(00)80161-6
22. Kiss T. Small nucleolar RNA-guided post-transcriptional modification of cellular RNAs. *EMBO J*. 2001;20(14):3617-3622. doi:10.1093/emboj/20.14.3617
23. Kiss T. Small Nucleolar RNAs: An Abundant Group of Noncoding RNAs with Diverse Cellular Functions. *Cell*. 2002;109(2):145-148. doi:10.1016/S0092-8674(02)00718-3

24. Maden BEH, Hughes JMX. Eukaryotic ribosomal RNA: the recent excitement in the nucleotide modification problem. Published online 1997:10.
25. Yu YT, Shu MD, Steitz JA. A new method for detecting sites of 2'-O-methylation in RNA molecules. *RNA*. 1997;3(3):324-331.
26. Qi Y, Purtell L, Fu M, et al. Hypothalamus specific re-introduction of Snord116 into otherwise Snord116 deficient mice increased energy expenditure. *J Neuroendocrinol*. Published online January 1, 2017:n/a-n/a. doi:10.1111/jne.12457
27. Polex-Wolf J, Lam BYH, Larder R, et al. Hypothalamic loss of Snord116 recapitulates the hyperphagia of Prader-Willi syndrome. *J Clin Invest*. 2018;128(3):960-969. doi:10.1172/JCI97007
28. Purtell L, Qi Y, Campbell L, Sainsbury A, Herzog H. Adult-onset deletion of the Prader-Willi syndrome susceptibility gene Snord116 in mice results in reduced feeding and increased fat mass. *Transl Pediatr*. 2017;6(2):88-97-97.
29. Ding F, Li HH, Zhang S, et al. SnoRNA Snord116 (Pwcr1/MBII-85) Deletion Causes Growth Deficiency and Hyperphagia in Mice. *PLOS ONE*. 2008;3(3):e1709. doi:10.1371/journal.pone.0001709
30. Skryabin BV, Gubar LV, Seeger B, et al. Deletion of the MBII-85 snoRNA Gene Cluster in Mice Results in Postnatal Growth Retardation. *PLoS Genet*. 2007;3(12). doi:10.1371/journal.pgen.0030235
31. Qi Y, Purtell L, Fu M, et al. Ambient temperature modulates the effects of the Prader-Willi syndrome candidate gene Snord116 on energy homeostasis. *Neuropeptides*. 2017;61:87-93. doi:10.1016/j.npep.2016.10.006
32. Burnett LC, LeDuc CA, Sulsona CR, et al. Deficiency in prohormone convertase PC1 impairs prohormone processing in Prader-Willi syndrome. *J Clin Invest*. 2016;127(1):293-305. doi:10.1172/JCI88648
33. Bittel DC, Kibiryeva N, Sell SM, Strong TV, Butler MG. Whole Genome Microarray Analysis of Gene Expression in Prader–Willi Syndrome. *Am J Med Genet A*. 2007;143A(5):430-442. doi:10.1002/ajmg.a.31606
34. Bochukova EG, Lawler K, Croizier S, et al. A Transcriptomic Signature of the Hypothalamic Response to Fasting and BDNF Deficiency in Prader-Willi Syndrome. *Cell Rep*. 2018;22(13):3401-3408. doi:10.1016/j.celrep.2018.03.018
35. Falaleeva M, Surface J, Shen M, de la Grange P, Stamm S. SNORD116 and SNORD115 change expression of multiple genes and modify each other's activity. *Gene*. 2015;572(2):266-273. doi:10.1016/j.gene.2015.07.023

Chapter 2. Literature Review

2.1 Clinical features of Prader-Willi Syndrome

Prader-Willi Syndrome (PWS) is a genetic disease characterized by developmental delay, infantile hypotonia, hormone deficiency, intellectual disability, hypogonadism, and hyperphagia that often leads to obesity. The incidence of PWS is estimated between 1/10,000 – 1/30,000 live births.[1–7] The phenotypes are multiphasic, with some phenotypes present throughout the patients' lifetime, and others that are only present for a certain phase of development. PWS clinical symptoms are traditionally divided into two phases: failure to thrive with slow development at infancy, and phase 2 being hyperphagia and the development of obesity from childhood into adulthood. However, a more detailed clinical timeline has been established:

- Prenatal - reduced fetal activity, small for gestational age, decreased birth weight, increased head/abdomen circumference ratio, polyhydramnios (excess amniotic fluid in the amniotic sac).[8–10]
- Birth - hypotonia, failure to thrive, weak suckling, growth hormone deficiency, hypogonadism/hypogenitalism, and cryptorchidism in males (undescended testicles).[1,4,11]
- 9 months – normal development [10]
- 2 years – body weight increase without changes in appetite or intake, some behavioral abnormalities [1,10–12]
- 4.5 years – hyperphagia with some satiety, intellectual disability, behavioral and emotional abnormalities continue to emerge [4,10–12]
- 8 years – hyperphagia without satiety [10]
- Adulthood – some satiety for few individuals [10]

Additional phenotypes include sleep disturbances, characteristic facial features, respiratory distress, short stature, small hands and feet, hypopigmentation, and abnormal hormone levels. Secondary symptoms arise from obesity including type 2 diabetes and related comorbidities. Cognitive and behavioral observations include aggression, impulsivity, cognitive rigidity, repetitive and compulsive behavior, skin picking, emotional outbursts, stubbornness,

and food related behavior including food seeking, stealing, hoarding, etc. Some patients show overlap with Autism-Spectrum Disorder (ASD), as well as bipolar disorder or other psychiatric illness.[1,4,7,11–13]

Complications of hyperphagia and obesity lead to the major morbidities and mortality of PWS patients, with early intervention of the food environment and dietary pattern helping to alleviate associated morbidities.[14,15] The leading cause of death for PWS patients is respiratory failure (31%) followed by cardiac disease/failure (16%) and gastrointestinal problems (10%).[15] Cases of respiratory failure are not correlated with obesity.[14] Quartile estimates for mortality rate by age is the following: 25% mortality at 20 years old, 50% mortality at 29 years old, 75% mortality at 42 years old, and 99% mortality at 60 years old.[15] Possible hyperphagia related deaths including accidents, aspiration, choking, and gastrointestinal perforation make up about 50% of all childhood deaths and about 1/3 of all reported deaths.[15] These possibly hyperphagia associated deaths disproportionately effect young males.[15]

The biological system that is most implicated in PWS is the endocrine system. The endocrine system generally consists of the hypothalamus and pituitary gland in the brain as central regulators, and various peripheral organs that receive and send hormonal signals through the bloodstream. Disruption of central endocrine regulation via the hypothalamus and pituitary gland is linked to the etiology of PWS. Endocrine related features of PWS include low levels of growth hormone (GH) and developmental delay in nearly all cases of PWS. Growth hormone supplementation is a standard treatment for PWS patients and is currently the only FDA approved treatment.

Hypogonadism is observed in nearly all cases of PWS and can be both pituitary and gonadal in origin.[1,11,16–18]

The thyroid system is either normal or mildly altered in PWS, with hypothyroidism debated to be present in 10-30% of cases and mostly central in nature, but observations are highly variable and inconclusive. It is possible that hypothyroidism is more prevalent in PWS newborns and children than adults, and growth hormone treatment at a young age may interact with the thyroid system.[1,11,17–23]

The status of the adrenal system is also debated, but adrenal insufficiency seems to be observed in about 10% of cases. Adrenal insufficiency may also be dependent on developmental phase and interactions with growth hormone treatment.[1,11,17,18,24,25]

Abnormal sleep patterns including central sleep apnea, obstructive sleep apnea, hypersomnia, and narcolepsy are observed with evidence of hypothalamic origin, including abnormal levels of the neuropeptide orexin (hypocretin).[1,11,17,18,26–29]

Oxytocin hypothalamus neurons are decreased in number, and lymphoblasts show low oxytocin receptor mRNA levels.[30,31] However, children show an increase in plasma oxytocin levels.[32] Of note, there is recent evidence that intranasal oxytocin and its functional analog may be a potential therapy for treating hyperphagia. While many studies show positive effects, there are variable results with some studies reporting no therapeutic effect, but overall, oxytocin treatment shows promise.[33–39]

Morphological abnormality of the PWS pituitary gland has also been observed using MRI, mostly showing a decrease in pituitary size compared to controls.[40–43] A recent study shows that about 30% of PWS patients have autoimmune antibodies reactive to the pituitary gland at a higher rate than control (5-6%).[44] Additionally, post-mortem PWS hypothalamus tissue shows an overall transcriptomic sign of inflammation.[45] The significance of these potential immune reactive contexts requires further investigation.

The hypothalamic system mediating energy homeostasis and feeding behavior is not completely characterized in PWS, although peripheral hormones have been investigated to a greater extent. Ghrelin, the appetite inducing peptide hormone secreted by the stomach, is elevated in PWS patients throughout their lifetime. Hyperghrelinemia is observed from infancy during poor feeding behavior, to childhood before the onset of hyperphagia, and adulthood during hyperphagia.[1,17,46] However, ghrelin receptor antagonists have no effect on PWS adult hyperphagia.[1,17,47] These studies show that it is unlikely that ghrelin levels are the main cause of the hyperphagic switch in PWS development, although abnormal neonatal ghrelin levels in mice may disrupt normal development of the hypothalamic feeding circuit.[48] Opposite to ghrelin, the appetite suppressing hormone Peptide YY (PYY) secreted from the intestines increases after feeding in a normal pattern in PWS children and adults.[49,50] Leptin, the appetite suppressing peptide hormone released from adipocytes in response to food intake, also appears to show a normal pattern in PWS patients.[51–53] Although the studies listed above imply normal hormonal signaling, there is less known about receptor expression at the target sites of these hormones in PWS. PWS lymphocytes show no difference in leptin receptor mRNA, and

PWS hypothalamus shows no difference in ghrelin receptor mRNA or PYY receptor mRNA.[52,54]

In summary, Prader-Willi Syndrome is a genetic developmental disorder with evidence of neuroendocrine dysfunction. The genetic cause of the disorder is well characterized, but not fully understood. Further investigation to bridge the gaps in knowledge hold promise for finding a therapeutic solution for PWS.

2.2 Genetics of Prader-Willi Syndrome

The genetic cause of PWS is a loss of function in the paternal chromosome 15q11 – q13. This genomic region only expresses genes from the paternal chromosome through epigenetic imprinting mechanisms in which the maternal genes are silenced, primarily through methylation. The large majority of PWS cases occur from *de novo* genetic events, in which the parents do not carry or pass the PWS genotypes. The loss of function in this genomic region is mostly caused by a *de novo* paternal genetic deletion (60-75% of cases) but can also be caused by uniparental disomy (UPD) of the maternal chromosome 15 (20-35%), or imprinting defects (1-5%).[1,7]

These three main subtypes of PWS are also associated with slightly varying phenotypes, but there is limited data on patients with imprinting defects. All subtypes share the hallmark phenotypes of hypotonia, hypogonadism, and hyperphagia. However, UPD patients exhibit higher risk of psychiatric illness, higher verbal IQ, and less maladaptive behavior. Patients with paternal deletion genotypes show an increase in PWS facial features, hypopigmentation, and higher visuospatial IQ.[1,13,55]

Maternal UPD of chromosome 15 (mUPD15) is due to errors in meiosis and has been associated with older age mothers.[4,7] Both copies of chromosome 15 (Chr15) are inherited from the mother and there are no copies from the father. There are 3 subtypes of mUPD15 categorized based on the degree of loss of heterozygosity.[7] Higher loss of heterozygosity in chromosome 15 leads to an increased risk of recessive disorder alleles and can lead to further deleterious genetic conditions. About 30% of mUPD15 patients show heterodisomy, 58% have partial heterodisomy, and 12% have total homodisomy.[7]

Imprinting defects leading to PWS are often caused by epimutations of chromosome 15 that lead to the silencing of the paternal alleles, as if they were the maternal chromosome. These may arise from errors in the imprinting process during spermatogenesis of the fathers, or embryogenesis. Imprinting defects can also be caused by deletions in the imprinting center (IC), a ~40kb genomic region within chromosome 15q11-13 that regulates the 2.5Mb differentially imprinted region of 15q11-13. Loss of function in the PWS-IC can lead to epigenetic silencing of the paternal alleles. There are rare cases where an imprinting center microdeletion is inherited from asymptomatic parents. Due to the nature of the imprinting process, the mutation in the IC can remain “silent” until the appropriate inheritance pattern occurs for symptoms to arise. The paternal grandmother can pass a PWS-IC deletion to an asymptomatic father who has a 50/50 chance of passing their PWS-IC mutation to an offspring, and thus a 50/50 chance of a having a child with PWS.[4,11,56–62]

The most common cause of PWS, a *de novo* deletion in the paternal chromosome 15q, also has varying subtypes. There are two common large deletions including a 5-6Mb large deletion type 1 (LD1) and a ~4.5Mb large deletion type 2 (LD2) (**Figure 1**). Behavioral and psychological phenotypes are generally more severe for the larger LD1 when compared to LD2.[6,55,63] Furthermore, if only the region unique to LD1 is lost, this can lead to a separate genomic syndrome of incomplete penetrance, characterized by neuropsychiatric and behavioral symptoms.[64] Of PWS patients with paternal chromosome 15 deletion, about 36-39% have LD1 and 55-56% have LD2. The remaining 6-8% of paternal deletion cases have atypical deletions that are either larger or smaller than LD1 and LD2.[7,65] This chromosomal region is prone to structural deletions due to the presence of segmental duplications, also known as low-copy repeats, at the common breakpoints. Segmental duplications are copies of >1kb stretches of DNA that are highly homologous that often mediate chromosomal rearrangements such as deletions, duplications, and inversions through non-allelic homologous recombination.[66–69] Large, highly homologous, repetitive chromosomal regions such as the PWS deletion region and pericentromeric regions are often difficult to sequence, map, and assemble, and also commonly show structural variation.[67–70] The distal PWS deletion region at Chr15q13.3, which is also sometimes deleted in large PWS deletions, was recently mapped with high structural resolution and shows structural variation within and between human genetic background.[4,66,67]

Of note, if loss of function occurs in the same common 15q11-q13 chromosome region on the maternal chromosome, it leads to a separate disease known as Angelman's syndrome.[1,4,11] This is due to loss of the paternally silenced gene *UBE3A* and partially silenced gene *ATP10A* that are downstream of the paternally expressed genes (**Figure 1**). The Angelman's syndrome imprinting center (AS-IC) is about 35kb upstream of the PWS-IC. Angelman's syndrome is characterized by microcephaly, seizures, developmental delay, intellectual disability, and behavioral issues.[11,61,62]

Figure 1

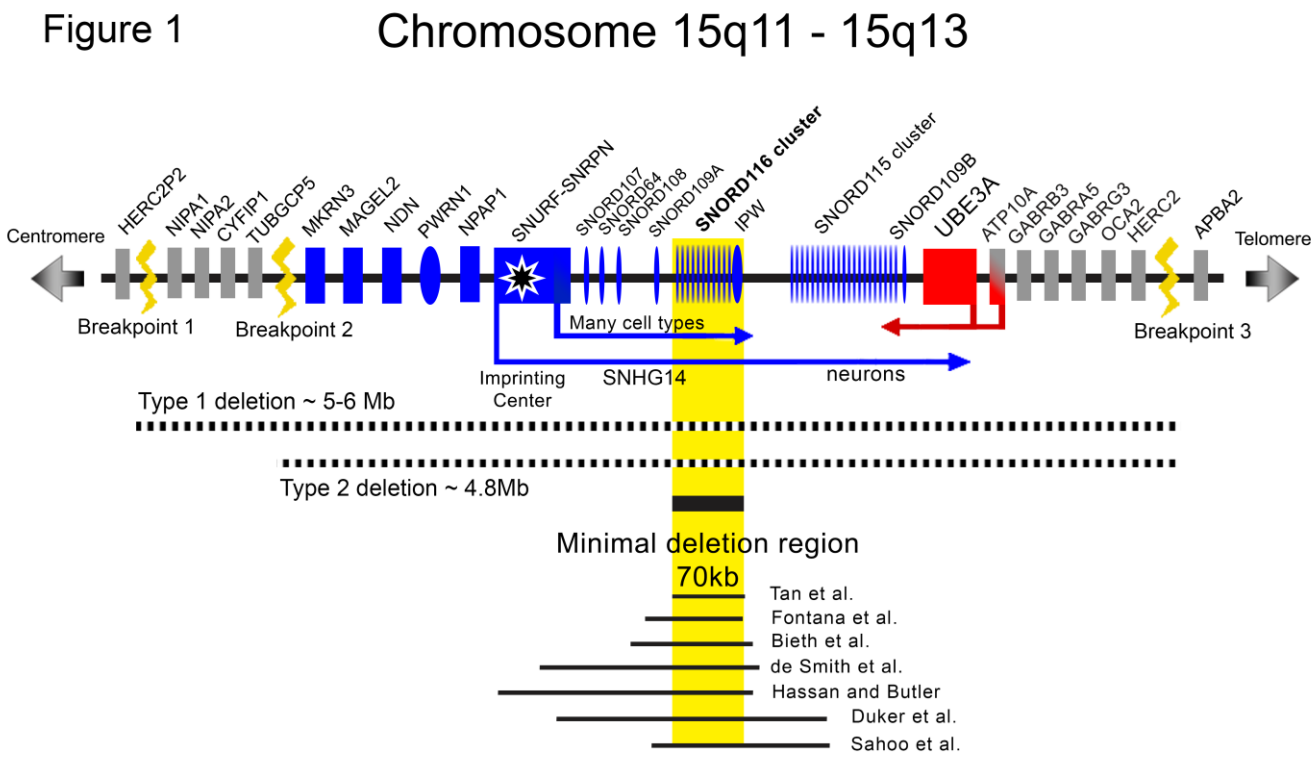

Figure 1. Prader-Willi Syndrome genomic locus on Chromosome 15. Protein coding genes are shown as rectangles, non-coding RNA genes are ovals, paternally expressed genes are blue, maternally expressed genes are red. The PWS minimal deletion region is highlighted in yellow with references below it depicting individual PWS microdeletion cases. Not to scale.

Observations of PWS patients presenting with atypical microdeletions have narrowed down the minimal critical deletion region of PWS to a 70kb stretch containing the *SNORD116* gene cluster and the *IPW* gene (**Figure 1**).[71–76] While this 70kb region of chromosome 15q has been identified as critical for PWS, the cases with microdeletions encompassing this region show some phenotypic variance (**Table 1**). All cases show hypotonia, hyperphagia,

developmental delay, obesity, and distinctive facial features, while a few cases show variability in hypogonadism, intellectual disability, short stature, sleep disturbances, and behavioral problems. In general, it seems that smaller sized deletions lead to less severe phenotypes. Of note, the case with the smallest deletion does not present hypogonadism, intellectual disability, or short stature. While the 2nd smallest deletion does not present failure to thrive, intellectual disability, short stature, or behavioral issues.[72,76]

Table 1	Sahoo et al.	de Smith et al.	Duker et al.	Bieth et al.	Hassan and Butler	Fontana et al.	Tan et al.
Deletion size (kbp)	175	187	236	118	210	80	71
Ethnicity	Caucasian	South Asian Indian	African-American	Caucasian	Caucasian	Caucasian	Caucasian
Gender	Male	Male	Male	Female	Female	Male	Male
Birth weight (g)	3218	2800	3020	2780	3334	2710	3140
Birth length (cm)	54.5	N/A	53	48	54.6	49	51
Age at examination (years)	4.8	19.5	11	23	26	18	17
Clinical features							
Hypotonia	+	+	+	+	+	+	+
Infantile feeding problems/FTT	+	+	+	+	+	−	+
Tube feeding	+	−	+	+	−	−	+
Start of excess weight gain (months)	18	24	6	18	30	Between 48–72	36
Hyperphagia	+	+	+	+	+	+	+
Overweight/Obesity	+	+	+	+	+	+	+
Distinctive facial features	+	N/A	+	+	+	+	+
Hypogonadism	+	+	+	+	N/A	+	−
Developmental delay	+	+	+	+	+	+	+
Mental retardation	+	+	+	+	N/A	−	−
Behavioral problems	+	+	+	+	+	−	+
Skin picking	+	+	−	+	+	−	+
Sleep disturbances/ apnea	+	N/A	+	+	N/A	−	+
Short stature	−	+	+	+	+	−	−
Small hands/feet for height	+	+	−	N/A	+	−	−
Eye abnormalities	−	N/A	+	N/A	N/A	+	−

FTT: failure to thrive; N/A: not available; +: present PWS characteristic; −: absent PWS characteristic.

Modified from Tan et al. 2020, used with permission from MDPI

2.3 *SNORD116* and related non-coding RNAs

While the minimal deletion region leading to PWS (PWS-MDR) has been identified, it is still unknown how loss of this PWS-MDR leads to PWS. There are many RNA products observed from this genomic locus with diverse functions (**Figure 2**). All RNA products from this region seemingly originate from or correlate with transcription of the SNURF-SNRPN gene, and transcription carries through the PWS-MDR past the *SNORD115* cluster and antisense to the *UBE3A* gene (**Figure 1**). While multiple transcription start sites may exist, this long noncoding RNA (lncRNA) transcript that carries through the PWS-MDR has gone by many names, but the current official gene name is Small Nucleolar RNA Host Gene 14 (*SNHG14*). Observed RNAs derived from *SNHG14* include lncRNAs that are transcribed from the exons along the locus, and undergo much alternative splicing.[77–82] Hosted within the introns of these lncRNA transcripts are small-nucleolar RNAs (snoRNAs) that are processed from introns and are protected from degradation through snoRNA-protein interactions.[83–85] These snoRNAs may also be further digested and processed to form smaller RNAs.[86,87] At the very 3' end of this locus, there is another ncRNA gene, *IPW*, that may be the 3' component of the lncRNAs. Additionally, lncRNAs capped on the 5' and 3' end by snoRNAs have also been observed.[88,89] Generally, all RNA products from this genomic locus are highly expressed in neurons and often have widespread tissue expression unless otherwise noted.[90]

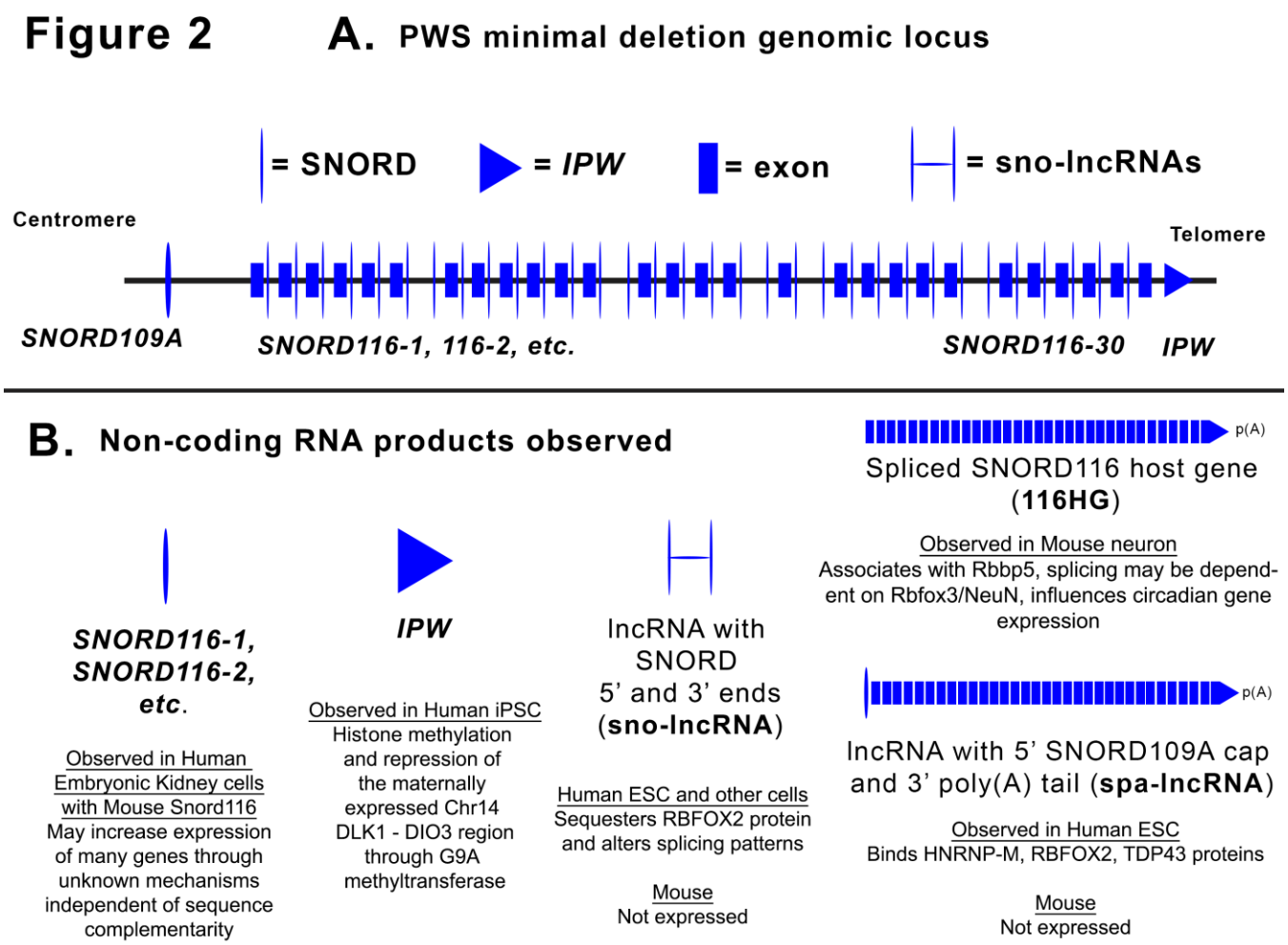

Figure 2. The PWS minimal deletion region and the non-coding RNA products observed from the locus. A. Genomic region with exons and genes labelled. **B.** RNA products observed from the genomic locus and their observed molecular characteristics. Original studies of the observed findings are discussed and cited in the main text.

The most identifiable and well characterized genes from this genomic locus are from the *SNORD116* gene cluster (previously known as HBII-85 in human and MBII-85 in mouse). This is a cluster of highly homologous, tandemly repeated non-coding RNA (ncRNA) genes of the small nucleolar RNA (snoRNA) classification. SnoRNAs are ncRNAs that are expressed in all eukaryotic cells, and they range from 50-150 nucleotides long. They primarily target and modify pre-ribosomal RNA (rRNA) or the spliceosome-associated small nuclear RNA (snRNA) through RNA sequence complementarity.[83,91–95] SnoRNAs usually localize to the nucleolus or cajal bodies.[96–98] There are two main classes of snoRNAs, categorized based on nucleotide motif conservation. These two classes are the C/D box snoRNAs, which 2'O-methylate target

RNAs, and the H/ACA box snoRNAs which pseudo-uridylate target RNAs.[83,91–96,99,100] Specifically, the PWS deletion locus snoRNAs contain C/D box nucleotide motifs, categorizing them into the class known as Small Nucleolar RNA with C/D box motifs (SNORD) (**Figure 3**). An individual SNORD from this gene cluster is known as *SNORD116*, and specific transcript IDs are labelled as *SNORD116-1*, *SNORD116-2*, etc. There is a total of 30 identified *SNORD116* copies in the human genome, although it is questionable how many of these are truly expressed and/or functional or how much variance in copy number there is between individuals.[92,101,102] Classically, SNORDs target other RNAs for modification through nucleotide complementarity in their anti-sense region just 5' of the D/D' box motifs (**Figure 3**). However, for *SNORD116* there are no predicted sequence complementarities to known RNAs, leaving *SNORD116*'s molecular function a mystery.

Figure 3. SNORD structure

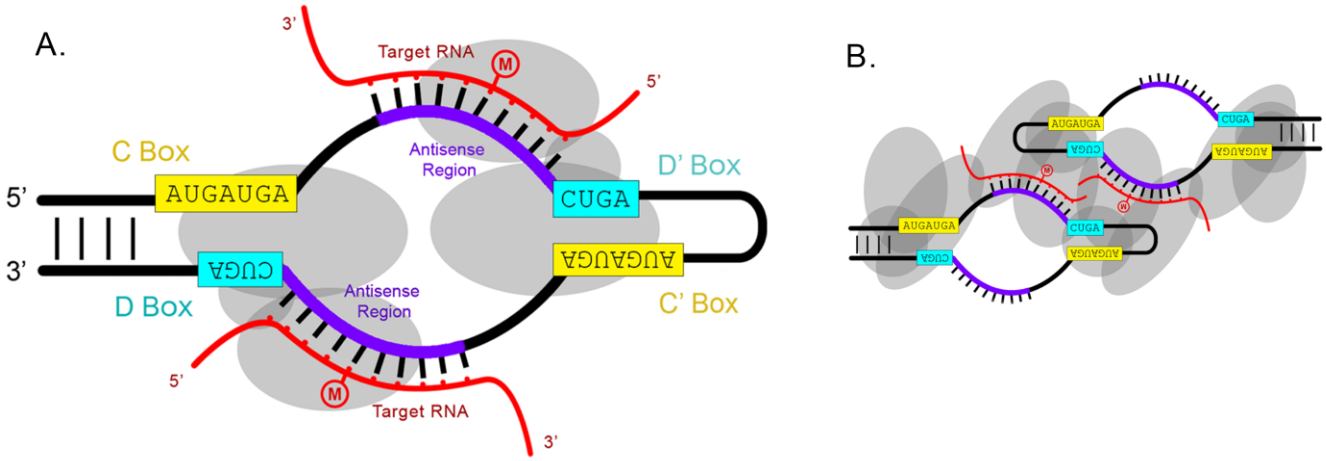

Figure 3. SNORD molecular structure. A. Mature monomeric SNORD structure with labelled components including C/C' boxes, D/D' boxes, antisense region, target RNA, methylated nucleotide, and key structural proteins that make up the snoRNP (grey ovals). **B.** One possible dimeric structure of SNORD. Informed by [94,190]

There have been observations of other SNORDs that have "non-canonical" mechanisms, because they do not target rRNAs or snRNAs.One well observed example of this is the *SNORD115* family of RNAs, which are located just downstream of the *SNORD116* cluster. The *SNORD115* RNAs have been shown to have high sequence complementarity to the serotonin 2C receptor (*HTR2C*) pre-mRNA, and can regulate alternative splicing and RNA

editing of this gene.[85,103–111] Additionally, mouse *Snord115* has been observed in non-canonical snoRNA-protein complexes (snoRNPs).[104] This includes a lack of RNA-protein interaction with the methyltransferase Fibrillarin that is needed for canonical SNORD function. However, there are variable observations of these non-canonical mechanisms that question their biological relevance and replicability.[87,110,112,113] This effect on *HTR2C* expression potentially explains some of the hyperphagic phenotypes observed in PWS that have deletions of *SNORD115*, as *HTR2C* has been implicated in feeding behavior.[114,115] However, the *SNORD115* cluster has been ruled out as a minimal causative deletion of PWS.[116] Regardless, *SNORD115* is an example of a non-canonical SNORD. In addition to the non-canonical functions of alternative splicing or RNA editing, it has also been observed that SNORDs can serve as precursors to miRNA and piRNA, although this has not been implicated for *SNORD116*.[117–121]

As mentioned previously, snoRNAs rely on RNA-protein interactions to form a snoRNP which is further processed to mature into a functional SNORD (**Figure 3**). As snoRNAs are often hosted within introns, the snoRNP protects the snoRNA from degradation, and the intronic RNA is degraded by exonuclease activity. This feature explains the expression of lncRNAs with snoRNA 5' and 3' ends observed from the PWS minimal deletion region. These "sno-lncRNAs" are expressed when there are two SNORD units close together within a single intron (**Figure 2**). Both copies of *SNORD116* are protected from exonuclease degradation, and the transcribed RNA linking the two SNORDs together are protected as well.[88,89] These sno-lncRNAs localize to their site of transcription, and associate with and sequester FOX protein family splicing factors, thus affect splicing patterns.[88] However the sno-lncRNAs associated with the PWS genomic locus are not observed in mice, showing species specific expression.[89]

The hosting of *SNORD116* and the sno-lncRNAs within the introns of their lncRNA host gene synchronizes the expression of the host RNA and the snoRNAs. The intron derived *SNORD116* is not expressed without the transcription of the host gene. Additionally, mouse *Snord116* is dependent on the splicing of its ncRNA host gene (116HG) for proper expression and function.[122] The splicing of mouse 116HG may require the neuronal splicing factor *Rbfox3*, also known as NeuN, for proper splicing and downstream expression of *Snord116*.[122] This splicing limits mouse *Snord116* expression to neuronal tissue, although nonspliced 116HG and ncRNAs from this locus are widely expressed in various cell types. Interestingly, the closely

related human *RBFOX2* splicing factor was found to associate with the sno-lncRNAs found in a variety of human cell types.[88] However, the *Rbfox3*/NeuN dependent splicing of 116HG was found in mouse, which doesn't appear to express mouse homologs of the sno-lncRNAs.[89] This potential dependency on *RBFOX3*/NeuN for human 116HG splicing and downstream *SNORD116* expression has not yet been demonstrated.

The spliced 116HG RNA has been observed to localize to its site of transcription, while the chromatin is decondensed of the active paternal allele in rat, mouse, and human neurons.[78,82] Chromatin decondensation and 116HG RNA levels are developmentally regulated in maturing neurons, and correlated with nucleolus size in mouse and human.[123,124] Fluorescent *in situ* hybridization (FISH) has shown 116HG localizes to its site of transcription, while processed *Snord116* transcripts diffuse throughout the nucleus and co-localize with pre-rRNA signal in primary rat hypothalamus cells.[82] In mouse neurons, spliced 116HG associates with *Rbbp*5 protein, which is involved in transcription activation through histone-3 lysine-4 (H3K4) methylation.[78] Mouse 116HG RNA also binds to genomic regions including its site of transcription, as well as other regions genome wide such as *Mtor* and *Ccdc12.* The RNA FISH signal of mouse spliced 116HG also shows circadian dependence, with higher spatial signal at Zeitgeber time +6 compared to Zeitgeber time +16.[78]

In addition to the spliced 116HG, a similar RNA has been observed. This RNA species is 5' capped with *SNORD109A* followed by the spliced 116HG exons, and 3'polyadenylated (SPA-lncRNA) (**Figure 2**).[77] This RNA species has been observed in human embryonic stem cells (hESCs) to sequester multiple RNA binding proteins including *RBFOX2*, *HNRNPM*, and *TDP43*.[77] Interestingly, the mouse genomic locus lacks a *SNORD109A* homolog and this SPA lncRNA is not observed in mouse embryonic stem cells (mESCs), although another SPA lncRNA originating upstream with a 5' cap of the *Snord107* homolog has been observed in mouse neurons but not mESCs, indicating that this class of RNA species is conserved.[77]

The very 3' end of the 116HG or SPA-lncRNA contains another ncRNA gene, *IPW* (**Figure 2**). This polyadenylated ncRNA is primarily expressed in brain, but widely expressed in other tissues.[125–127] *IPW* has been implicated to regulate an imprinted locus on Chromosome 14, the *DLK1 – DIO3* region, in human induced pluripotent stem cells (iPSCs). *IPW* mediates this regulation through binding interactions with the G9A methyltransferase, and downstream

repressive effects of the maternally expressed genes in the Chr14 imprinted region through histone-3 lysine-9 trimethylation (H3K9me3).[128]

It is important to be aware of the many RNA products observed at the genomic PWS-MDR, as genomic deletion models are often used in mouse and human studies. Some studies implicate their studied RNA of interest in downstream molecular effects through different knockout models. However, some claims may overreach when attributing a specific RNA species to data observed in genomic deletion models. Nevertheless, consistency of findings between PWS deletion models and non-disease state models certainly shows high biological relevance. The molecular mechanisms listed for the above ncRNAs have been curated to minimize conclusions that originate from large genomic locus deletions and knockouts. Additionally, genomic deletions may alter unidentified chromatin-scale *cis*-acting or *trans*-acting elements, further confounding findings in genomic deletion models.

Interestingly, expression of *SNORD116* from the silenced maternal allele can be restored by knockout of zinc-finger protein ZNF274 or modification of the ZNF274 DNA binding sites located within a subset of *SNORD116* copies.[129,130] ZNF274 binding enables a repressive H3K9 methyltransferase that silences the maternal alleles at the PWS-MDR independently of the PWS-IC.[129,130]

To re-focus on *SNORD116*, there are few studies with hints to its molecular mechanism. As mentioned previously, RNA FISH shows rat neuron *Snord116* RNA colocalizes with pre-rRNA to the nucleolus, canonical localizations for snoRNAs.[82] However, there is a lack of predicted target RNAs for *SNORD116*. The overexpression of functional mouse *Snord116* (highly homologous to at least one copy of human *SNORD116*) in HEK293T kidney cells changed the RNA expression level of many genes, but none were predicted to interact with *Snord116* through sequence complementarity.[112] Additionally, there was no evidence of alternative splicing, potentially mirroring *Snord115*'s non-canonical functions. However, due to the overall upregulation in other genes' expression levels, it was proposed that *Snord116* may increase RNA stability or transcription.[112] Although *Snord116* may be dependent on *Rbfox3*/NeuN splicing factors in mouse for proper expression, the overexpression construct used was optimized at the splicing sites for efficient expression and there is evidence for functional *Snord116* expressed in the study.[112,122] Outside of this *Snord116* overexpression study there is a lack of molecular studies that directly investigate *Snord116* while minimizing

confounds of the PWS-MDR. Many studies have been conducted in the context of genomic deletion models that delete the whole *SNORD116* gene cluster. One reason for this approach is the availability of a PWS model mouse that harbors a deletion in the *SNORD116* gene cluster and *IPW*, a region nearly homologous to the PWS-MDR in humans.

2.4 Prader-Willi Syndrome mouse models

Mouse models for PWS have proven valuable to further elucidate PWS etiology and potential treatments. However, as with all models, they are not perfect. The human Chr15 PWS region is syntenic to a region on mouse Chr7. The PWS large deletion locus is mostly conserved between mouse and human with a few differences including potential chromosome structural variation or the absence of a few gene homologs including *PWRN1, NPAP1 SNORD108*, *SNORD109A*, and *SNORD109B* (**Figure 1**). As mentioned previously, the lack of a *SNORD109A* homolog in mouse likely leads to no expression of a mouse homolog of the SPA-lncRNA expressed in the human locus (**Figure 2**).[77] The sno-lncRNAs from the human locus are also not observed in mouse[89] and the mouse homolog for *IPW* shows relatively weak conservation to the human sequence. Lastly, the mouse *Snord116* sequences show very high homogeneity within mouse, while the human *SNORD116* sequences show more heterogeneity within human (**Figure 4**). Between mouse and human *SNORD116* copies, the sequences are relatively homologous.

Figure 4

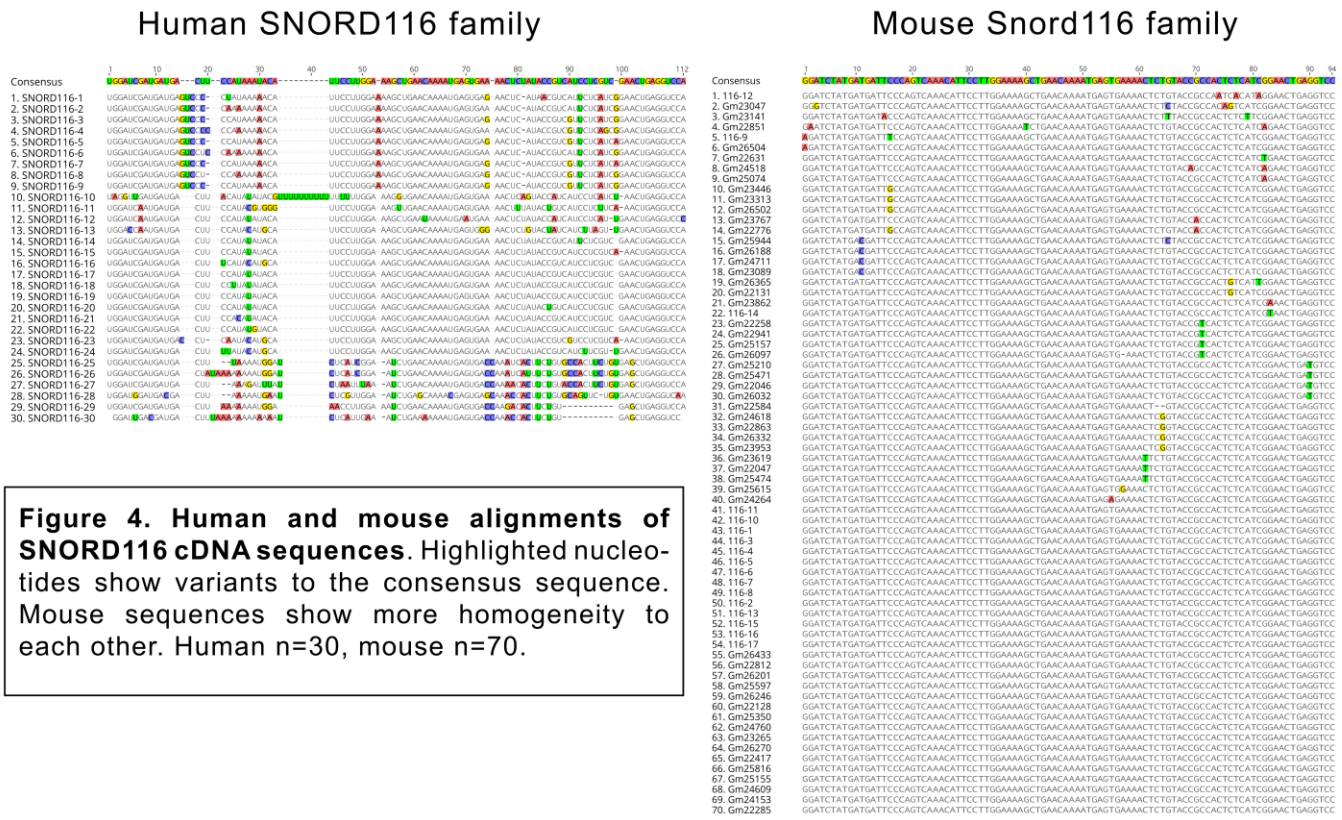

Figure 4. Human and mouse alignments of SNORD116 cDNA sequences. Highlighted nucleotides show variants to the consensus sequence. Mouse sequences show more homogeneity to each other. Human n=30, mouse n=70.

Various mouse models have been generated to investigate PWS and the genomic locus: PWS-IC, AS-IC, and *Snurf-Snrpn* mutations; a large deletion encompassing the *Snurf* gene to the *Ube3a* gene; a large deletion syntenic for human PWS LD1; deletion of *Ndn;* deletion of *Magel2*; deletion of *Ipw* and the *Snord115* cluster; and deletion of *Ipw* and the *Snord116* cluster.[131] The focus of the current study and review is on the mouse models with deletions encompassing *Ipw* and the *Snord116* cluster (*Snord116*del mice). Two mouse models generated independently involve a deletion in the region encompassing the *Snord116* cluster and *IPW*.[131,132] These mouse models share some phenotypes with human PWS, the most prominent phenotype being postnatal developmental delay.

Table 2 shows major findings from this mouse model of PWS. To summarize, nearly all findings include developmental delay, low body weight, and low circulating/liver insulin-like growth factor 1 (IGF1), a biomarker for growth hormone activity. The mouse models also fail to develop hypogonadism, obesity, and often show low body fat percentage, distinct contrasts from PWS patients. Energy expenditure is generally increased, while some studies find either

increased fatty acid oxidation or carbohydrate oxidation dependent on the situation. The presence of hyperphagia is a debated topic, with some studies finding no change, while others claim increased food intake relative to body weight. Circadian systems are disrupted at the behavioral, neurocircuit, epigenetic, and molecular level. Peripheral hormones such as ghrelin show some variation between studies, but mice are also resistant to ghrelin receptor inhibitors, like PWS patients.

Many hypothalamic neuropeptides and related genes show varying results between studies, this includes neuropeptide Y (*Npy*), Agouti-related peptide (*Agrp*), Pro-opiomelanocortin (*Pomc*), hypocretin/orexin (*Hcrt*), Pro-Melanin concentrating hormone (*Pmch*), growth hormone releasing hormone (*Ghrh*), Prohormone convertase 1 (*Pcsk1*), and Nescient helix-loop-helix 2 (*Nhlh2*). Generally, *Npy, Agrp,* and *Pomc* show increased mRNA expression between multiple studies. Although these neuropeptides have many functions, they generally work on opposite sides of the appetite homeostasis system, with *Npy* and *Agrp* stimulating appetite, and *Pomc* suppressing appetite. Selective *Snord116* deletion only in Npy-expressing neurons also recapitulates most phenotypes of the whole-body deletion mouse models. Additionally, thermal regulation of PWS mouse models may be disrupted and thermo-neutral habitations at 30°C may normalize some phenotypes.

Generally, it seems that PWS mouse models are stuck in the early phase of PWS associated with developmental delay. They do not transition to a distinct hyperphagia and develop obesity like PWS patients do. However, there is some evidence that knockdown of *Snord116* after mouse maturity may have effects on hyperphagia and obesity that are more indicative of human PWS. This outcome adds to the hypothesis that PWS mouse models fail to transition to the later stages of PWS, and that *Snord116* deletion may possibly recapitulate obesity and hyperphagia if given the right developmental context.

Table 2. Major findings from *Snord116* deletion mice

Snord116 cluster deletion models	Phenotypes	Reference
Congenital deletion (Paternal inheritance)	• Postnatal developmental delay • Postnatal lethality (15%) in C57BL/6J mice	Skryabin et al. 2007 [131]
Congenital deletion (Paternal inheritance)	• Postnatal developmental delay • Low body weight and body fat percentage with normal and high-fat diet • Deficiencies in motor learning • Anxiety-like behavior • Increased food intake relative to body weight • Increased circulating ghrelin • Decreased hepatic *Igf1* mRNA (low growth hormone function) • Normal fertility with delayed sexual maturation in females • Increased carbohydrate oxidation in dark hours • Increased oxygen consumption • Better maintenance of core body temperature during cold exposure	Ding et al. 2008 [132]
Congenital deletion (Paternal inheritance)	• No changes in neonatal hypothalamus RNA via microarray	Ding et al. 2010 [133]
Congenital deletion (Paternal inheritance)	• Increased fatty acid oxidation in light hours • No altered food intake • Increased energy expenditure • Altered circadian gene expression (*Mtor, Cry1, Per2, Clock*)	Powell et al. 2013 [78]
Congenital deletion (Paternal inheritance)	• Some increased food intake • No anorexic effects of ghrelin receptor inhibitors	Lin et al. 2014 [134]
Congenital deletion (Paternal and Maternal inheritance)	• Task-dependent alterations to locomotion • Anxiety-like behavior • Normal Sociability • Normal social recognition memory, • Normal spatial working memory, • Normal fear-associated behaviors	Zieba et al. 2015 [135]
Congenital deletion (Paternal inheritance)	• Defects in prohormone processing of proinsulin, pro-GH–releasing hormone, and proghrelin • Reduction in prohormone processing gene pathway (*Pcsk1* and *Nhlh2*) • Increased *Agrp* and *Npy* mRNA (hypothalamus) • Increased food intake relative to body weight • No difference in fatty acid or carbohydrate oxidation • Decreased serum IGF1 and liver *Igf1*	Burnett et al. 2016 [136]
1. Congenital deletion (Paternal inheritance) **2.** Conditional congenital deletion (NPY neurons, paternal inheritance)	• Reduced skeletal growth, bone size, bone mass, bone density • Increased *Npy* and *Pomc* mRNA (arcuate nucleus hypothalamus)	Khor et al. 2016 [137]
1. Congenital deletion (Paternal inheritance) **2.** Congenital deletion (Paternal and Maternal	• Better performance in the working-for-food behavioral task	Lassi et al. 2016 [138]

inheritance)		
Congenital deletion (Paternal inheritance)	• Alterations in REM sleep EEG theta wave signal • Reduction in gray matter volume of theta-wave-relevant brain areas • Higher peripheral body temperature	Lassi et al. 2016 [139]
1. Congenital deletion (Paternal and Maternal inheritance) **2.** Conditional congenital deletion (NPY neurons, paternal and maternal inheritance)	• Developmental delay • Low body weight and body fat percentage • Respiratory exchange ratio dependent on age • Increased food intake relative to body weight • Increased energy expenditure relative to body weight • Resistant to high-fat diet induced obesity • <u>Conditional deletion</u> • Increased *Npy* and *Pomc* mRNA levels (conditional NPY neuron knockout) • • <u>Non-conditional deletion</u> • Normal ghrelin level • Decreased serum IGF1 • Increased neuropeptide mRNA levels: *Pomc, Npy, Hcrt, Pmch, Ghrh*	Qi et al. 2016 [140]
1. Congenital deletion (Paternal and Maternal inheritance) **2.** Conditional congenital deletion (NPY neurons, paternal and maternal inheritance)	• <u>30 °C habitation vs 22 °C</u> • Normalizes food intake relative to body weight • Normalizes energy expenditure relative to body weight • Normalizes *Npy* and *Pomc* mRNA levels	Qi et al. 2017 [141]
Congenital deletion (Paternal and Maternal inheritance) **With** Mid-hypothalamus deletion rescue at 6 weeks	• Further reduction of body weight and weight gain (rescued by 30 °C habitation) • Increased energy expenditure • Increased carbohydrate oxidation	Qi et al. 2017 [142]
Conditional deletion (whole-body knockdown at 8 weeks)	• Reduced feeding • Increased fat mass	Purtell et al. 2017 [143]
1. Congenital deletion (Paternal inheritance) **2.** Conditional deletion (mediobasal hypothalamus deletion at 10-12 weeks old)	• <u>Congenital deletion</u> • Normal food intake • No change in *Nhlh2, Pcsk1, Pomc, Lepr, Npy, Agrp,* mRNA (hypothalamus) • <u>Conditional deletion</u> • Increased food intake • Obesity in some mice • Increased *Socs3* mRNA in obese mice (hypothalamus)	Polex-Wolf et al. 2018 [144]
Congenital deletion (Paternal inheritance)	• Disrupted circadian pattern of chromosome methylation	Coulson et al. 2018 [145]
Congenital deletion (Paternal inheritance) **With** Ubiquitous expression of	• <u>WT background</u> • Brain specific splicing of *116HG* dependent on *Rbfox3*/NeuN • Co-localization of transgenic *116HG* / *Snord116* with	Coulson et al. 2018 [122]

Snord116 transgene on Chr7 (47Mb from endogenous *Snord116*)	endogenous equivalents • <u>Paternal deletion background</u> • No expression of transgenic *116HG* / *Snord116* on paternal deletion background	
1. Congenital deletion (Paternal inheritance) **2.** Congenital deletion (Paternal inheritance) ***With*** Ghrelin gene deletion **3.** Congenital deletion (Paternal inheritance) ***With*** Ghrelin receptor gene deletion	• Ghrelin receptor agonist rescues neonatal mortality • Increased plasma Acylated ghrelin • Decreased plasma IGF1 • No major effects of ghrelin gene deletions	Rodriguez et al. 2018 [146]
Congenital deletion (Paternal inheritance)	• Deficits in novel object recognition, location memory, and tone cue fear conditioning • Normal exploratory and motor abilities	Adhikari et al. 2019 [147]
Congenital deletion (Paternal inheritance)	• Altered neuronal firing dynamics in the lateral hypothalamus associated with sleep homeostasis • High proportion of neurons non-responsive to food intake (lateral hypothalamus) • Impaired orexin (hypocretin) neuron system (lateral hypothalamus) mediating sleep homeostasis, REM sleep, and thermoregulatory responses	Pace et al. 2020 [148]

2.5 Impaired prohormone processing in Prader-Willi Syndrome

In late 2016, Burnett et al. showed that peptide hormone processing was dysregulated in PWS mouse models and neurons differentiated from iPSCs of PWS patients (PWS iPSC-neurons). Many peptide hormones and neuropeptides are post-translationally cleaved and processed to form smaller peptides that are often the functional peptide, or have more potency, or vary in function. With impaired prohormone processing, key peptides in the endocrine system are disrupted and endocrine signaling is impaired. Specifically, proinsulin, pro-GH–releasing hormone, and proghrelin showed defects in prohormone processing in Snord116del mice.[136] In conjunction with these findings, prohormone convertase 1 (PC1), a key enzyme involved in prohormone processing, was expressed at lower levels in PWS mice and PWS iPSC-neurons compared to controls. The reduced levels of PC1, encoded by the gene *PCSK1*, was proposed to be a major causative factor in the etiology of PWS, as many symptoms of PWS are shared by patients with defects in PC1. Additionally, *NHLH2*, a transcriptional activator of the *PCSK1* gene, was also downregulated in PWS mouse models and PWS iPSC-neurons.[136] Therefore, it is possible that dysregulation of *NHLH2* upstream of *PCSK1* lowers the expression of *PCSK1* protein and leads to impaired prohormone processing and PWS symptoms. Additionally, *Nhlh2* $^{-/-}$ mice show many phenotypic similarities to PWS patients and PWS mouse models including hypogonadism and obesity. A comparison of these phenotypes is shown in **Table 3**. The theory of impaired prohormone processing in PWS is an enticing explanation, however, it is unknown how loss of the *SNORD116* gene cluster in mice and PWS iPSC-neurons leads to lower levels of *NHLH2* and *PCSK1*.

While reduction in *NHLH2* and *PCSK1* explains many clinical features of PWS, it does not have comprehensive support. PC1 deficient patients display impaired POMC processing resulting in pale skin and adrenal insufficiency, neonatal malabsorptive diarrhea, diabetes insipidus, and rarely show GH deficiency, all symptoms that deviate from PWS patients.[149] Additionally, studies have failed to find lower expression of *PCSK1*/*NHLH2* in mRNA sequencing studies of both PWS patient post-mortem hypothalamus and PWS mouse model hypothalamus.[45,144]

Table 3. Phenotype comparison of PWS patients and mouse models

PWS Symptom/Endocrine Abnormality	*Nhlh2* KO mouse	*Snord116*del mouse	Adult onset *Snord116*del mouse
Infantile poor weight gain	Yes	Yes	-
Developmental delay	Yes	Yes	-
GH Deficiency	No	Yes	-
Excessive weight gain 0.5 years – 6 years	Adult-onset obesity	**No**	-
Obesity	Adult-onset	**No**	Yes[144]/Some fat gain[143]
Hyperphagia	No	**Debated**	Yes[144]/No[143]
Hypogonadism	Yes	**No**	No
Delayed Sexual Maturation	Yes	Yes	-

Furthermore, a study in late 2020 found that loss of *MAGEL2*, a gene deleted in large deletions of PWS, disrupts neuropeptide processing through aberrant regulation of processing enzymes such as PC1.[150] Neuropeptide secretory vesicles are reduced as well as active forms of neuropeptides. Loss of *MAGEL2* results in aberrant endosomal trafficking and secretory granule regulation, instead leading to increased lysosomal degradation of key proteins such as PC1 and reduced mature neuropeptides. While this finding harmonizes with the theory of aberrant pro-hormone processing in PWS, it fails to explain dysregulation of PC1 in models with *Snord116* microdeletions.

2.6 The proposed role of *NHLH2* in Prader-Willi Syndrome

NHLH2 is a basic helix-loop-helix (bHLH) transcription factor involved in neural development, energy homeostasis, and gonadal development.[151–158] *Nhlh2* $^{-/-}$ mice show developmental delay, hypogonadism, and adult-onset obesity preceded by reduced voluntary activity and energy expenditure.[155] Loss of *Nhlh2* impairs development of gonadotropin releasing hormone (GnRH) neurons, peripheral innervation and vascularization of adipose tissue, and development of precerebellar neurons.[151,153,159] High *Nhlh2* expression is also associated with poor prognosis in neuroblastoma.[160–163]

Nhlh2 is co-expressed in kisspeptin/neurokinin B/dynorphin (KBDy) neurons, thyrotropin releasing hormone (TRH) neurons, and POMC neurons of the mouse hypothalamus.[164,165] KBDy neurons are hypothalamic neurons controlling GnRH neurons' pulsed release of GnRH, which regulates release of downstream gonadotropins such as luteinizing hormone (LH) and follicle-stimulating hormone (FSH) that are needed for proper gonadal development at the testes and ovaries.[166] Little is known about the role of *Nhlh2* in KBDy neurons, although there is growing work in this field showing that a large percentage of KBDy neurons co-express *Nhlh2* in the rodent hypothalamus (e.g. [164] and unpublished work).

Co-expression of *Nhlh2* is present in TRH neurons of the hypothalamus which are upstream regulators of thyroid stimulating hormone (TSH) and the thyroid system.[167] Loss of *Nhlh2* leads to lower expression of TRH mRNA and peptide in mouse hypothalamus, although prohormone processing does not seem to be affected.[165] Implications for low TRH levels includes hypothyroidism.

Hypothalamic POMC neurons are major appetite suppressors, although there are many POMC-derived peptides involved in diverse functions. Loss of function in the human POMC gene results in red hair, low cortisol levels, and hyperphagic early-onset obesity.[168] Loss of *Nhlh2* impairs the prohormone processing of the POMC peptide. Loss of *Nhlh2* in mouse hypothalamus leads to reduction in PC1 and PC2 which results in impaired POMC peptide processing. This results in low levels of the primary appetite suppressing peptide of interest, alpha melanocyte stimulating hormone (aMSH).[165] Low levels of aMSH, an agonist for melanocortin 4 receptor (MC4R) in the hypothalamus, impairs the energy homeostasis system.[168] Mutations in MC4R are one of the most common causes of monogenic obesity, as

stimulation of MC4R is associated with appetite suppression.[169] Of note, the AgRP neuropeptide inhibits MC4R and causes an increase in appetite.[168] Additionally, mice with *Nhlh2* deletions specific to only GnRH neurons show less POMC neurons in some hypothalamic subnuclei and visceral obesity.[152] POMC neurons can also increase TRH activity, as TRH neurons have MC4R receptors.[170]

Nhlh2 is a transcription factor that activates transcription of the genes *Mc4r*, *Pcsk1*, *Pcsk2*, *Maoa*, *Ndn*, and *Ascl1*.[151,163,165,171–174] **Figure 5** summarizes the *Nhlh2* molecular regulatory network. As described previously, MC4R is critical for the regulation of appetite suppression and energy homeostasis. *Pcsk1* and *Pcsk2* products, (PC1 and PC2), are critical for a broad spectrum of peptide processing, and particularly for POMC signaling in *Nhlh2* positive POMC neurons.[165] The *Maoa* gene encodes monoamine oxidase A (MAO-A), which is associated with psychiatric symptoms such as depression and aggression. In the brain, MAO-A is known to degrade monoamine neurotransmitters such as serotonin, dopamine, and norepinephrine. Many antidepressant drugs act as inhibitors of MAO-A. *Nhlh2* activates transcription of *Maoa*, which influences anxiety-like behavior, PTSD-like behavior, and exploratory behavior in mice.[172,173]

The *Ndn* gene, encoding the Necdin protein, is coincidentally located at the PWS large deletion region on Chr15q. Necdin is a melanoma antigen (MAGE) family protein, which is part of the protein endosomal recycling / ubiquitination / degradation pathway that promotes recycling. Necdin plays a role in GnRH neuron development, leptin receptor cell surface abundance, and axonal outgrowth.[151,175–177]

The *Ascl1* gene encodes a basic helix-loop-helix (bHLH) transcription factor and is involved in neurogenesis, neuronal commitment, and differentiation.[163,178–180] *Ascl1* and downstream targets are needed for proper hypothalamic and ventral telencephalon development and differentiation.[180,181] There is some evidence that *NHLH2* may promote transcription of *ASCL1* in a neuroblastoma context.[160,163] Additionally, *ASCL1* may induce expression of *NHLH2* in embryonic neuronal development and embryonic carcinoma.[180,181] This relationship suggests there may be a feedback loop with *NHLH2* and *ASCL1* in neuroblastoma. However, approaches examining targets of *ASCL1* fail to show *NHLH2* or its potential upstream regulators.[178] More research is needed in this field.

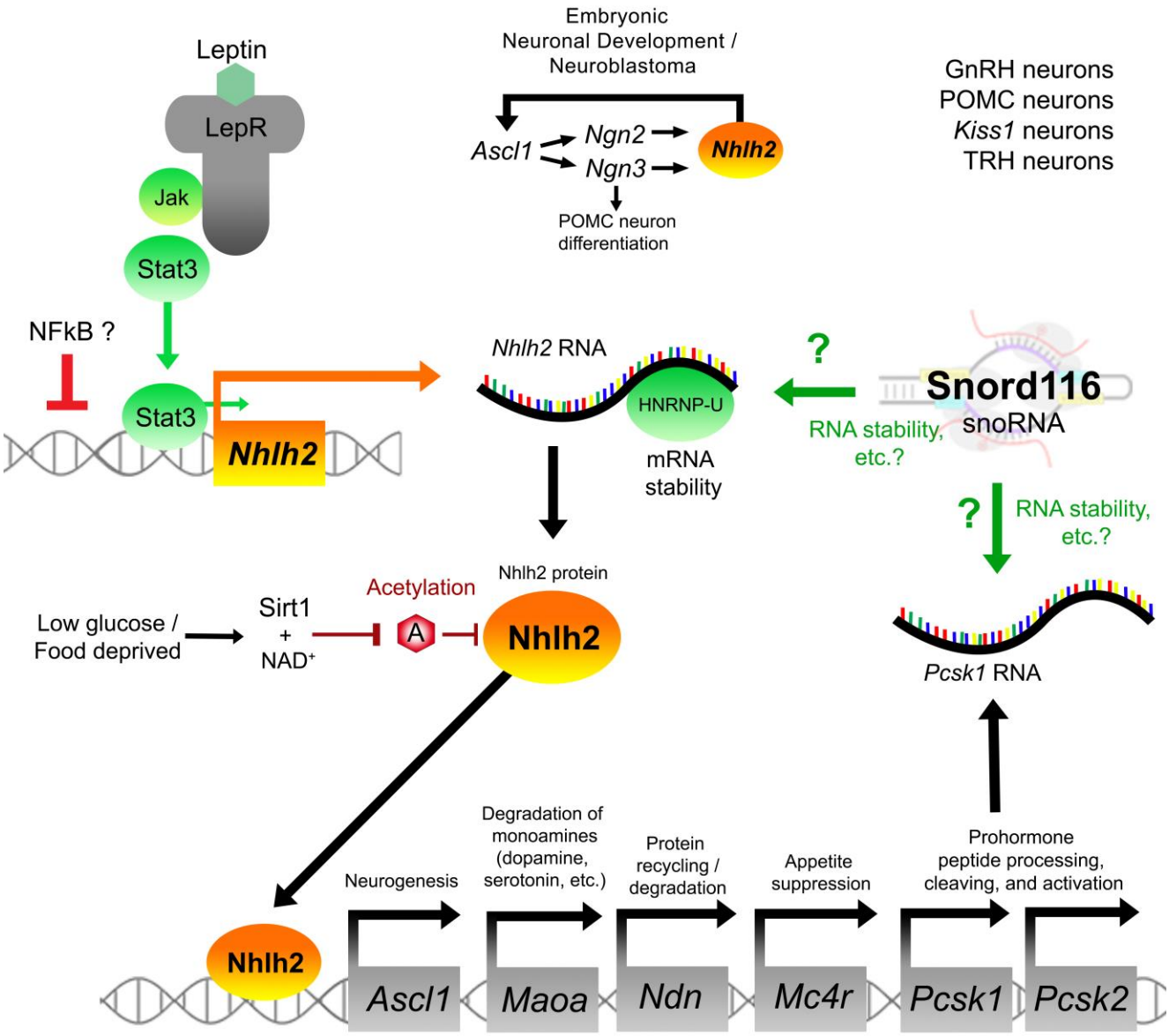

Figure 5. Molecular regulatory network of Nhlh2. Positive regulatory components are indicated with arrows or green shapes. Inhibitory components are indicated with red T shapes. Original findings are discussed and cited in the main text.

Related to *Ascl1, Nhlh2* expression is induced by the neurogenin bHLH transcription factor genes *Ngn2* and *Ngn3*, transcription factors involved in neuronal differentiation and development.[172,181] However as with *Ascl1*, this regulation may depend on developmental context, as there are conflicting results.[182] The post-translational acetylation status of Nhlh2 protein is likely energy dependent, with de-acetylation and activation of Nhlh2 occurring during low energy states and fasted conditions via the NAD^+-dependent de-acetylase Sirt1.[173,183] Additionally, the tumor suppressor gene p53 may upregulate *NHLH2* in a lung cancer cell line.[184]

One of the most well-established upstream regulators of *Nhlh2* is the leptin system. The adipocyte cytokine leptin is released by adipose tissue in response to feeding and activates leptin receptors (LepR) in many cell types and tissues including hypothalamic neurons. Like many cytokine receptors, intracellular signal transduction through LepR is mediated by janus kinase (JAK) and signal transducer and activator of transcription (STAT) pathways.[185,186] In hypothalamic neurons, leptin stimulates LepR and activates Stat3, a transcription factor that binds to the promoter of *Nhlh2*, promoting transcription.[156,187] LepR is present on POMC neurons and TRH neurons of the hypothalamus, which co-express *Nhlh2* and increase their activity with leptin stimulation.[168,170]

At the transcript level, *NHLH2* mRNA is stabilized by the Heterogeneous nuclear ribonucleoprotein U (HNRNP-U) an RNA binding protein, in HEK293 cells.[188] Additionally, a human SNV in the 3' untranslated region (3'UTR) of *Nhlh2* mRNA destabilizes the mRNA and results in decreased expression.[189] These observations of post-transcriptional regulation of *Nhlh2* may provide examples of the possible role Snord116 may play in *Nhlh2* regulation. Due to the snoRNA background and classification of *Snord116*, it is expected that its molecular mechanism involves targeting and binding other RNAs through sequence complementarity to carry out further function, whether that is RNA modification such as methylation, destabilization, stabilization, splicing mechanisms, or other outcomes.

There is evidence presented by Burnett et al. that suggests *Snord116* may regulate *Nhlh2*. However, subsequent studies have failed to find a change in *Nhlh2* or *Pcsk1* expression in PWS models. This key intersection in PWS research requires further investigation. Does *Snord116* truly regulate *Nhlh2* at the molecular level, and if so, how? We hypothesize that *Snord116* regulates *Nhlh2* at the transcript level and stabilizes its RNA. The answer to these questions may guide PWS research field for years to come, as it may answer the compelling theory of impaired prohormone processing in PWS etiology. The current study may partially explain the molecular etiology of PWS and serve as a model for the molecular function of *Snord116*, and perhaps the PWS microdeletion genomic locus.

Problem statement and Specific Aims

Loss of the *SNORD116* gene cluster causes Prader-Willi Syndrome. However, the molecular function of *SNORD116* is unknown, and its poorly understood why loss of this gene cluster causes PWS. Some recent evidence suggests that *SNORD116* may regulate the neuroendocrine transcription factor *NHLH2,* explaining many PWS phenotypes. This study investigates if *Snord116* regulates *Nhlh2*, and the potential molecular mechanisms that may mediate this.

Our overall objective is to identify the relationship between *Snord116* and *Nhlh2*. Our central hypothesis is that products from the *Snord116* gene cluster regulate *Nhlh2* at the RNA transcript.

Aim 1: Characterize the molecular relationship between *Snord116* and *Nhlh2*. Using *in vitro* experiments, the effect of *Snord116* expression on *Nhlh2* expression will be observed in the context of variable 3'UTRs and RNA stability to clarify the molecular relationship between *Snord116* and *Nhlh2*.

Aim 2: Characterize *Snord116*$^{m+/p-}$ mouse hypothalamus gene expression under various feeding conditions. The *in vivo* effect of mouse paternal allele deletion of the *Snord116* gene cluster on mouse hypothalamus RNA expression will be observed in the context of feeding conditions that mediate *Nhlh2* signaling and a dietary supplement that supports weight loss and reduction of body fat.

2.7 References

1. Chung MS, Langouët M, Chamberlain SJ, Carmichael GG. Prader-Willi syndrome: reflections on seminal studies and future therapies. *Open Biol*. 2020;10(9):200195. doi:10.1098/rsob.200195
2. Vogels A, Van Den Ende J, Keymolen K, et al. Minimum prevalence, birth incidence and cause of death for Prader–Willi syndrome in Flanders. *Eur J Hum Genet*. 2004;12(3):238-240. doi:10.1038/sj.ejhg.5201135
3. Whittington JE, Holland AJ, Webb T, Butler J, Clarke D, Boer H. Population prevalence and estimated birth incidence and mortality rate for people with Prader-Willi syndrome in one UK Health Region. *J Med Genet*. 2001;38(11):792-798. doi:10.1136/jmg.38.11.792
4. Cassidy SB, Schwartz S, Miller JL, Driscoll DJ. Prader-Willi syndrome. *Genet Med*. 2012;14(1):10-26. doi:10.1038/gim.0b013e31822bead0
5. Butler MG, Thompson T. Prader-Willi Syndrome: Clinical and Genetic Findings. *The Endocrinologist*. 2000;10(4 Suppl 1):3S-16S.
6. Butler MG, Bittel DC, Kibiryeva N, Talebizadeh Z, Thompson T. Behavioral Differences Among Subjects With Prader-Willi Syndrome and Type I or Type II Deletion and Maternal Disomy. *Pediatrics*. 2004;113(3 Pt 1):565-573. doi:10.1542/peds.113.3.565
7. Butler MG, Hartin SN, Hossain WA, et al. Molecular genetic classification in Prader-Willi syndrome: a multisite cohort study. *J Med Genet*. 2019;56(3):149-153. doi:10.1136/jmedgenet-2018-105301
8. Gross N, Rabinowitz R, Gross-Tsur V, Hirsch HJ, Eldar-Geva T. Prader–Willi syndrome can be diagnosed prenatally. *Am J Med Genet A*. 2015;167(1):80-85. doi:https://doi.org/10.1002/ajmg.a.36812
9. Butler MG, Sturich J, Myers SE, Gold J-A, Kimonis V, Driscoll DJ. Is gestation in Prader-Willi syndrome affected by the genetic subtype? *J Assist Reprod Genet*. 2009;26(8):461-466. doi:10.1007/s10815-009-9341-7
10. Miller JL, Lynn CH, Driscoll DC, et al. Nutritional Phases in Prader–Willi Syndrome. *Am J Med Genet A*. 2011;155A(5):1040-1049. doi:10.1002/ajmg.a.33951
11. Butler MG, Miller JL, Forster JL. Prader-Willi Syndrome - Clinical Genetics, Diagnosis and Treatment Approaches: An Update. *Curr Pediatr Rev*. 2019;15(4):207-244. doi:10.2174/1573396315666190716120925
12. Dimitropoulos A, Feurer ID, Butler MG, Thompson T. Emergence of Compulsive Behavior and Tantrums in Children with Prader-Willi Syndrome. *Am J Ment Retard AJMR*. 2001;106(1):39-51. doi:10.1352/0895-8017(2001)106<0039:EOCBAT>2.0.CO;2
13. Yang L, Zhan G, Ding J, et al. Psychiatric Illness and Intellectual Disability in the Prader–Willi Syndrome with Different Molecular Defects - A Meta Analysis. *PLoS ONE*. 2013;8(8). doi:10.1371/journal.pone.0072640
14. Manzardo AM, Loker J, Heinemann J, Loker C, Butler MG. Survival Trends from the Prader-Willi Syndrome Association (USA) 40-Year Mortality Survey. *Genet Med Off J Am Coll Med Genet*. 2018;20(1):24-30. doi:10.1038/gim.2017.92
15. Butler MG, Manzardo AM, Heinemann J, Loker C, Loker J. Causes of Death in Prader-Willi Syndrome: Prader-Willi Syndrome Association (USA) 40-Year Mortality Survey. *Genet Med Off J Am Coll Med Genet*. 2017;19(6):635-642. doi:10.1038/gim.2016.178

16. Radicioni AF, Giorgio GD, Grugni G, et al. Multiple forms of hypogonadism of central, peripheral or combined origin in males with Prader–Willi syndrome. *Clin Endocrinol (Oxf)*. 2012;76(1):72-77. doi:https://doi.org/10.1111/j.1365-2265.2011.04161.x
17. Angulo MA, Butler MG, Cataletto ME. Prader-Willi syndrome: a review of clinical, genetic, and endocrine findings. *J Endocrinol Invest*. 2015;38:1249-1263. doi:10.1007/s40618-015-0312-9
18. Emerick JE, Vogt KS. Endocrine manifestations and management of Prader-Willi syndrome. *Int J Pediatr Endocrinol*. 2013;2013(1):14. doi:10.1186/1687-9856-2013-14
19. Vaiani E, Herzovich V, Chaler E, et al. Thyroid axis dysfunction in patients with Prader-Willi syndrome during the first 2 years of life. *Clin Endocrinol (Oxf)*. 2010;73(4):546-550. doi:https://doi.org/10.1111/j.1365-2265.2010.03840.x
20. Iughetti L, Vivi G, Balsamo A, et al. Thyroid function in patients with Prader-Willi syndrome: an Italian multicenter study of 339 patients. *J Pediatr Endocrinol Metab*. 2019;32(2):159-165. doi:10.1515/jpem-2018-0388
21. Konishi A, Ida S, Shoji Y, Etani Y, Kawai M. Central hypothyroidism improves with age in very young children with Prader-Willi syndrome. *Clin Endocrinol (Oxf)*. 2020;n/a(n/a). doi:https://doi.org/10.1111/cen.14323
22. Festen D a. M, Visser TJ, Otten BJ, Wit JM, Duivenvoorden HJ, Hokken-Koelega ACS. Thyroid hormone levels in children with Prader–Willi syndrome before and during growth hormone treatment. *Clin Endocrinol (Oxf)*. 2007;67(3):449-456. doi:https://doi.org/10.1111/j.1365-2265.2007.02910.x
23. Butler MG, Theodoro M, Skouse JD. Thyroid Function Studies in Prader–Willi Syndrome. *Am J Med Genet A*. 2007;143A(5):488-492. doi:10.1002/ajmg.a.31683
24. Edgar OS, Lucas-Herald AK, Shaikh MG. Pituitary-Adrenal Axis in Prader Willi Syndrome. *Diseases*. 2016;4(1). doi:10.3390/diseases4010005
25. Rosenberg AGW, Pellikaan K, Poitou C, et al. Central Adrenal Insufficiency Is Rare in Adults With Prader–Willi Syndrome. *J Clin Endocrinol Metab*. 2020;105(7):e2563-e2571. doi:10.1210/clinem/dgaa168
26. Sedky K, Bennett DS, Pumariega A. Prader Willi Syndrome and Obstructive Sleep Apnea: Co-occurrence in the Pediatric Population. *J Clin Sleep Med JCSM Off Publ Am Acad Sleep Med*. 2014;10(4):403-409. doi:10.5664/jcsm.3616
27. Manzardo AM, Johnson L, Miller JL, Driscoll DJ, Butler MG. Higher plasma orexin A levels in children with Prader–Willi syndrome compared with healthy unrelated sibling controls. *Am J Med Genet A*. 2016;170(8):2097-2102. doi:https://doi.org/10.1002/ajmg.a.37749
28. Nevsimalova S, Vankova J, Stepanova I, Seemanova E, Mignot E, Nishino S. Hypocretin deficiency in Prader–Willi syndrome. *Eur J Neurol*. 2005;12(1):70-72. doi:https://doi.org/10.1111/j.1468-1331.2004.00969.x
29. Omokawa M, Ayabe T, Nagai T, et al. Decline of CSF orexin (hypocretin) levels in Prader–Willi syndrome. *Am J Med Genet A*. 2016;170(5):1181-1186. doi:https://doi.org/10.1002/ajmg.a.37542
30. Bittel DC, Kibiryeva N, Sell SM, Strong TV, Butler MG. Whole Genome Microarray Analysis of Gene Expression in Prader–Willi Syndrome. *Am J Med Genet A*. 2007;143A(5):430-442. doi:10.1002/ajmg.a.31606
31. Swaab DF, Purba JS, Hofman MA. Alterations in the hypothalamic paraventricular nucleus and its oxytocin neurons (putative satiety cells) in Prader-Willi syndrome: a study of five cases. *J Clin Endocrinol Metab*. 1995;80(2):573-579. doi:10.1210/jcem.80.2.7852523

32. Johnson L, Manzardo AM, Miller JL, Driscoll DJ, Butler MG. Elevated Plasma Oxytocin Levels in Children with Prader–Willi Syndrome Compared with Healthy Unrelated Siblings. *Am J Med Genet A*. 2016;170(3):594-601. doi:10.1002/ajmg.a.37488
33. Damen L, Grootjen LN, Juriaans AF, et al. Oxytocin in young children with Prader-Willi syndrome: Results of a randomized, double-blind, placebo-controlled, crossover trial investigating 3 months of oxytocin. *Clin Endocrinol (Oxf)*. 2020;n/a(n/a). doi:https://doi.org/10.1111/cen.14387
34. Hollander E, Levine KG, Ferretti CJ, et al. Intranasal oxytocin versus placebo for hyperphagia and repetitive behaviors in children with Prader-Willi Syndrome: A randomized controlled pilot trial. *J Psychiatr Res*. Published online November 4, 2020. doi:10.1016/j.jpsychires.2020.11.006
35. Kuppens RJ, Donze SH, Hokken-Koelega ACS. Promising effects of oxytocin on social and food-related behaviour in young children with Prader–Willi syndrome: a randomized, double-blind, controlled crossover trial. *Clin Endocrinol (Oxf)*. 2016;85(6):979-987. doi:https://doi.org/10.1111/cen.13169
36. Rice LJ, Einfeld SL, Hu N, Carter CS. A review of clinical trials of oxytocin in Prader–Willi syndrome. *Curr Opin Psychiatry*. 2018;31(2):123-127. doi:10.1097/YCO.0000000000000391
37. Miller JL, Tamura R, Butler MG, et al. Oxytocin treatment in children with Prader–Willi syndrome: A double-blind, placebo-controlled, crossover study. *Am J Med Genet A*. 2017;173(5):1243-1250. doi:10.1002/ajmg.a.38160
38. Tauber M, Boulanouar K, Diene G, et al. The Use of Oxytocin to Improve Feeding and Social Skills in Infants With Prader–Willi Syndrome. *Pediatrics*. 2017;139(2). doi:10.1542/peds.2016-2976
39. Dykens EM, Miller J, Angulo M, et al. Intranasal carbetocin reduces hyperphagia in individuals with Prader-Willi syndrome. *JCI Insight*. 2018;3(12). doi:10.1172/jci.insight.98333
40. Miller JL, Goldstone AP, Couch JA, et al. Pituitary abnormalities in Prader–Willi syndrome and early onset morbid obesity. *Am J Med Genet A*. 2008;146A(5):570-577. doi:https://doi.org/10.1002/ajmg.a.31677
41. Iughetti L, Bosio L, Corrias A, et al. Pituitary height and neuroradiological alterations in patients with Prader-Labhart-Willi syndrome. *Eur J Pediatr*. 2008;167(6):701-702. doi:10.1007/s00431-007-0555-3
42. Nieuwpoort IC van, Sinnema M, Castelijns JA, Twisk JWR, Curfs LMG, Drent ML. The GH/IGF-I Axis and Pituitary Function and Size in Adults with Prader-Willi Syndrome. *Horm Res Paediatr*. 2011;75(6):403-411. doi:10.1159/000323442
43. Lukoshe A, van Dijk SE, van den Bosch GE, van der Lugt A, White T, Hokken-Koelega AC. Altered functional resting-state hypothalamic connectivity and abnormal pituitary morphology in children with Prader-Willi syndrome. *J Neurodev Disord*. 2017;9. doi:10.1186/s11689-017-9188-7
44. Grugni G, Crinò A, De Bellis A, et al. Autoimmune pituitary involvement in Prader–Willi syndrome: new perspective for further research. *Endocrine*. 2018;62(3):733-736. doi:10.1007/s12020-018-1666-5
45. Bochukova EG, Lawler K, Croizier S, et al. A Transcriptomic Signature of the Hypothalamic Response to Fasting and BDNF Deficiency in Prader-Willi Syndrome. *Cell Rep*. 2018;22(13):3401-3408. doi:10.1016/j.celrep.2018.03.018

46. Kweh FA, Miller JL, Sulsona CR, et al. Hyperghrelinemia in Prader-Willi Syndrome Begins in Early Infancy Long Before the Onset of Hyperphagia. *Am J Med Genet A*. 2015;0(1):69-79. doi:10.1002/ajmg.a.36810
47. Waele KD, Ishkanian SL, Bogarin R, et al. Long-acting octreotide treatment causes a sustained decrease in ghrelin concentrations but does not affect weight, behaviour and appetite in subjects with Prader–Willi syndrome. *Eur J Endocrinol*. 2008;159(4):381-388. doi:10.1530/EJE-08-0462
48. Steculorum SM, Collden G, Coupe B, et al. Neonatal ghrelin programs development of hypothalamic feeding circuits. *J Clin Invest*. 2015;125(2):846-858. doi:10.1172/JCI73688
49. Purtell L, Sze L, Loughnan G, et al. In adults with Prader–Willi syndrome, elevated ghrelin levels are more consistent with hyperphagia than high PYY and GLP-1 levels. *Neuropeptides*. 2011;45(4):301-307. doi:10.1016/j.npep.2011.06.001
50. Bizzarri C, Rigamonti AE, Luce A, et al. Children with Prader–Willi syndrome exhibit more evident meal-induced responses in plasma ghrelin and peptide YY levels than obese and lean children. *Eur J Endocrinol*. 2010;162(3):499-505. doi:10.1530/EJE-09-1033
51. Butler MG, Moore J, Morawiecki A, Nicolson M. Comparison of Leptin Protein Levels in Prader-Willi Syndrome and Control Individuals. *Am J Med Genet*. 1998;75(1):7-12.
52. Goldstone AP, Brynes AE, Thomas EL, et al. Resting metabolic rate, plasma leptin concentrations, leptin receptor expression, and adipose tissue measured by whole-body magnetic resonance imaging in women with Prader-Willi syndrome. *Am J Clin Nutr*. 2002;75(3):468-475. doi:10.1093/ajcn/75.3.468
53. Lindgren AC, Marcus C, Skwirut C, et al. Increased Leptin Messenger RNA and Serum Leptin Levels in Children with Prader-Willi Syndrome and Nonsyndromal Obesity. *Pediatr Res*. 1997;42(5):593-596. doi:10.1203/00006450-199711000-00007
54. TALEBIZADEH Z, KIBIRYEVA N, BITTEL DC, BUTLER MG. Ghrelin, peptide YY and their receptors: Gene expression in brain from subjects with and without Prader-Willi syndrome. *Int J Mol Med*. 2005;15(4):707-711.
55. Hartley SL, MacLean WE, Butler MG, Zarcone J, Thompson T. Maladaptive Behaviors and Risk Factors Among the Genetic Subtypes of Prader-Willi Syndrome. *Am J Med Genet A*. 2005;136(2):140-145. doi:10.1002/ajmg.a.30771
56. Ohta T, Gray TA, Rogan PK, et al. Imprinting-mutation mechanisms in Prader-Willi syndrome. *Am J Hum Genet*. 1999;64(2):397-413.
57. Yang T, Adamson TE, Resnick JL, et al. A mouse model for Prader-Willi syndrome imprinting-centre mutations. *Nat Genet*. 1998;19(1):25-31. doi:10.1038/ng0598-25
58. Saitoh S, Buiting K, Rogan PK, et al. Minimal definition of the imprinting center and fixation of chromosome 15q11-q13 epigenotype by imprinting mutations. *Proc Natl Acad Sci U S A*. 1996;93(15):7811-7815.
59. Buiting K, Saitoh S, Gross S, et al. Inherited microdeletions in the Angelman and Prader–Willi syndromes define an imprinting centre on human chromosome 15. *Nat Genet*. 1995;9(4):395-400. doi:10.1038/ng0495-395
60. Kantor B, Makedonski K, Green-Finberg Y, Shemer R, Razin A. Control elements within the PWS/AS imprinting box and their function in the imprinting process. *Hum Mol Genet*. 2004;13(7):751-762. doi:10.1093/hmg/ddh085
61. Horsthemke B, Wagstaff J. Mechanisms of imprinting of the Prader–Willi/Angelman region. *Am J Med Genet A*. 2008;146A(16):2041-2052. doi:https://doi.org/10.1002/ajmg.a.32364

62. Buiting K, Groß S, Lich C, Gillessen-Kaesbach G, El-Maarri O, Horsthemke B. Epimutations in Prader-Willi and Angelman Syndromes: A Molecular Study of 136 Patients with an Imprinting Defect. *Am J Hum Genet*. 2003;72(3):571-577.
63. Bittel DC, Kibiryeva N, Butler MG. Expression of 4 Genes Between Chromosome 15 Breakpoints 1 and 2 and Behavioral Outcomes in Prader-Willi Syndrome. *Pediatrics*. 2006;118(4):e1276-e1283. doi:10.1542/peds.2006-0424
64. Cox DM, Butler MG. The 15q11.2 BP1–BP2 Microdeletion Syndrome: A Review. *Int J Mol Sci*. 2015;16(2):4068-4082. doi:10.3390/ijms16024068
65. Kim S-J, Miller JL, Kuipers PJ, et al. Unique and atypical deletions in Prader–Willi syndrome reveal distinct phenotypes. *Eur J Hum Genet*. 2012;20(3):283-290. doi:10.1038/ejhg.2011.187
66. Sharp AJ, Mefford HC, Li K, et al. A recurrent 15q13.3 microdeletion syndrome associated with mental retardation and seizures. *Nat Genet*. 2008;40(3):322-328. doi:10.1038/ng.93
67. Mostovoy Y, Yilmaz F, Chow SK, et al. Genomic regions associated with microdeletion/microduplication syndromes exhibit extreme diversity of structural variation. *Genetics*. 2021;(iyaa038). doi:10.1093/genetics/iyaa038
68. Bailey JA, Yavor AM, Massa HF, Trask BJ, Eichler EE. Segmental Duplications: Organization and Impact Within the Current Human Genome Project Assembly. *Genome Res*. 2001;11(6):1005-1017. doi:10.1101/gr.187101
69. Bailey JA, Church DM, Ventura M, Rocchi M, Eichler EE. Analysis of Segmental Duplications and Genome Assembly in the Mouse. *Genome Res*. 2004;14(5):789-801. doi:10.1101/gr.2238404
70. Levy-Sakin M, Pastor S, Mostovoy Y, et al. Genome maps across 26 human populations reveal population-specific patterns of structural variation. *Nat Commun*. 2019;10. doi:10.1038/s41467-019-08992-7
71. Bieth E, Eddiry S, Gaston V, et al. Highly restricted deletion of the SNORD116 region is implicated in Prader–Willi Syndrome. *Eur J Hum Genet*. 2015;23(2):252-255. doi:10.1038/ejhg.2014.103
72. Tan Q, Potter KJ, Burnett LC, et al. Prader–Willi-Like Phenotype Caused by an Atypical 15q11.2 Microdeletion. *Genes*. 2020;11(2). doi:10.3390/genes11020128
73. Sahoo T, del Gaudio D, German JR, et al. Prader-Willi phenotype caused by paternal deficiency for the HBII-85 C/D box small nucleolar RNA cluster. *Nat Genet*. 2008;40(6):719-721. doi:10.1038/ng.158
74. Duker AL, Ballif BC, Bawle EV, et al. Paternally inherited microdeletion at 15q11.2 confirms a significant role for the SNORD116 C/D box snoRNA cluster in Prader–Willi syndrome. *Eur J Hum Genet*. 2010;18(11):1196-1201. doi:10.1038/ejhg.2010.102
75. de Smith AJ, Purmann C, Walters RG, et al. A deletion of the HBII-85 class of small nucleolar RNAs (snoRNAs) is associated with hyperphagia, obesity and hypogonadism. *Hum Mol Genet*. 2009;18(17):3257-3265. doi:10.1093/hmg/ddp263
76. Fontana P, Grasso M, Acquaviva F, et al. SNORD116 deletions cause Prader-Willi syndrome with a mild phenotype and macrocephaly. *Clin Genet*. 2017;92(4):440-443. doi:https://doi.org/10.1111/cge.13005
77. Wu H, Yin Q-F, Luo Z, et al. Unusual Processing Generates SPA LncRNAs that Sequester Multiple RNA Binding Proteins. *Mol Cell*. 2016;64(3):534-548. doi:10.1016/j.molcel.2016.10.007

78. Powell WT, Coulson RL, Crary FK, et al. A Prader–Willi locus lncRNA cloud modulates diurnal genes and energy expenditure. *Hum Mol Genet*. 2013;22(21):4318-4328. doi:10.1093/hmg/ddt281
79. Coulson RL, Powell WT, Yasui DH, Dileep G, Resnick J, LaSalle JM. Prader-Willi locus Snord116 RNA processing requires an active endogenous allele and neuron-specific splicing by Rbfox3/NeuN. *bioRxiv*. Published online April 20, 2018:305557. doi:10.1101/305557
80. Powell WT, Coulson RL, Gonzales ML, et al. R-loop formation at Snord116 mediates topotecan inhibition of Ube3a-antisense and allele-specific chromatin decondensation. *Proc Natl Acad Sci U S A*. 2013;110(34):13938-13943. doi:10.1073/pnas.1305426110
81. Runte M, Hüttenhofer A, Groß S, Kiefmann M, Horsthemke B, Buiting K. The IC-SNURF–SNRPN transcript serves as a host for multiple small nucleolar RNA species and as an antisense RNA for UBE3A. *Hum Mol Genet*. 2001;10(23):2687-2700. doi:10.1093/hmg/10.23.2687
82. Vitali P, Royo H, Marty V, Bortolin-Cavaillé M-L, Cavaillé J. Long nuclear-retained non-coding RNAs and allele-specific higher-order chromatin organization at imprinted snoRNA gene arrays. *J Cell Sci*. 2010;123(1):70-83. doi:10.1242/jcs.054957
83. Falaleeva M, Welden JR, Duncan MJ, Stamm S. C/D-box snoRNAs form methylating and non-methylating ribonucleoprotein complexes: Old dogs show new tricks. *BioEssays*. 2017;39(6):n/a-n/a. doi:10.1002/bies.201600264
84. Deschamps-Francoeur G, Garneau D, Dupuis-Sandoval F, et al. Identification of discrete classes of small nucleolar RNA featuring different ends and RNA binding protein dependency. *Nucleic Acids Res*. 2014;42(15):10073-10085. doi:10.1093/nar/gku664
85. Cavaillé J, Buiting K, Kiefmann M, et al. Identification of brain-specific and imprinted small nucleolar RNA genes exhibiting an unusual genomic organization. *Proc Natl Acad Sci U S A*. 2000;97(26):14311-14316.
86. Shen M, Eyras E, Wu J, et al. Direct cloning of double-stranded RNAs from RNase protection analysis reveals processing patterns of C/D box snoRNAs and provides evidence for widespread antisense transcript expression. *Nucleic Acids Res*. 2011;39(22):9720-9730. doi:10.1093/nar/gkr684
87. Bortolin-Cavaillé M-L, Cavaillé J. The SNORD115 (H/MBII-52) and SNORD116 (H/MBII-85) gene clusters at the imprinted Prader–Willi locus generate canonical box C/D snoRNAs. *Nucleic Acids Res*. 2012;40(14):6800-6807. doi:10.1093/nar/gks321
88. Yin Q-F, Yang L, Zhang Y, et al. Long Noncoding RNAs with snoRNA Ends. *Mol Cell*. 2012;48(2):219-230. doi:10.1016/j.molcel.2012.07.033
89. Zhang X-O, Yin Q-F, Wang H-B, et al. Species-specific alternative splicing leads to unique expression of sno-lncRNAs. *BMC Genomics*. 2014;15:287. doi:10.1186/1471-2164-15-287
90. Galiveti CR, Raabe CA, Konthur Z, Rozhdestvensky TS. Differential regulation of non-protein coding RNAs from Prader-Willi Syndrome locus. *Sci Rep*. 2014;4. doi:10.1038/srep06445
91. Bachellerie J-P, Cavaillé J, Hüttenhofer A. The expanding snoRNA world. *Biochimie*. 2002;84(8):775-790. doi:10.1016/S0300-9084(02)01402-5
92. Jorjani H, Kehr S, Jedlinski DJ, et al. An updated human snoRNAome. *Nucleic Acids Res*. 2016;44(11):5068-5082. doi:10.1093/nar/gkw386

93. Bergeron D, Fafard-Couture É, Scott MS. Small nucleolar RNAs: continuing identification of novel members and increasing diversity of their molecular mechanisms of action. *Biochem Soc Trans*. 2020;48(2):645-656. doi:10.1042/BST20191046
94. Bratkovič T, Božič J, Rogelj B. Functional diversity of small nucleolar RNAs. *Nucleic Acids Res*. 2020;48(4):1627-1651. doi:10.1093/nar/gkz1140
95. Boivin V, Faucher-Giguère L, Scott M, Abou-Elela S. The cellular landscape of mid-size noncoding RNA. *Wiley Interdiscip Rev RNA*. 2019;10(4). doi:10.1002/wrna.1530
96. Kiss T. Small nucleolar RNA-guided post-transcriptional modification of cellular RNAs. *EMBO J*. 2001;20(14):3617-3622. doi:10.1093/emboj/20.14.3617
97. Boisvert F-M, van Koningsbruggen S, Navascués J, Lamond AI. The multifunctional nucleolus. *Nat Rev Mol Cell Biol*. 2007;8(7):574-585. doi:10.1038/nrm2184
98. Matera AG, Terns RM, Terns MP. Non-coding RNAs: lessons from the small nuclear and small nucleolar RNAs. *Nat Rev Mol Cell Biol*. 2007;8(3):209-220. doi:10.1038/nrm2124
99. Kiss-László Z, Henry Y, Kiss T. Sequence and structural elements of methylation guide snoRNAs essential for site-specific ribose methylation of pre-rRNA. *EMBO J*. 1998;17(3):797-807. doi:10.1093/emboj/17.3.797
100. Kiss T. Small Nucleolar RNAs: An Abundant Group of Noncoding RNAs with Diverse Cellular Functions. *Cell*. 2002;109(2):145-148. doi:10.1016/S0092-8674(02)00718-3
101. Keshavarz M, Krebs-Wheaton R, Refki P, et al. Natural copy number differences of tandemly repeated small nucleolar RNAs in the Prader-Willi syndrome genomic region regulate individual behavioral responses in mammals. *bioRxiv*. Published online January 13, 2020:476010. doi:10.1101/476010
102. Castle JC, Armour CD, Löwer M, et al. Digital Genome-Wide ncRNA Expression, Including SnoRNAs, across 11 Human Tissues Using PolyA-Neutral Amplification. *PLoS ONE*. 2010;5(7). doi:10.1371/journal.pone.0011779
103. Kishore S, Stamm S. The snoRNA HBII-52 Regulates Alternative Splicing of the Serotonin Receptor 2C. *Science*. 2006;311(5758):230-232. doi:10.1126/science.1118265
104. Soeno Y, Taya Y, Stasyk T, Huber LA, Aoba T, Hüttenhofer A. Identification of novel ribonucleo-protein complexes from the brain-specific snoRNA MBII-52. *RNA*. 2010;16(7):1293-1300. doi:10.1261/rna.2109710
105. Kishore S, Stamm S. Regulation of Alternative Splicing by snoRNAs. *Cold Spring Harb Symp Quant Biol*. 2006;71:329-334. doi:10.1101/sqb.2006.71.024
106. Kishore S, Khanna A, Zhang Z, et al. The snoRNA MBII-52 (SNORD 115) is processed into smaller RNAs and regulates alternative splicing. *Hum Mol Genet*. 2010;19(7):1153-1164. doi:10.1093/hmg/ddp585
107. Raabe CA, Voss R, Kummerfeld D-M, et al. Ectopic expression of Snord115 in choroid plexus interferes with editing but not splicing of 5-Ht2c receptor pre-mRNA in mice. *Sci Rep*. 2019;9(1):4300. doi:10.1038/s41598-019-39940-6
108. Vitali P, Basyuk E, Le Meur E, et al. ADAR2-mediated editing of RNA substrates in the nucleolus is inhibited by C/D small nucleolar RNAs. *J Cell Biol*. 2005;169(5):745-753. doi:10.1083/jcb.200411129
109. Garfield AS, Davies JR, Burke LK, et al. Increased alternate splicing of Htr2c in a mouse model for Prader-Willi syndrome leads disruption of 5HT2C receptor mediated appetite. *Mol Brain*. 2016;9(1):95. doi:10.1186/s13041-016-0277-4

110. Hebras J, Marty V, Personnaz J, et al. Reassessment of the involvement of Snord115 in the serotonin 2c receptor pathway in a genetically relevant mouse model. Gingeras TR, Zoghbi HY, eds. *eLife*. 2020;9:e60862. doi:10.7554/eLife.60862
111. Bratkovič T, Modic M, Camargo Ortega G, Drukker M, Rogelj B. Neuronal differentiation induces SNORD115 expression and is accompanied by post-transcriptional changes of serotonin receptor 2c mRNA. *Sci Rep*. 2018;8(1):5101. doi:10.1038/s41598-018-23293-7
112. Falaleeva M, Surface J, Shen M, de la Grange P, Stamm S. SNORD116 and SNORD115 change expression of multiple genes and modify each other's activity. *Gene*. 2015;572(2):266-273. doi:10.1016/j.gene.2015.07.023
113. Kishore S, Gruber AR, Jedlinski DJ, Syed AP, Jorjani H, Zavolan M. Insights into snoRNA biogenesis and processing from PAR-CLIP of snoRNA core proteins and small RNA sequencing. *Genome Biol*. 2013;14(5):R45. doi:10.1186/gb-2013-14-5-r45
114. Tecott LH, Sun LM, Akana SF, et al. Eating disorder and epilepsy in mice lacking 5-HT 2C serotonin receptors. *Nature*. 1995;374(6522):542-546. doi:10.1038/374542a0
115. Xu Y, Jones JE, Kohno D, et al. 5-HT2CRs Expressed by Pro-Opiomelanocortin Neurons Regulate Energy Homeostasis. *Neuron*. 2008;60(4-2):582-589. doi:10.1016/j.neuron.2008.09.033
116. Runte M, Varon R, Horn D, Horsthemke B, Buiting K. Exclusion of the C/D box snoRNA gene cluster HBII-52 from a major role in Prader–Willi syndrome. *Hum Genet*. 2005;116(3):228-230. doi:10.1007/s00439-004-1219-2
117. Ono M, Scott MS, Yamada K, Avolio F, Barton GJ, Lamond AI. Identification of human miRNA precursors that resemble box C/D snoRNAs. *Nucleic Acids Res*. 2011;39(9):3879-3891. doi:10.1093/nar/gkq1355
118. Scott MS, Ono M, Yamada K, Endo A, Barton GJ, Lamond AI. Human box C/D snoRNA processing conservation across multiple cell types. *Nucleic Acids Res*. 2012;40(8):3676-3688. doi:10.1093/nar/gkr1233
119. Brameier M, Herwig A, Reinhardt R, Walter L, Gruber J. Human box C/D snoRNAs with miRNA like functions: expanding the range of regulatory RNAs. *Nucleic Acids Res*. 2011;39(2):675-686. doi:10.1093/nar/gkq776
120. Zhong F, Zhou N, Wu K, et al. A SnoRNA-derived piRNA interacts with human interleukin-4 pre-mRNA and induces its decay in nuclear exosomes. *Nucleic Acids Res*. 2015;43(21):10474-10491. doi:10.1093/nar/gkv954
121. Taft RJ, Glazov EA, Lassmann T, Hayashizaki Y, Carninci P, Mattick JS. Small RNAs derived from snoRNAs. *RNA*. 2009;15(7):1233-1240. doi:10.1261/rna.1528909
122. Coulson RL, Powell WT, Yasui DH, Dileep G, Resnick J, LaSalle JM. Prader–Willi locus Snord116 RNA processing requires an active endogenous allele and neuron-specific splicing by Rbfox3/NeuN. *Hum Mol Genet*. 2018;27(23):4051-4060. doi:10.1093/hmg/ddy296
123. Leung KN, Vallero RO, DuBose AJ, Resnick JL, LaSalle JM. Imprinting regulates mammalian snoRNA-encoding chromatin decondensation and neuronal nucleolar size. *Hum Mol Genet*. 2009;18(22):4227-4238. doi:10.1093/hmg/ddp373
124. Le Meur E, Watrin F, Landers M, Sturny R, Lalande M, Muscatelli F. Dynamic developmental regulation of the large non-coding RNA associated with the mouse 7C imprinted chromosomal region. *Dev Biol*. 2005;286(2):587-600. doi:10.1016/j.ydbio.2005.07.030

125. Wevrick R, Francke U. An Imprinted Mouse Transcript Homologous to the Human Imprinted in Prader-Willi Syndrome (IPW) Gene. *Hum Mol Genet*. 1997;6(2):325-332. doi:10.1093/hmg/6.2.325
126. Wevrick R, Kerns JA, Francke U. Identification of a novel paternally expressed gene in the Prader - Willi syndrome region. *Hum Mol Genet*. 1994;3(10):1877-1883. doi:10.1093/hmg/3.10.1877
127. Chen W, Xu D, Ma C, et al. The molecular structure and imprinting status of the IPW (imprinted gene in the Prader-Willi syndrome region) gene in cattle. *Anim Genet*. 2019;50(5):417-422. doi:https://doi.org/10.1111/age.12815
128. Stelzer Y, Sagi I, Yanuka O, Eiges R, Benvenisty N. The noncoding RNA IPW regulates the imprinted DLK1 - DIO3 locus in an induced pluripotent stem cell model of Prader-Willi syndrome. *Nat Genet*. 2014;46(6):551-557. doi:10.1038/ng.2968
129. Langouët M, Gorka D, Orniacki C, et al. Specific ZNF274 binding interference at SNORD116 activates the maternal transcripts in Prader-Willi syndrome neurons. *Hum Mol Genet*. 2020;29(19):3285-3295. doi:10.1093/hmg/ddaa210
130. Langouët M, Glatt-Deeley HR, Chung MS, et al. Zinc finger protein 274 regulates imprinted expression of transcripts in Prader-Willi syndrome neurons. *Hum Mol Genet*. 2018;27(3):505-515. doi:10.1093/hmg/ddx420
131. Skryabin BV, Gubar LV, Seeger B, et al. Deletion of the MBII-85 snoRNA Gene Cluster in Mice Results in Postnatal Growth Retardation. *PLoS Genet*. 2007;3(12). doi:10.1371/journal.pgen.0030235
132. Ding F, Li HH, Zhang S, et al. SnoRNA Snord116 (Pwcr1/MBII-85) Deletion Causes Growth Deficiency and Hyperphagia in Mice. *PLOS ONE*. 2008;3(3):e1709. doi:10.1371/journal.pone.0001709
133. Ding F, Li HH, Li J, Myers RM, Francke U. Neonatal Maternal Deprivation Response and Developmental Changes in Gene Expression Revealed by Hypothalamic Gene Expression Profiling in Mice. *PLoS ONE*. 2010;5(2). doi:10.1371/journal.pone.0009402
134. Lin D, Wang Q, Ran H, et al. Abnormal Response to the Anorexic Effect of GHS-R Inhibitors and Exenatide in Male Snord116 Deletion Mouse Model for Prader-Willi Syndrome. *Endocrinology*. 2014;155(7):2355-2362. doi:10.1210/en.2013-2083
135. Zieba J, Low JK, Purtell L, et al. Behavioural characteristics of the Prader–Willi syndrome related biallelic Snord116 mouse model. *Neuropeptides*. 2015;53:71-77. doi:10.1016/j.npep.2015.06.009
136. Burnett LC, LeDuc CA, Sulsona CR, et al. Deficiency in prohormone convertase PC1 impairs prohormone processing in Prader-Willi syndrome. *J Clin Invest*. 2016;127(1):293-305. doi:10.1172/JCI88648
137. Khor E-C, Fanshawe B, Qi Y, et al. Prader-Willi Critical Region, a Non-Translated, Imprinted Central Regulator of Bone Mass: Possible Role in Skeletal Abnormalities in Prader-Willi Syndrome. *PLoS ONE*. 2016;11(1). doi:10.1371/journal.pone.0148155
138. Lassi G, Maggi S, Balzani E, Cosentini I, Garcia-Garcia C, Tucci V. Working-for-Food Behaviors: A Preclinical Study in Prader-Willi Mutant Mice. *Genetics*. 2016;204(3):1129-1138. doi:10.1534/genetics.116.192286
139. Lassi G, Priano L, Maggi S, et al. Deletion of the Snord116/SNORD116 Alters Sleep in Mice and Patients with Prader-Willi Syndrome. *Sleep*. 2016;39(3):637-644. doi:10.5665/sleep.5542

140. Qi Y, Purtell L, Fu M, et al. Snord116 is critical in the regulation of food intake and body weight. *Sci Rep*. 2016;6. doi:10.1038/srep18614
141. Qi Y, Purtell L, Fu M, et al. Ambient temperature modulates the effects of the Prader-Willi syndrome candidate gene Snord116 on energy homeostasis. *Neuropeptides*. 2017;61:87-93. doi:10.1016/j.npep.2016.10.006
142. Qi Y, Purtell L, Fu M, et al. Hypothalamus specific re-introduction of Snord116 into otherwise Snord116 deficient mice increased energy expenditure. *J Neuroendocrinol*. Published online January 1, 2017:n/a-n/a. doi:10.1111/jne.12457
143. Purtell L, Qi Y, Campbell L, Sainsbury A, Herzog H. Adult-onset deletion of the Prader-Willi syndrome susceptibility gene Snord116 in mice results in reduced feeding and increased fat mass. *Transl Pediatr*. 2017;6(2):88-97-97.
144. Polex-Wolf J, Lam BYH, Larder R, et al. Hypothalamic loss of Snord116 recapitulates the hyperphagia of Prader-Willi syndrome. *J Clin Invest*. 2018;128(3):960-969. doi:10.1172/JCI97007
145. Coulson RL, Yasui DH, Dunaway KW, et al. Snord116-dependent diurnal rhythm of DNA methylation in mouse cortex. *Nat Commun*. 2018;9. doi:10.1038/s41467-018-03676-0
146. Rodriguez JA, Bruggeman EC, Mani BK, et al. Ghrelin Receptor Agonist Rescues Excess Neonatal Mortality in a Prader-Willi Syndrome Mouse Model. *Endocrinology*. 2018;159(12):4006-4022. doi:10.1210/en.2018-00801
147. Adhikari A, Copping NA, Onaga B, et al. Cognitive deficits in the Snord116 deletion mouse model for Prader-Willi syndrome. *Neurobiol Learn Mem*. 2019;165:106874. doi:10.1016/j.nlm.2018.05.011
148. Pace M, Falappa M, Freschi A, et al. Loss of Snord116 impacts lateral hypothalamus, sleep, and food-related behaviors. *JCI Insight*. 2020;5(12). doi:10.1172/jci.insight.137495
149. Polex-Wolf J, Yeo GSH, O'Rahilly S. Impaired prohormone processing: a grand unified theory for features of Prader-Willi syndrome? *J Clin Invest*. 2017;127(1):98-99. doi:10.1172/JCI91307
150. Chen H, Victor AK, Klein J, et al. Loss of MAGEL2 in Prader-Willi syndrome leads to decreased secretory granule and neuropeptide production. *JCI Insight*. 2020;5(17). doi:10.1172/jci.insight.138576
151. Krüger M, Ruschke K, Braun T. NSCL-1 and NSCL-2 synergistically determine the fate of GnRH-1 neurons and control necdin gene expression. *EMBO J*. 2004;23(21):4353-4364. doi:10.1038/sj.emboj.7600431
152. Schmid T, Günther S, Mendler L, Braun T. Loss of NSCL-2 in Gonadotropin Releasing Hormone Neurons Leads to Reduction of Pro-Opiomelanocortin Neurons in Specific Hypothalamic Nuclei and Causes Visceral Obesity. *J Neurosci*. 2013;33(25):10459-10470. doi:10.1523/JNEUROSCI.5287-12.2013
153. Schmid T, Krüger M, Braun T. NSCL-1 and -2 control the formation of precerebellar nuclei by orchestrating the migration of neuronal precursor cells. *J Neurochem*. 2007;102(6):2061-2072. doi:https://doi.org/10.1111/j.1471-4159.2007.04694.x
154. Suzuki Y, Tsuruga E, Yajima T, Takeda M. Expression of bHLH Transcription Factors NSCL1 and NSCL2 in the Mouse Olfactory System. *Chem Senses*. 2003;28(7):603-608. doi:10.1093/chemse/bjg051
155. Coyle CA, Jing E, Hosmer T, Powers JB, Wade G, Good DJ. Reduced voluntary activity precedes adult-onset obesity in Nhlh2 knockout mice. *Physiol Behav*. 2002;77(2):387-402. doi:10.1016/S0031-9384(02)00885-5

156. Vella KR, Burnside AS, Brennan KM, Good DJ. Expression of the Hypothalamic Transcription Factor Nhlh2 is Dependent on Energy Availability. *J Neuroendocrinol*. 2007;19(7):499-510. doi:10.1111/j.1365-2826.2007.01556.x
157. Good DJ, Porter FD, Mahon KA, Parlow AF, Westphal H, Kirsch IR. Hypogonadism and obesity in mice with a targeted deletion of the Nhlh2 gene. *Nat Genet*. 1997;15(4):397-401. doi:10.1038/ng0497-397
158. Johnson SA, Marín-Bivens CL, Miele M, Coyle CA, Fissore R, Good DJ. The Nhlh2 transcription factor is required for female sexual behavior and reproductive longevity. *Horm Behav*. 2004;46(4):420-427. doi:10.1016/j.yhbeh.2004.03.006
159. Ruschke K, Ebelt H, Klöting N, et al. Defective Peripheral Nerve Development Is Linked to Abnormal Architecture and Metabolic Activity of Adipose Tissue in Nscl-2 Mutant Mice. *PLoS ONE*. 2009;4(5). doi:10.1371/journal.pone.0005516
160. Aoyama M, Ozaki T, Inuzuka H, et al. LMO3 Interacts with Neuronal Transcription Factor, HEN2, and Acts as an Oncogene in Neuroblastoma. *Cancer Res*. 2005;65(11):4587-4597. doi:10.1158/0008-5472.CAN-04-4630
161. Giwa A, Fatai A, Gamieldien J, Christoffels A, Bendou H. Identification of novel prognostic markers of survival time in high-risk neuroblastoma using gene expression profiles. *Oncotarget*. 2020;11(46):4293-4305. doi:10.18632/oncotarget.27808
162. Brown L, Espinosa R, Le Beau MM, Siciliano MJ, Baer R. HEN1 and HEN2: a subgroup of basic helix-loop-helix genes that are coexpressed in a human neuroblastoma. *Proc Natl Acad Sci U S A*. 1992;89(18):8492-8496.
163. Isogai E, Ohira M, Ozaki T, Oba S, Nakamura Y, Nakagawara A. Oncogenic LMO3 Collaborates with HEN2 to Enhance Neuroblastoma Cell Growth through Transactivation of Mash1. *PLoS ONE*. 2011;6(5). doi:10.1371/journal.pone.0019297
164. Mickelsen LE, Flynn WF, Springer K, et al. Cellular taxonomy and spatial organization of the murine ventral posterior hypothalamus. *eLife*. 2020;9. doi:10.7554/eLife.58901
165. Jing E, Nillni EA, Sanchez VC, Stuart RC, Good DJ. Deletion of the Nhlh2 Transcription Factor Decreases the Levels of the Anorexigenic Peptides α Melanocyte-Stimulating Hormone and Thyrotropin-Releasing Hormone and Implicates Prohormone Convertases I and II in Obesity. *Endocrinology*. 2004;145(4):1503-1513. doi:10.1210/en.2003-0834
166. Moore AM, Coolen LM, Porter DT, Goodman RL, Lehman MN. KNDy Cells Revisited. *Endocrinology*. 2018;159(9):3219-3234. doi:10.1210/en.2018-00389
167. Ortiga-Carvalho TM, Chiamolera MI, Pazos-Moura CC, Wondisford FE. Hypothalamus-Pituitary-Thyroid Axis. In: *Comprehensive Physiology*. American Cancer Society; 2016:1387-1428. doi:10.1002/cphy.c150027
168. Harno E, Gali Ramamoorthy T, Coll AP, White A. POMC: The Physiological Power of Hormone Processing. *Physiol Rev*. 2018;98(4):2381-2430. doi:10.1152/physrev.00024.2017
169. Farooqi IS. Monogenic human obesity syndromes. In: Kalsbeek A, Fliers E, Hofman MA, Swaab DF, van Someren EJW, Buijs RM, eds. *Progress in Brain Research*. Vol 153. Hypothalamic Integration of Energy Metabolism. Elsevier; 2006:119-125. doi:10.1016/S0079-6123(06)53006-7
170. Harris M, Aschkenasi C, Elias CF, et al. Transcriptional regulation of the thyrotropin-releasing hormone gene by leptin and melanocortin signaling. *J Clin Invest*. 2001;107(1):111-120.

171. Wankhade UD, Good DJ. Melanocortin 4 Receptor is a Transcriptional Target of Nescient Helix-Loop-Helix-2. *Mol Cell Endocrinol*. 2011;341(1-2):39-47. doi:10.1016/j.mce.2011.05.022
172. Libert S, Pointer K, Bell EL, et al. SIRT1 Activates MAO-A in the Brain to Mediate Anxiety and Exploratory Drive. *Cell*. 2011;147(7):1459-1472. doi:10.1016/j.cell.2011.10.054
173. Li W, Guo B, Tao K, et al. Inhibition of SIRT1 in hippocampal CA1 ameliorates PTSD-like behaviors in mice by protections of neuronal plasticity and serotonin homeostasis via NHLH2/MAO-A pathway. *Biochem Biophys Res Commun*. 2019;518(2):344-350. doi:10.1016/j.bbrc.2019.08.060
174. Fox DL, Good DJ. Nescient Helix-Loop-Helix 2 Interacts with Signal Transducer and Activator of Transcription 3 to Regulate Transcription of Prohormone Convertase 1/3. *Mol Endocrinol*. 2008;22(6):1438-1448. doi:10.1210/me.2008-0010
175. Lee S, Walker CL, Karten B, et al. Essential role for the Prader–Willi syndrome protein necdin in axonal outgrowth. *Hum Mol Genet*. 2005;14(5):627-637. doi:10.1093/hmg/ddi059
176. Miller NLG, Wevrick R, Mellon PL. Necdin, a Prader–Willi syndrome candidate gene, regulates gonadotropin-releasing hormone neurons during development. *Hum Mol Genet*. 2009;18(2):248-260. doi:10.1093/hmg/ddn344
177. Wijesuriya TM, De Ceuninck L, Masschaele D, et al. The Prader-Willi syndrome proteins MAGEL2 and necdin regulate leptin receptor cell surface abundance through ubiquitination pathways. *Hum Mol Genet*. 2017;26(21):4215-4230. doi:10.1093/hmg/ddx311
178. Park NI, Guilhamon P, Desai K, et al. ASCL1 Reorganizes Chromatin to Direct Neuronal Fate and Suppress Tumorigenicity of Glioblastoma Stem Cells. *Cell Stem Cell*. 2017;21(2):209-224.e7. doi:10.1016/j.stem.2017.06.004
179. Itoh F, Nakane T, Chiba S. Gene expression of MASH-1, MATH-1, neuroD and NSCL-2, basic helix-loop-helix proteins, during neural differentiation in P19 embryonal carcinoma cells. *Tohoku J Exp Med*. 1997;182(4):327-336. doi:10.1620/tjem.182.327
180. McNay DEG, Pelling M, Claxton S, Guillemot F, Ang S-L. Mash1 Is Required for Generic and Subtype Differentiation of Hypothalamic Neuroendocrine Cells. *Mol Endocrinol*. 2006;20(7):1623-1632. doi:10.1210/me.2005-0518
181. Pelling M, Anthwal N, McNay D, et al. Differential requirements for neurogenin 3 in the development of POMC and NPY neurons in the hypothalamus. *Dev Biol*. 2011;349(2):406-416. doi:10.1016/j.ydbio.2010.11.007
182. Perez SE. Neurogenins promote sensory neurogenesis. Published online March 17, 1999:14.
183. Mattar P, Langevin LM, Markham K, et al. Basic Helix-Loop-Helix Transcription Factors Cooperate To Specify a Cortical Projection Neuron Identity. *Mol Cell Biol*. 2008;28(5):1456-1469. doi:10.1128/MCB.01510-07
184. Kannan K, Amariglio N, Rechavi G, et al. DNA microarrays identification of primary and secondary target genes regulated by p53. *Oncogene*. 2001;20(18):2225-2234. doi:10.1038/sj.onc.1204319
185. Watanabe S, Arai K. Roles of the JAK-STAT system in signal transduction via cytokine receptors. *Curr Opin Genet Dev*. 1996;6(5):587-596. doi:10.1016/S0959-437X(96)80088-8
186. Ladyman SR, Grattan DR. JAK-STAT and feeding. *JAK-STAT*. 2013;2(2). doi:10.4161/jkst.23675

187. Rayyan NA, Zhang J, Burnside AS, Good DJ. Leptin Signaling Regulates Hypothalamic Expression of Nescient helix-loop-helix 2 (Nhlh2) Through Signal Transducer and Activator 3 (Stat3). *Mol Cell Endocrinol*. 2014;384(0):134-142. doi:10.1016/j.mce.2014.01.017
188. Yugami M, Kabe Y, Yamaguchi Y, Wada T, Handa H. hnRNP-U enhances the expression of specific genes by stabilizing mRNA. *FEBS Lett*. 2007;581(1):1-7. doi:https://doi.org/10.1016/j.febslet.2006.11.062
189. AL_Rayyan N, Wankhade U, Bush K, Good DJ. Two Single Nucleotide Polymorphisms in the Human Nescient Helix Loop Helix 2 (NHLH2) Gene Reduce mRNA Stability and DNA Binding. *Gene*. 2013;512(1):134-142. doi:10.1016/j.gene.2012.09.068
190. Yu G, Zhao Y, Li H. The multistructural forms of box C/D ribonucleoprotein particles. *RNA*. 2018;24(12):1625-1633. doi:10.1261/rna.068312.118

Chapter 3. Phylogenetic analysis of the *SNORD116* locus

Matthew A. Kocher and Deborah J. Good

Genes 2017, doi:10.3390/genes8120358

Reproduced with permission from Multidisciplinary Digital Publishing Institute – (MDPI)

3.1 Abstract

Abstract: The *SNORD116* small nucleolar RNA locus (*SNORD116@*) is contained within the long noncoding RNA host gene *SNHG14* on human chromosome 15q11-q13. The *SNORD116* locus is a cluster of 28 or more small nucleolar (sno) RNAs; C/D box (SNORDs). Individual RNAs within the cluster are tandem, highly similar sequences, referred to as *SNORD116-1*, *SNORD116-2*, etc., with the entire set referred to as *SNORD116@*. There are also related *SNORD116* loci on other chromosomes, and these additional loci are conserved among primates. Inherited chromosomal 15q11-q13 deletions, encompassing the *SNORD116@* locus, are causative for the paternally-inherited/maternally-imprinted genetic condition, Prader–Willi syndrome (PWS). Using in silico tools, along with molecular-based and sequenced-based confirmation, phylogenetic analysis of the *SNORD116@* locus was performed. The consensus sequence for the *SNORD116@* snoRNAs from various species was determined both for all the *SNORD116* snoRNAs, as well as those grouped using sequence and location according to a human grouping convention. The implications of these findings are put in perspective for studying *SNORD116* in patients with inherited Prader–Willi syndrome, as well as model organisms.

3.2 Introduction

While we have known about the RNA molecule for over 100 years [1], RNA was originally thought to take just three major forms: transfer RNA, ribosomal RNA and the messenger RNA that codes for protein [2]. As our genomes were further dissected and more sophisticated technologies for sequencing and quantifying small RNAs were developed, both long and small families of non-coding RNA were discovered. In fact, mRNA makes up only 1–2% of the total expressed RNA, with the rest of the transcribed RNA remaining untranslated

[3–5]. One of these families of non-transcribed RNAs is the small nucleolar RNA family, or snoRNAs. This family of short, 60–170-nt RNAs includes two major groups, the C/D box snoRNAs and H/ACA snoRNAs, as well as subfamilies of each, which are so named by the motifs they contain (C/D or H/ACA boxes) [6]. These motifs specify RNA secondary structure, and interaction with both other RNAs and RNA-binding proteins [6]

The fact that humans and many other animals transcribe these snoRNA only leads to more questions, as many of the targets for these snoRNAs are not known; and in many cases, it is not clear what the very function of each is [6]. In this short communication, which focuses on the C/D box snoRNA group *SNORD116@*, the question of whether conservation of sequence between species can be used to identify regions that are key for the regulatory and functional properties of a snoRNA group such as *SNORD116@* will be investigated. The human *SNORD116@* locus (previously known as *HBII-85*) encodes up to 30 snoRNAs that belong to the C/D box family of snoRNAs [7]. In several publications, the human *SNORD116@* locus snoRNAs have been grouped by location on the chromosome into three groups, with Group I consisting of *SNORD116-1–SNORD116-9*, Group II of *SNORD116-10–SNORD116-23* and Group III of *SNORD116-24–SNORD116-27* [8]. Later studies included *SNORD116-28* and *SNORD116-29* snoRNAs in the human locus within Group III [9]. No known RNA targets have been identified for *SNORD116@*, although the related and adjacent *SNORD115@* locus RNAs share an 18-nucleotide sequence complementarity to the serotonin receptor 2C pre-mRNA and appear to mediate differential splicing by promoting the inclusion of an alternative exon when *SNORD115* is present [10]. Both *SNORD116@* and *SNORD115@* are deleted in the genetically-inherited syndrome Prader–Willi syndrome (PWS; Online Mendelian Inheritance in Man (OMIM) #176270), https://www.omim.org/ [7]. However, the smallest known deletions that still cause clinical PWS contain or overlap with *SNORD116* [11], suggesting that deletion of the *SNORD116@* locus plays a direct causative role in PWS.

PWS results from a 15q11-q13 deletion in an imprinted region that is normally active only from the paternal allele. Thus, deletion of the paternally-inherited allele causes PWS, while deletion of a maternally-inherited allele has no known effect, as the maternally-inherited allele is not expressed [11]. Individuals with PWS display developmental delay and hypogonadism, accompanied by intellectual disabilities [12]. With an occurrence rate of one in 15,000–25,000 individuals, PWS is considered to be the leading cause of life-threatening

childhood, genetically-inherited obesity [12]. The central 485-kb PWS region contains the *SNURF-SNRPN* region, which is most frequently deleted in PWS [13]. This region contains at least 148 expressed exons, including *SNORD116@* and *SNORD115@* loci. Fine analysis of the deleted regions of many clinically-diagnosed patients revealed one family with Angelman syndrome (due to maternal deletion on 15q), whose deletion extended to *SNORD115@*, but who did not show PWS phenotypes [14]. Three separate patients have been diagnosed with PWS caused by different, overlapping microdeletions in 15q, which all encompass the *SNORD116@* locus. However, these patients do not show some of the facial and hand features typical of PWS, but do show macrocephaly and tall stature, phenotypes not in typical PWS presentation. A single patient with a 118-kb microdeletion, which only includes *IPW*, *SNORD109A* and *SNORD116@*, plus a small amount of intergenic region on either side of that cluster, has all of the clinical features of PWS [15]. Importantly, paternally-deleted *Snord116*$^{p-/m+}$ mice re-capitulate many, although not all, of the clinical phenotypes seen in human PWS; namely, they fail to develop obesity [16,17].

Using pluripotent stem cell-induced neurons from the microdeletion patients, along with the *Snord116*$^{p-/m+}$ mouse model, Burnett and colleagues were able to show that the *Nhlh2/NHLH2* gene is significantly downregulated in PWS [18]. Mice with a deletion of *Nhlh2* show adult-onset obesity [19], suggesting that the obese phenotype of PWS patients may involve *SNORD116*-mediated regulation of *NHLH2*. Considering the human clinical cases and the mouse *Snord116*$^{p-/m+}$ knockout model together, a strong case can be made that deletion of *SNORD116@* is the most plausible mechanism for the development of the main clinical phenotypes of PWS. Thus, it is imperative that we start to understand what the *SNORD116* snoRNAs do and to identify any RNA or protein targets that interact with them. In addition, large deletions within the PWS locus, such as those encompassing the *MAGEL*, *SNORD115@* and *NDN* loci, complicate the genotype-phenotype relationship as these losses likely extend the phenotypic landscape of the condition, compared to patients with the smaller or microdeletion patients.

In this study, *SNORD116@* sequences from humans and other species were compared phylogenetically, at the level of nucleotide sequence to identify conserved regions. The regions of the *SNORD116* snoRNA with the greatest potential for target-specific interactions are discussed, as well as how function may vary between primate and rodent species.

3.3 Results and Discussion

A number of papers and reviews have compared the mouse *Snord116@* sequences and genomic locus on murine chromosome 7, to the human *SNORD116@* locus on human chromosome 15 (for a recent review, see [7]). While the overall structure and gene organization is similar between these two species and mouse deletion models of *Snord116* replicate many, but not all of the phenotypes of PWS [16,17], there are differences between the copy numbers for the human and mouse *SNORD116@* locus (Table 1). In addition, there are differences in the variability of the sequences between mice and humans. Using the Ensembl browser [20], there are 70 paralogs within the murine *Snord116* family, and these are organized into two clusters, separated by approximately 50 kb (Table 1), not to be confused with the *Snord115* cluster, which is separated further still. The total size of the *Snord116* cluster on mouse chromosome 7 is 179,261 base pairs. In addition, of the 17 annotated *Snord116* snoRNAs, most are nearly identical in sequence. Compare this to the 30 human *SNORD116* annotated snoRNAs; while close in sequence, they are not nearly identical like mice. Rather, human *SNORD116* snoRNAs can be divided by sequence into three paralogous groups [8,9]. In considering the structure of the human and mouse locus and comparing this to other species (Table 1), it appears that the murine locus had a duplication event at some point after divergence between Rodentia (mouse and rat) and Lagomorpha (rabbit). The *Snord116* locus is similarly large in rat, although fewer *Snord116* snoRNAs have been discovered in rat, compared to mice. Additionally, no orthologues of the *SNORD116* gene were found outside of the class Mammalia [16]

Table 1. SNORD116 snoRNA clusters in different species.

Common Name *Genus species*	Chromosome	Synteny with Human Chromosome 15	Cluster Size (bp)	Strand	Number of Transcripts (with Perfectly Homologous C/C′ and D/D′ Boxes)	Number of Annotated Transcripts
Human *Homo sapiens*	15	-	56,781	Forward	30 (24)	30
Chimpanzee *Pan troglodytes*	15	yes	66,103	Forward	28 (22)	0
Rhesus macaque *Macaca mulatta*	7	yes	61,342 *	Forward	29 (26)	29
Rabbit *Oryctolagus cuniculus*	17	yes	72,915	Reverse	29 (22)	0
Rat *Rattus norvegicus*	1	yes	163,162 @	Reverse	26 (15)	26
Mouse *Mus musculus*	7	yes	45,634 (Cluster 1) 133,627 (Cluster 2) ^	Reverse	71 (64)	17

* Missing one ~6.5 kb contig within the cluster; @ missing six contigs, totaling ~50 kb within the region; ^ missing one ~50 kb contig between clusters.

In addition to the *SNORD116* clusters found on chromosomes syngeneic to human chromosome 15 (Table 1), primates have paralogs on other chromosomes (Table 2). These paralogs are singly located paralogs to *SNORD116*, identified by BLAST analysis, but not found within the human chromosome 15 cluster (or syngeneic primate clusters). Most of these only possess partial C/C' and D/D' motifs, showing slight variance in nucleotides within a given motif. The importance of these other *SNORD116* paralogs is not currently known, and due to the lack of complete C/C' and D/D' box motifs, it is questionable whether these genes are expressed and processed to form a mature snoRNA-protein complex (snoRNP), as the C/D motifs are required to escape degradation [21]. They were not included in further consensus analyses.

Table 2. Non-cluster paralogs to *SNORD116.*

Human Chromosome Number (Accession Number)	Location in Humans	Presence of Homologous C/C′ and D/D′ Boxes to *SNORD116*	Chimpanzee Chromosome (synteny)/Location/ Homologous C/D Boxes?	Rhesus Macaque Chromosome (synteny)/Location/Homologous C/D Boxes?
1(ENST00000365628.1)	Intronic	No	3 (no)/intergenic/yes	1 (yes)/intronic/no
9(ENST00000517176.1)	Intronic	No	9 (yes)/intronic/no	15 (yes)/intronic/no
13(ENST00000391251.1)	Intergenic	No	N/A (scaffold) (yes)/intergenic/no	17 (yes)/intergenic/no

In order to begin to understand the relatedness and relationships between both paralogs and orthologs within the SNORD116 locus, a consensus sequence for each species *SNORD116* cluster was generated (Figure 1). To do this, the sequences of each of the *SNORD116* transcripts within the species cluster were compared. A consensus sequence was generated by using a threshold frequency for single nucleotide inclusion in the consensus of 90% of the *SNORD116* snoRNAs. Nucleotides that did not meet the 90% threshold were indicated using IUPAC ambiguity codes. As shown, the location and sequence of the C/C' and D/D' boxes are conserved across species, with the exception of the C' box in rat and the D box in rat and rabbit (Figure 1), which calls into question whether the transcripts that lack a complete C/C' or D/D' box are processed and expressed. In doing this comparison, 53 out of 98 (54%) nucleotides are conserved cross-species (when allowing non-perfect matches to ambiguous nucleotides; i.e., T is acceptable homology under a W site). Forty-nine out 98 (50%) nucleotides are conserved when using strict homology that only allows perfect matches; i.e., T is not an acceptable homology under a W site. The highest homology appears to include the region from 5' of the D' box through the C' box, confirming our hypothesis that this analysis would yield homologous domains outside of the C/C' and D/D' domains.

When comparing consensus sequences for groups, it is important to note the difference in grouping method for rat *Snord116* sequences. Because it differs from the primate and rabbit grouping method, it may not show the best fit with the rest of the Group I consensus sequences. For this reason, to explore which groups showed the most homology to the human groups, consensus sequences of various groups and animals were compared to the human consensus sequences of Groups I, II and III (Table 3). In fact, rat's Group I appears to fit slightly better with human's Group II, but only when using non-strict homology. Additionally, the mouse 116@ consensus sequence does not appear to cluster strongly within a human group consensus. Depending on either non-strict or strict homology rules, the mouse 116@ consensus sequence shows greater homology with either human Group II or Group I, respectively. This effect may be due in part to the higher number of ambiguous nucleotides found in human Group II (16) vs. Group I (8), combined with the lack of any ambiguous nucleotides in the mouse 116@ consensus sequence. This analysis is therefore inconclusive in the grouping of mouse Snord116 sequences into either human Group I or II, but indicates an exclusion from human Group III.

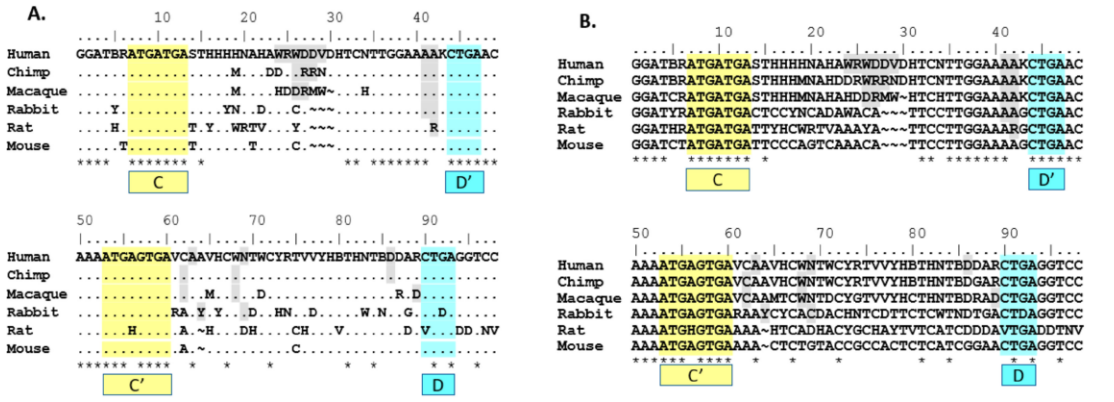

Figure 1. Comparison of genomic sequences of the *SNORD116* locus from model organisms used for most biological research. Sequences from human (*Homo sapiens*), chimpanzee (*Pan troglodytes*), rhesus (*Macaca mulatta*), rabbit (*Oryctolagus cuniculus*), rat (*Rattus norvegicus*) and mouse (*Mus musculus*) were analyzed and the composite sequence shown. Nucleotides AGCT shown are present in 90% or greater of the transcripts at that position, while IUPAC codes are used for positions with one or more variable nucleotides. (**A**) Alignment of *SNORD116@* consensus sequences displaying sites of non-strict homology. A dot (.) indicates non-strict homology with the human sequence for the given nucleotide position. (**B**) Alignment showing all nucleotides of consensus sequences used in (**A**). Sequences used for the analysis were obtained from Ensembl builds. The build and the number of SNORD116 sequences analyzed are shown after the common name of the organism: human (n = 30, GRCh38.p10), chimp (n = 28, CHIMP2.1.4), rhesus (n = 29, Mmul_8.0.1), rabbit (n = 29, OryCun_2.0), rat (n = 26, Rnor_6.0) and mouse (n = 17, GRCm38.p5). The C and C′ boxes are highlighted in yellow, while the D and D′ boxes are highlighted in blue. Nucleotides that do not meet the 90% frequency threshold are indicated using IUPAC ambiguity codes. Grey-shading indicates regions of insertion/deletion in some sites of the group. Frequency for qualifying as in/del site is 10% or greater. A dot (.) indicates non-strict homology with the human sequence for the given nucleotide position. A tilde (~) indicates a gap in consensus sequence compared to the aligned consensus sequence. An asterisk (*) indicates perfect homology with the human sequence for all nucleotides in the site above.

Table 3. Homology comparison of consensus sequences for *SNORD116* groupings between human and rat, rabbit and mouse. The number of homologous nucleotide sites is displayed.

	Non-Strict Homology			Strict Homology		
	Human Group I 96 Nucleotides	**Human Group II 92 Nucleotides**	**Human Group III 96 Nucleotides**	**Human Group I 96 Nucleotides**	**Human Group II 92 Nucleotides**	**Human Group III 96 Nucleotides**
Rat 116@	64 (66.7%)	65 (70.7%)	52 (54.2%)	59 (61.5%)	57 (62.0%)	30 (31.3%)
Rat Group I	76 (79.2%)	79 (85.9%)	65 (67.7%)	69 (71.9%)	66 (71.7%)	48 (50.0%)
Rat Group II	64 (66.7%)	60 (65.2%)	53 (55.2%)	59 (61.5%)	55 (59.8%)	40 (41.7%)
Rabbit 116@	73 (76.0%)	69 (75.0%)	58 (60.4%)	68 (70.8%)	60 (65.2%)	45 (46.9%)
Rabbit Group I	86 (89.6%)	78 (84.8%)	64 (66.7%)	78 (81.3%)	64 (69.6%)	47 (49.0%)
Rabbit Group II	57 (59.4%)	59 (64.1%)	48 (50.0%)	54 (56.3%)	53 (57.6%)	41 (42.7%)
Mouse 116@	81 (84.4%)	81 (88.0%)	64 (66.7%)	75 (78.1%)	66 (71.7%)	47 (49.0%)

Patterns of homology observed in Table 3 informed alignments of between-species group consensus sequences in Figure 2. Due to different methods for defining and clustering rat groups, both rat Group I and Group II consensus sequences were excluded from group alignments in Figure 2. Rabbit Group I was included in the Group I between-species consensus sequence alignment due to the same grouping method used in primates and human, as well as the consistent fit with the human Group I consensus sequence as shown in Table 3. Rabbit Group II was excluded from the Group II alignment due to a lack of strong preferential fit to human Group II.

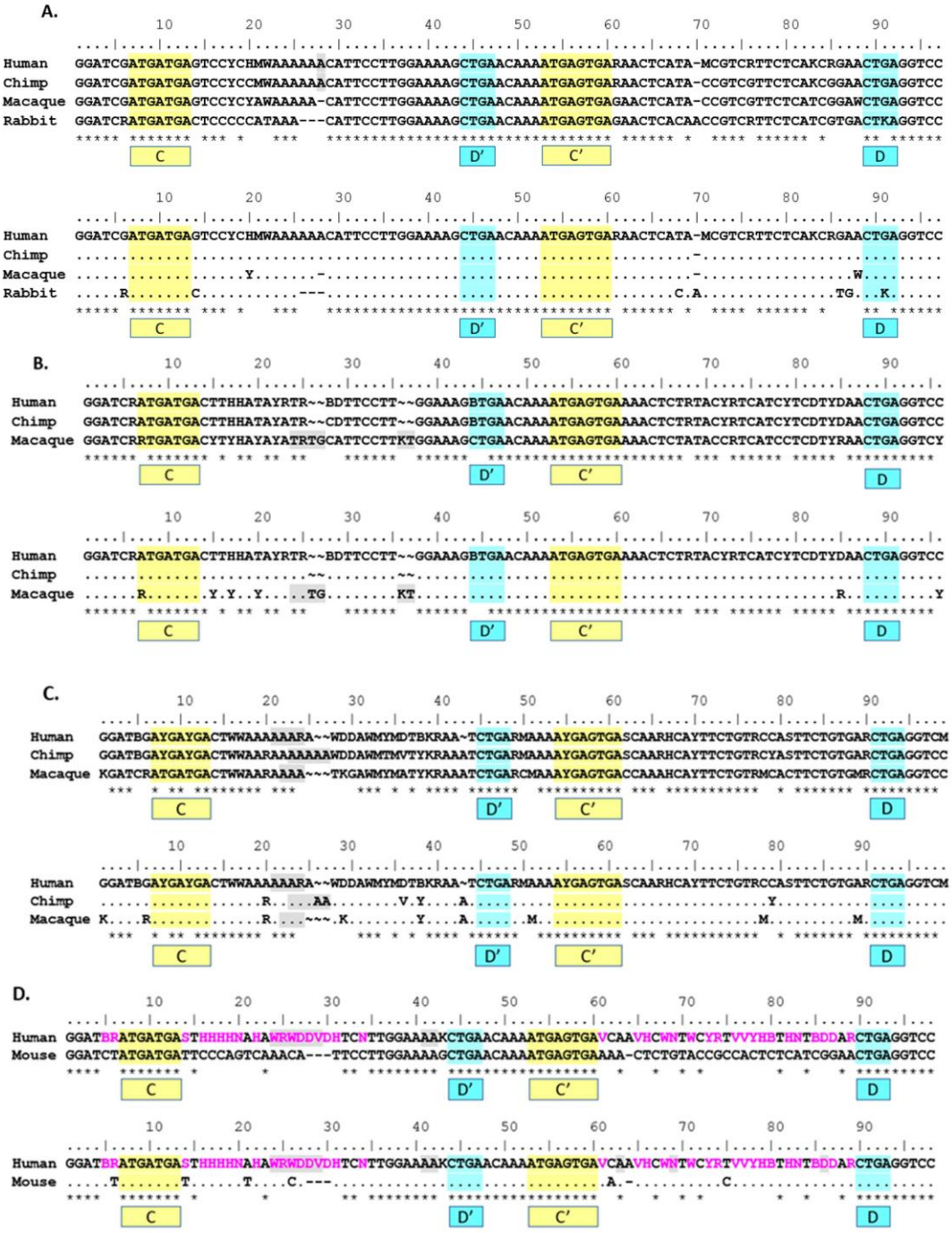

Figure 2. Consensus sequences for respective SNORD116@ transcript clusters (groups). Threshold frequency for single nucleotide inclusion in the consensus is 90%. Nucleotides that do not meet or exceed the 90% frequency threshold are indicated using IUPAC ambiguity codes. In/del sites are highlighted in light gray. Frequency for qualifying as in/del site is 10% or greater. C/C′ boxes highlighted in yellow. D/D′ boxes highlighted in light blue. A dot (.) indicates non-strict homology with human sequence for the given nucleotide position. A tilde (~) indicates a gap in consensus sequence compared to other consensus sequences. An asterisk (*) indicates perfect homology with the human sequence for all nucleotides in the site above. (**A**) Group I consensus analysis; (**B**) Group II consensus analysis; (**C**) Group 3 consensus analysis; (**D**) Mouse-human consensus analysis. For this analysis, nucleotides using IAPUC codes are pink.

The use of phylogenetic sequence analysis on *SNORD116* family members allows for an expansion of the homologous regions from just the C/C' and D/D' boxes to sequences outside of those regions, especially within the 5' sequences of the transcripts and the region spanning D' and C'. This finding was conserved using the human groupings for groups I, II and III (Figure 2A–C). Based on the proposed structure of a C/D box snoRNA, it is the region 5' of the D/D' box that may interact with target RNA and/or RNA binding proteins [7]. This predicted functional region is consistent with the expected variability in *SNORD116* transcripts, as this is the antisense region that hybridizes to putative RNA targets for modification. Such variation observed would allow a wide range of putative targets if structural function is not compromised.

The direct comparison between mouse and human 116@ consensus sequences shows homology in the C/C' and D/D' boxes, as well as the 5' and 3' ends that form the stem structure in a functional SNORD. Additionally, nearly all the sequence is homologous in the non-strict sense, yet due to the high variation in human sequences, the antisense region 5' of the D' box shows a low strict homology indicated by the asterisks (*) in Figure 2D. Mouse 116@ is certainly very homologous when compared to human 116@, as mouse possesses no ambiguous nucleotides in the consensus sequence, whereas human possesses 37 ambiguous sites. As Groups II and III are largely responsible for this variance, this finding could partially explain why the expression of Groups II and III is relatively low [9]. For the region 5' of the D' box (nucleotides 32–42), there is highly strict homology, and contrastingly, the region 5' of the D box (75–89) shows very low strict homology. This could be interpreted in multiple ways. Implications include that the region near the D' box could play a large structural role, perhaps contributing to the stability of the individual snoRNAs or that this region may be important for the shared phenotypes seen in *Snord116* deletion mice and PWS patients.

It is important to note that the consensus sequences are created from a multiple sequence alignment. The specific alignment used will influence the resulting consensus sequences. Although we are confident that our alignments are good fits, alternative alignment methods may lead to different results. Slight variation is possible in highly variant regions, where alignments do not fit as smoothly, and the parameters used for allowing gaps is one aspect that can influence this. With different alignment methods, the majority of our results would be consistent, but the details could change, such as the sites that use IUPAC ambiguity codes in the 116@ consensus alignments. Our finding that this region is highly variant would

still hold true. The results from the grouped alignments are less prone to variance, as their alignments have better fits. We have included alignments of individual *SNORD116* sequences used in the Supplementary Data.

Finally, it is important to further note the proposed mechanisms for the expression of the *SNORD116@* locus in the context of this analysis. The classical SNORD mechanism is a release from introns following an RNA splicing event in which the escape from degradation, processing and maturation of the SNORD is carried out by key RNA binding proteins to form a functional snoRNP complex. This mechanism is likely to be conserved, as it is necessary for expression, yet some SNORDs have shown differential dependence on RNA binding proteins [22]. Additionally, further proposed mechanisms of *SNORD116@* include the product of processed RNAs derived from snoRNA degradation that may or may not regulate downstream targets [23]. Jorjani and colleagues showed that an overwhelming majority of RNA seq reads from *SNORD116* Group I were processed sequence reads (<40 nt) rather than long form sequences across multiple cell types. Reads from other groups were comparatively less processed [6]. Although there is a lack of evidence indicating the use of the micro-RNA machinery, it remains a possibility that these small SNORD-derived RNAs are functional [24]. Furthermore, there is a possibility that the *SNORD116* locus may express long non-coding RNAs (lncRNAs) with snoRNA ends as “caps” [25,26]. These rely on the snoRNP processing mechanism to escape degradation, but the functional unit does not rely on the *SNORD116* sequence itself as the canonical SNORD mechanism does. Rather, the region outside the SNORD carries out the proposed function of binding splicing factors and affecting alternative splicing. This possibility would weaken the relevance of the current analysis. Though there are many proposed mechanisms regarding *SNORD116*, these may not be mutually exclusive, but rather provide many layers of functionality. Importantly, experiments have been performed using various cell types, and there are likely to be unique tissue-specific patterns. Future studies will need to address these caveats.

3.4 Conclusions

Phylogenetic analysis of the *SNORD116* cluster on human chromosome 15q has identified nucleotides that are conserved cross-species. It is hoped that this type of analysis for

SNORD116@, as well as other snoRNAs could help to identify functional domains, as well as regions that are susceptible to genetically-inherited phenotypes. In particular, the region from 5' of the D' box through the C' box is highly homologous between species. Perhaps comparison between well-characterized SNORDs and orphan SNORDs may provide insight into the mechanisms of other orphan SNORDs and help to target regions for future bench research. Additionally, prior studies have lacked specificity in sensing members of *SNORD116* transcripts; often using methods that are sensitive to all the transcripts or a representative transcript. The degree of nucleotide variation between and within mouse and human sequences may inform new methods for detecting and analyzing the expression of individual transcripts for this complex locus.

It is hoped that these studies will lead to a better understanding of the genetic imprinting condition, PWS. While the single PWS patient who carries the smallest known microdeletion encompassing all of the *SNORD116@*, *IPW* and *SNORD109A* locus is informative of the minimal causative genotype, additional studies on *SNORD109A* and *IPW* are warranted. Furthermore, some additional small processed RNA species, which appear to be derived from the *SNORD116@* locus, have been detected, but contain only partial sequences, as compared to the full *SNORD116@* sequences [23]. Little is known about the biological relevance of these, but they do warrant further investigation.

One of the reasons for undertaking this work was to attempt to use phylogenetic comparisons to determine where there may be functional and non-functional domains, as well as whether the *SNORD116*$^{m+/p-}$ mouse model could be justified as a functional model of the human *SNORD1116@* deletion. We believe our results suggest that the *SNORD116*$^{m+/p-}$ mouse can be used as a simplified version of a human Group I or Group II *SNORD116* deletion, with the caveat that the overlapping phenotypes of PWS with the *SNORD116*$^{m+/p-}$ mouse may be due to the loss of *SNORD116* Groups I and II, and that the other RNAs, namely Group III, may account for the non-overlapping phenotypes. This hypothesis remains to be proven. It remains to be determined to which human *SNORD116* groups the mouse *Snord116* correlates functionally rather than by sequence homology. As we move from this phylogenetic analysis of *SNORD116@* to future studies, characterization of the differential expression and gene regulatory targets of *SNORD116@* across various species and tissue types, especially

those tissues—namely brain, pancreas and muscle—that are affected in PWS patients will hopefully provide possible drug and genetic targets for basic scientists to direct therapies.

Supplementary Materials: The following are available online at www.mdpi.com/2073-4425/8/12/358/s1. Supplemental Figures S1–S6, as well as supplemental Tables S1 and S2.

Acknowledgments: This work was supported by the Foundation for Prader-Willi Research, Walnut, CA. Publication costs were supported by Virginia Tech Libraries Open Access Subvention Fund.

Author Contributions: Matthew A. Kocher and Deborah J. Good both conceived of, designed and performed the experiments, the analysis of the data and the writing of the manuscript.

Conflicts of Interest: The authors declare no conflict of interest. The founding sponsors had no role in the design of the study; in the collection, analyses or interpretation of data; in the writing of the manuscript; nor in the decision to publish the results.

3.5 Methods

Data Acquisition

Sequences were obtained from Ensembl Release 90, using genome assemblies GRCh38.p10 (human), CHIMP2.1.4 (chimpanzee), Mmul_8.0.1 (rhesus macaque), OryCun_2.0 (rabbit), Rnor_6.0 (rat) and GRCm38.p5 (mouse). The tracks used for analysis were: genes (Ensembl) (every species except human and mouse), GENCODE 27 (human tracks) and GENCODE M15 (mouse tracks). The GENCODE project (https://www.gencodegenes.org/) provides reference sequence information for both human and mouse genomes, and merges both Havana manual gene annotation and the Ensembl automated gene annotation. The numbers indicate the version used in this study.

Sequence Analysis

Sequences were aligned using Clustal Omega multiple sequence alignment (https://www.ebi. ac.uk/Tools/msa/clustalo, EMBL-EBI, Wellcome Genome Campus, Hinxton, Cambridgeshire, CB10 1SD, UK/), MAFFT, multiple alignment program for amino acid or nucleotide sequences, Version 7 (https://mafft.cbrc.jp/alignment/server/, Computation Biology Research Consortium, Tokyo, Japan), and BioEdit biological sequence alignment editor, Version 7.2.6.1 (http://www.mbio.ncsu.edu/bioedit/ bioedit.html, Ibis Therapeutics, Carlsbad, CA, USA). Consensus sequences were created in BioEdit using a threshold frequency of inclusion in the consensus of 90%. Sites that did not meet the threshold were notated using IUPAC ambiguity codes. Sequences are displayed as DNA rather than RNA, indicating T's in place of U's for all analyses.

Sequence Subgrouping

Human SNORD116@ followed a previous grouping method [8,9] consisting of Groups I, II and III. Additionally, Group I within chimp, rhesus and rabbit was defined as transcripts with 95% homology to the 1st *SNORD116* transcript downstream of the *SNURF/SNRPN* site. Group I transcripts in human are found tandem along the genome in the direction of transcription. For the purpose of the analyses, this is how transcripts were 'numbered' for species that are not annotated with numbered *SNORD116* names (i.e., rhesus, chimp and rabbit *SNORD116-1*s were classified as the closest *SNORD116* downstream of the *SNURF/SNRPN* transcription site). The tandem SNORD transcripts that follow were classified as 116-2, 116-3, and so on. This resembles the naming scheme of human *SNORD116* individual transcripts.

Mouse and rat *Snord116@* members do not follow this naming scheme. For example, Snord116s 116-1, 116-2 and 116-3 are not found tandem to each other or closest to the *Snurf/Snrpn* locus. Rat Snord116s were instead classified into Group I by using a template *Snord116* transcript that resulted in the largest group of transcripts with 95% homology (*Snord116.3*). Mice Snord116s were not grouped, as all 70 potential Snord116 sequences show 95% homology or more.

For primates, Groups II and III were informed by previous groupings of human *SNORD116* [8,9]. Sequences within a species were grouped according to clusters of high homology that show tandem appearance in the *SNORD116@* locus, with Group I including

genes closest to Group II transcripts on the genome. In rabbit and rat, further groupings beyond Group I showed much less homology. The remaining ungrouped sequences outside of Group I were grouped using a homology threshold of 80%, excluding any sequence with a lower homology. This left 2 sequences ungrouped in both rat and rabbit.

Group I: human (116-1–116-9); chimp (1–4, 6–8); macaque (1–9); rabbit (1–19); rat (116.3, 116.7, 116.8, 116.15, 116.16, 116.19, 116.23, 116.24, 116.25, 116.31, 116.35).

Group II: human (116-10–116-24); chimp (9–22); macaque (10–24); rabbit (20–27); rat (116.6, 116.20, 116.10, 116.21, 116.29, 116.12, 116.11, 116.27, 116.1, 116.34, 116.13, 116.28, 116.33).

Group III: human (116-25–116-30); chimp (23–28); macaque (25–29).

Ungrouped: chimp (5); rabbit (28, 29); rat (116.9, 116.17); mouse (116@).

Sequence Accession Codes

Ensembl *SNORD116* transcript sequences used are provided with Ensembl accession codes and are displayed in order of shortest distance from the *SNURF/SNRPN* locus within the respective species (Supplemental Tables S1 and S2). In species without individually-annotated and numbered *SNORD116* transcripts (e.g., macaque, chimp, rabbit), predicted gene names are omitted, and instead, the sequences are numbered starting from the one that is the shortest distance from the *SNURF/SNRPN* locus. All sequences are listed in order of the chromosome, starting with the sequence closest to the *SNURF/SNRPN* locus. Sequence alignments used for each species can be found in Supplemental Figures S1–S6.

3.6 References

1. Levene, P.A.; Jacobs, W.A. Über inosinsäure. Eur. J. Inorg. Chem. 1909, 42, 1198–1203.
2. Gros, F.; Gilbert, W.; Hiatt, H.H.; Attardi, G.; Spahr, P.F.; Watson, J.D. Molecular and biological characterization of messenger RNA. Cold Spring Harb. Symp. Quant. Biol. 1961, 26, 111–132.
3. Carninci, P.; Kasukawa, T.; Katayama, S.; Gough, J.; Frith, M.C.; Maeda, N.; Oyama, R.; Ravasi, T.; Lenhard, B.; Wells, C.; et al. The transcriptional landscape of the mammalian genome. Science 2005, 309, 1559–1563.
4. Ensemble Consortium; Birney, E.; Stamatoyannopoulos, J.A.; Dutta, A.; Guigo, R.; Gingeras, T.R.; Margulies, E.H.; Weng, Z.; Snyder, M.; Dermitzakis, E.T.; et al. Identification and analysis of functional elements in 1% of the human genome by the encode pilot project. Nature 2007, 447, 799–816.
5. Pennisi, E. Genomics. ENCODE project writes eulogy for junk DNA. Science 2012, 337, 1159, 1161.
6. Jorjani, H.; Kehr, S.; Jedlinski, D.J.; Gumienny, R.; Hertel, J.; Stadler, P.F.; Zavolan, M.; Gruber, A.R. An updated human snoRNAome. Nucleic Acids Res. 2016, 44, 5068–5082.
7. Cavaille, J. Box C/D small nucleolar RNA genes and the Prader-Willi syndrome: A complex interplay. Wiley Interdiscip. Rev. RNA 2017, 8.
8. Runte, M.; Huttenhofer, A.; Gross, S.; Kiefmann, M.; Horsthemke, B.; Buiting, K. The IC-SNURF-SNRPN transcript serves as a host for multiple small nucleolar RNA species and as an antisense RNA for UBE3A. Hum. Mol. Genet. 2001, 10, 2687–2700.
9. Castle, J.C.; Armour, C.D.; Lower, M.; Haynor, D.; Biery, M.; Bouzek, H.; Chen, R.; Jackson, S.; Johnson, J.M.; Rohl, C.A.; et al. Digital genome-wide ncRNA expression, including SnoRNAs, across 11 human tissues using polya-neutral amplification. PLoS ONE 2010, 5.
10. Kishore, S.; Stamm, S. The snoRNA HBII-52 regulates alternative splicing of the serotonin receptor 2C. Science 2006, 311, 230–232.
11. Hassan, M.; Butler, M.G. Prader-Willi syndrome and atypical submicroscopic 15q11-q13 deletions with or without imprinting defects. Eur. J. Med. Genet. 2016, 59, 584–589.
12. Foundation for Prader-Willi Research. About Prader-willi Syndrome. Available online: https://www.fpwr. org/about-prader-willi-syndrome/ (accessed on 31 October 2017).
13. Cheon, C.K. Genetics of Prader-Willi syndrome and Prader-Will-Like syndrome. Ann. Pediatr. Endocrinol. Metab. 2016, 21, 126–135.
14. Runte, M.; Varon, R.; Horn, D.; Horsthemke, B.; Buiting, K. Exclusion of the C/D box snoRNA gene cluster HBII-52 from a major role in Prader-Willi syndrome. Hum. Genet. 2005, 116, 228–230.
15. Bieth, E.; Eddiry, S.; Gaston, V.; Lorenzini, F.; Buffet, A.; Conte Auriol, F.; Molinas, C.; Cailley, D.; Rooryck, C.; Arveiler, B.; et al. Highly restricted deletion of the SNORD116 region is implicated in Prader-Willi syndrome. Eur. J. Hum. Genet. 2015, 23, 252–255.
16. Ding, F.; Li, H.H.; Zhang, S.; Solomon, N.M.; Camper, S.A.; Cohen, P.; Francke, U. SnoRNA Snord116 (Pwcr1/MBII-85) deletion causes growth deficiency and hyperphagia in mice. PLoS ONE 2008, 3.

17. Skryabin, B.V.; Gubar, L.V.; Seeger, B.; Pfeiffer, J.; Handel, S.; Robeck, T.; Karpova, E.; Rozhdestvensky, T.S.; Brosius, J. Deletion of the MBII-85 snoRNA gene cluster in mice results in postnatal growth retardation. PLoS Genet. 2007, 3.
18. Burnett, L.C.; LeDuc, C.A.; Sulsona, C.R.; Paull, D.; Rausch, R.; Eddiry, S.; Carli, J.F.; Morabito, M.V.; Skowronski, A.A.; Hubner, G.; et al. Deficiency in prohormone convertase PC1 impairs prohormone processing in Prader-Willi syndrome. J. Clin. Investig. 2017, 127, 293–305.
19. Good, D.J.; Porter, F.D.; Mahon, K.A.; Parlow, A.F.; Westphal, H.; Kirsch, I.R. Hypogonadism and obesity in mice with a targeted deletion of the Nhlh2 gene. Nat. Genet. 1997, 15, 397–401.
20. Aken, B.L.; Ayling, S.; Barrell, D.; Clarke, L.; Curwen, V.; Fairley, S.; Fernandez Banet, J.; Billis, K.; Garcia Giron, C.; Hourlier, T.; et al. The ensembl gene annotation system. Database 2016, 2016.
21. Cavaille, J.; Bachellerie, J.P. Processing of fibrillarin-associated snornas from pre-mrna introns: An exonucleolytic process exclusively directed by the common stem-box terminal structure. Biochimie 1996, 78, 443–456. Genes 2017, 8, 358 11 of 11
22. Deschamps-Francoeur, G.; Garneau, D.; Dupuis-Sandoval, F.; Roy, A.; Frappier, M.; Catala, M.; Couture, S.; Barbe-Marcoux, M.; Abou-Elela, S.; Scott, M.S. Identification of discrete classes of small nucleolar RNA featuring different ends and RNA binding protein dependency. Nucleic Acids Res. 2014, 42, 10073–10085.
23. Shen, M.; Eyras, E.; Wu, J.; Khanna, A.; Josiah, S.; Rederstorff, M.; Zhang, M.Q.; Stamm, S. Direct cloning of double-stranded RNAs from RNase protection analysis reveals processing patterns of C/D box snoRNAas and provides evidence for widespread antisense transcript expression. Nucleic Acids Res. 2011, 39, 9720–9730.
24. Kishore, S.; Gruber, A.R.; Jedlinski, D.J.; Syed, A.P.; Jorjani, H.; Zavolan, M. Insights into snoRNA biogenesis and processing from PAR-CLIP of snoRNA core proteins and small RNA sequencing. Genome Biol. 2013, 14.
25. Wu, Q.; Zhou, X.; Han, X.; Zhuo, Y.; Zhu, S.; Zhao, Y.; Wang, D. Genome-wide identification and functional analysis of long noncoding RNAs involved in the response to graphene oxide. Biomaterials 2016, 102, 277–291.
26. Yin, Q.F.; Yang, L.; Zhang, Y.; Xiang, J.F.; Wu, Y.W.; Carmichael, G.G.; Chen, L.L. Long noncoding RNAs with snoRNA ends. Mol. Cell 2012, 48, 219–230.

Chapter 4. *Snord116* Post-transcriptionally Increases *Nhlh2* mRNA Stability: Implications for Human Prader-Willi Syndrome

Matthew A. Kocher[1], Fenix W. Huang[2], Erin Le[3], and Deborah J. Good[1,3]*

[1]Translational Biology, Medicine and Health Graduate Program, 1 Riverside Circle, Virginia Tech, Roanoke, VA 24016

[2]Biocomplexity Institute & Initiative, University of Virginia, 995 Research Park Blvd, Town Center III, 4th Floor, Charlottesville, VA 22911

[3]Department of Human Nutrition, Foods, and Exercise, 1981 Kraft Drive (0913), Integrated Life Sciences Building, Virginia Tech, Blacksburg, VA 24060

Human Molecular Genetics 2021, under review

4.1 Abstract

The smallest genomic region causing Prader-Willi Syndrome (PWS) deletes the non-coding RNA *SNORD116* cluster; however, the function of *SNORD116* remains a mystery. Previous work in the field revealed the tantalizing possibility that expression of *NHLH2*, a gene previously implicated in both obesity and hypogonadism, was downregulated in PWS patients and differentiated stem cells. *In silico* RNA:RNA modeling identified several potential interaction domains between *SNORD116* and *NHLH2* mRNA. One of these interaction domains was highly conserved in most vertebrate *NHLH2* mRNAs examined. A construct containing the *Nhlh2* mRNA, including its 3'-UTR, linked to a c-myc tag was transfected into a hypothalamic neuron cell line in the presence and absence of exogenously-expressed *Snord116*. *Nhlh2* mRNA expression was upregulated in the presence of *Snord116* dependent on the length and type of 3'UTR used on the construct. Furthermore, use of actinomycin D to stop new transcription in N29/2 cells demonstrated that the upregulation occurred through increased stability of the *Nhlh2* mRNA in the 45 minutes immediately following transcription. *In silico* modeling also revealed that a single nucleotide variant (SNV) in the *NHLH2* mRNA could

reduce the predicted interaction strength of the *NHLH2:SNORD116* diad. Indeed, use of an *Nhlh2* mRNA construct containing this SNV significantly reduces the ability of *Snord116* to increase *Nhlh2* mRNA levels. For the first time, these data identify a motif and mechanism for SNORD116-mediated regulation of *NHLH2*, clarifying the mechanism by which deletion of the *SNORD116* snoRNAs locus leads to PWS phenotypes.

4.2 Introduction

Prader-Willi Syndrome (PWS) is a devastating human genetic condition, affecting up to 1 in 10,000 live births. Affected infants present with hypotonia, as well as weak suckling and failure to thrive (1). Adolescents are hypogonadal and males show cryptorchidism, with hypogonadotropic hypogonadism at puberty (1). Hyperphagia typically begins around age 2 years (1), and results in morbid obesity in adulthood unless drastic calorie limitation is initiated.

PWS is most often due to a de novo paternal deletion of the chromosome 15q11-q13 region (at least 60% of cases) (1). The paternally-inherited 15q deletion minimally contains the *SNORD116* locus, (a group of 30 small nucleolar RNAs “snoRNAs”), and the *IPW* gene (2). The *SNORD116* snoRNAs are “orphan” snoRNAs meaning that they have no predicted RNA targets.

A significant gap in knowledge exists in our understanding of how deletion of this region of 15q leads to the complex phenotypes of PWS. A hint about this came in late 2016 when Burnett and colleagues showed two mRNAs--*NHLH2* and *PCSK1* were downregulated in human PWS induced pluripotent stem cell (iPSC)-derived neurons, and in the *Snord116*$^{m+/p-}$ mouse—a model animal for PWS (3). As noted in their paper, targeted deletion of *Nhlh2* (N2KO) in mice results in phenotypes that overlap that of human PWS, and the *Snord116*$^{m+/p-}$ mouse (3).

N2KO mice show an initial delay in total body weight until about 7 weeks of age in males, and then a later onset obesity, significant in both sexes by around 13 weeks of age (4). Total body fat in the females becomes significantly higher than age-matched wild-type females in the 13-19 week ages, while in males, body fat levels are significantly higher in animals older than 20 weeks old (4). Both of these phenotypes are similar in developmental stages to PWS patients. Likewise, N2KO mice demonstrate male cryptorchidism, with hypogonadotropic

hypogonadism in males and females at puberty (5, 6). Low physical activity levels are characteristic of both N2KO mice (4) and PWS patients—the latter showing low infantile movement (1) as well as overall physical activity levels and response to exercise (7). Both N2KO mice (KJ/hour, in preparation) and PWS patients (Kcal/day) (8) demonstrate low energy expenditure levels, contributing to overall lower metabolism levels for both the model organism and the human counterparts.

Nhlh2 is a neuronal basic helix-loop-helix transcription factor that controls genes within the leptin-melanocortin pathway (9), including prohormone convertase 1/3 (*PCSK1/3*) (10), melanocortin-4-receptor (*MC4R*) (11), and even a locus within the imprinted region of chromosome 15q, necdin (NDN) (12). Reduced expression of *NHLH2* in PWS patients could explain both the obesity and hypogonadal phenotypes of these patients. However, a significant gap in knowledge exists about how deletion of the paternal 15q region would lead to lower *NHLH2* levels.

Our expertise in *NHLH2* regulation and function, combined with the findings by Burnett and colleagues led us to ask if *SNORD116* might regulate *NHLH2* levels at a molecular level. We specifically focused on *SNORD116* due to the finding that the *Snord116*$^{m+/p-}$ mouse as well as iPSC derived neurons from patients with a minimal deletion that included *SNORD116* showed the lower *NHLH2/Nhlh2* protein and mRNA expression levels (3). In this paper, using *in silico* tools and a mouse hypothalamic neuron cell line, we demonstrate the mechanism by which *Snord116* controls levels of *Nhlh2*. Together, these results effectively change *SNORD116* from an orphan snoRNA, to one with a verified target, identify a *SNORD116* interaction motif that can be used to search for more targets, and provide a molecular genetic mechanism for how deletion of the 15q11-q13 region in humans leads to PWS.

4.3 Results

In silico determination of an *NHLH2: SNORD116-3* interaction motif

As the SNORD116 locus codes for orphan snoRNAs, meaning that there were no known interaction targets for any of its 30 snoRNAs, *in silico* tools were used to determine if any region of the *NHLH2* mRNA showed strong interactions with any of the 30 *SNORD116* snRNAs. Both the mouse and human *NHLH2* genes contain three exons, with only a small

coding region at the beginning of exon 3, and a long 3' untranslated region (UTR) (**Figure 1A**).

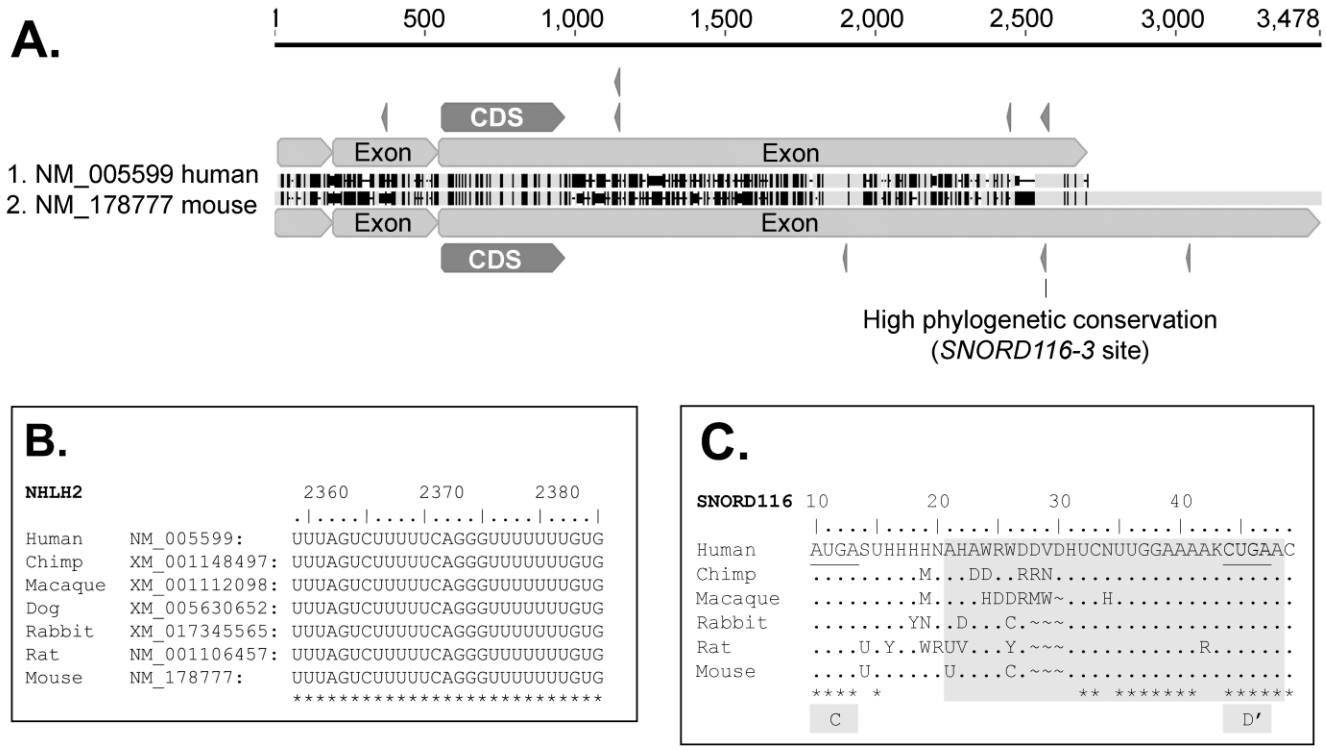

Figure 1. Strongest predicted RNA:RNA interaction between SNORD116 and NHLH2 is found within highly conserved regions. A., Nucleotide alignment for human and mouse NHLH2 mRNA sequences with predicted SNORD116 interaction sites. Predicted interaction sites are displayed in small antisense arrows above or below the given sequence. Light gray regions in the aligned sequences show identity agreement, black regions show disagreements, and horizontal lines show gaps in alignment. One region with high phylogenetic agreement and predicted SNORD116 interaction sites found in both human and mouse are labelled. **B.**, Phylogenetic alignment of NHLH2 3'UTR predicted interaction site among vertebrates. Nucleotide numbers above the alignment are based on human NHLH2, NM_005599. NCBI reference sequence numbers used for the analysis are shown. * indicates perfect non-ambiguous homology with the human sequence for all nucleotides in the site above. **C.**, Phylogenetic Alignment of consensus SNORD116. Underlines indicate C/D' box motifs. Boxed region indicates predicted interaction site with NHLH2, which includes the canonical snoRNA antisense region. * indicates perfect non-ambiguous homology with the human sequence for all nucleotides in the site above. Human n = 30, chimp n = 28, rhesus n = 29, rabbit n = 29, rat n = 26, and mouse n = 17.

Within the 3'-UTR, several regions of high homology exist between mouse and human *NHLH2.* An *in silico* RNA:RNA interaction analysis using all of the Human *SNORD116* snoRNAs, and the human *NHLH2* mRNA sequence indicated that at least one of the 30 *SNORD116* transcripts had the potential to form a highly stable RNA:RNA interaction. As shown in **Figure 1A**, the location of the putative interaction region is within a larger region showing 100% conservation between mouse and human *NHLH2* (as indicated by the gray shading). *In silico* RNA:RNA analysis identified other *SNORD116*:NHLH2 dyads with lower interaction energies (shown as arrow heads, **Figure 1A**), but these interactions were not pursued further, as they did not interact with homologous regions in the mouse and human *NHLH2* mRNA, were not located in the snoRNA antisense region, and had much lower interaction energies compared to that for *SNORD116-3*: *NHLH2*. The putative *SNORD116-3: NHLH2* interaction motif is highly conserved in vertebrates (**Figure 1B-C**). For *NHLH2,* this region is 100% conserved in the

vertebrates shown (**Figure 1B**), and in 70/77 vertebrates tested phylogenetically (data not shown). *SNORD116* consensus sequences for all paralogs within a cluster show high phylogenetic conservation in the predicted interaction region (**Figure 1C**). Critically, the *SNORD116-3* predicted interaction is in the canonical antisense region just 5' of the D' box, conserved in all species shown (**Figure 1C**). Of note, the *SNORD116-3* interaction motif on the *NHLH2* 3'UTR is found in 2 of 2 of the human *NHLH2* splice variants, and 2 of 2 of the murine splice variants that are registered in the RefSeq database (**Supplemental Figure 1**).

Numerous single nucleotide variants (SNV) exist within the NHLH2 and SNORD116-3 genomic loci, although none have been characterized as having clinical significance. However, an analysis of the effect of each naturally-occurring SNVs on the *NHLH2* 3'UTR in the region of this motif revealed five of these that disrupted the energy of interaction, as predicted using *in silico* RNA:RNA interaction analyses. Each of these disrupting SNVs were found towards the 3' end of the motif (**Figure 2A**) and reduce the predicted strength of interaction from -13.4 kcal/mol for the wildtype, to -9.4 for both rs1218168750 and rs1051613841 (**Figure 2B**). As shown in **Figure 2C**, compared to **2D,** rs1051613841 was predicted to disrupt the stem area of the *NHLH2:SNORD116-3* dyad. The predicted mouse secondary structure for the wildtype (**Figure 2E**) and mutagenized form (**Figure 2F**) are also shown.

A.

```
                  2359                        2385
Human NM_005599 - UUUAGUCUUUUUCAGGGUUUUUUUGUG
                                 1     2     3 45
Mouse NM_178777 - UUUAGUCUUUUUCAGGGUUUUUUUGUG
                  2424                        2450
```

B.

Number	Variant ID	Alleles	SNORD116-3 interaction energy (kcal/mol)	Minor Allele Frequency	Database
1	rs1218168750	U>A	-9.4	A=0.000008/1	TOPMED
2	rs1429739555	U>A	-12.4	A=0.00003/1	GnomAD
3	rs1263227328	U>G	-10.3	G=0.000008/1	TOPMED
4	**rs1051613841**	**U>C**	**-9.4**	**C=0.000008/1**	**TOPMED**
5	rs1435274872	G>A	-10.4	A=0.000008/1	TOPMED
WT	-	-	-13.4	-	-

C.

NHLH2_NM_005599

```
          2359                            2385
            |                               |
5'-AAU...AGAU     U           UU           UCUC...AAA-3'
             UUUAG CUUUUUCAGGG     UUUUUGUG
             ||:|| |||||:||:||     |||||:||
             AAGUC GAAAAGGUUCC     AAAAAUAC
3'-ACC...AAAC                  UUAC         CCCC...GGU-5'
            |                               |
           48                               21
```

SNORD116-3 NR_003318.1

interaction energy = -13.4311 kcal/mol

D.

NM_005599_SNV_rs1051613841

```
          2359               2375
            |                  |
5'-AAU...AGAU     U            UUUUUUUGCG..AAA-3'
             UUUAG CUUUUUCAGGG
             ||:|| |||||:||:||
             AAGUC GAAAAGGUUCC
3'-ACC...AAAC                   UUACAAAAAUAC...GGU-5'
            |                  |
           48                  33
```

SNORD 116-3 NR_003318.1

interaction energy = -9.42051 kcal/mol

E. **Nhlh2_NM_178777**

```
            2424              2440
              |                 |
5'-AGG...AGAU     U            UUUUUUUGUG...UCC-3'
             UUUAG CUUUUUCAGGG
             ||:|| |||||:||:||
             AAGUC GAAAAGGUUCC
3'-CCU...AAAC                  UUACAAACUG...AGG-5'
             |                 |
            45                30
```

Mouse Snord116-1 ENSMUST00000179518.1

interaction energy = -7.70926 kcal/mol

F. **Nhlh2_NM_178777_U2449C**

```
            2424              2440
              |                 |
5'-AGG...AGAU     U            UUUUUUUGCG..UCC-3'
             UUUAG CUUUUUCAGGG
             ||:|| |||||:||:||
             AAGUC GAAAAGGUUCC
3'-CCU...AAAC                  UUACAAACUG...AGG-5'
             |                 |
            45                30
```

Mouse Snord116-1 ENSMUST00000179518.1

interaction energy = -7.60017 kcal/mol

Figure 2. Single nucleotide variants have the potential to reduce the predicted NHLH2: SNORD116 motif interaction energy. A., RNA alignment of the predicted SNORD116 interaction region for mouse and human NHLH2 with five human SNVs displayed. **B.**, Reference SNV data provided from NCBI SNP database, including accession number, and major allele frequency (MAF). The predicted effect on the SNORD116-3 interaction energy (kcal/mol) with NHLH2 is shown. **C.**, INTA-RNA predicted structure of the wild-type NHLH2:SNORD116-3 interaction. **D.**, INTA-RNA predicted structure of the NHLH2:SNORD116-3 interaction containing NHLH2 SNV rs1051613841 **E.**, INTA-RNA predicted structure of the wild-type mouse Nhlh2:Snord116 interaction used in the current study. **F.**, INTA-RNA predicted structure of the mutagenized mouse sequence U2449C. SNV site of interest is labelled in bold, underlined, and/or with arrows .

The intact *NHLH2*:*SNORD116-3* interaction motif mediates high *Nhlh2* expression levels.

N29/2 hypothalamic cells have been previously used to measure *Nhlh2* expression at the transcriptional and posttranscriptional levels (13, 14). A set of constructs, using a myc-tag motif to differentiate endogenous *Nhlh2* from the transfected *Nhlh2* with different 3' tails were used to measure Nhlh2 response to Snord116 in hypothalamic cells. These constructs all contained the myc-tagged *Nhlh2* (mouse) coding region linked to either high-expression SV-40 3'UTR, a partial *Nhlh2* 3' UTR (13), a full-length *Nhlh2* 3'-UTR, or a full-length *Nhlh2* 3'-UTR containing the rs1051613841 SNV (**Figure 3A**). Each were transfected into N29/2 hypothalamic neurons (15) which express low levels of *Snord116,* and *Nhlh2* during regular growth phase. Addition of a mouse *Snord116* consensus expression plasmid (which is most phylogenetically homologous to group 1 SNORD116 snoRNAs (16)) to cells expressing the full-length *Nhlh2-myc* mRNA construct led to a ~15-fold increase of *Nhlh2-myc mRNA* levels

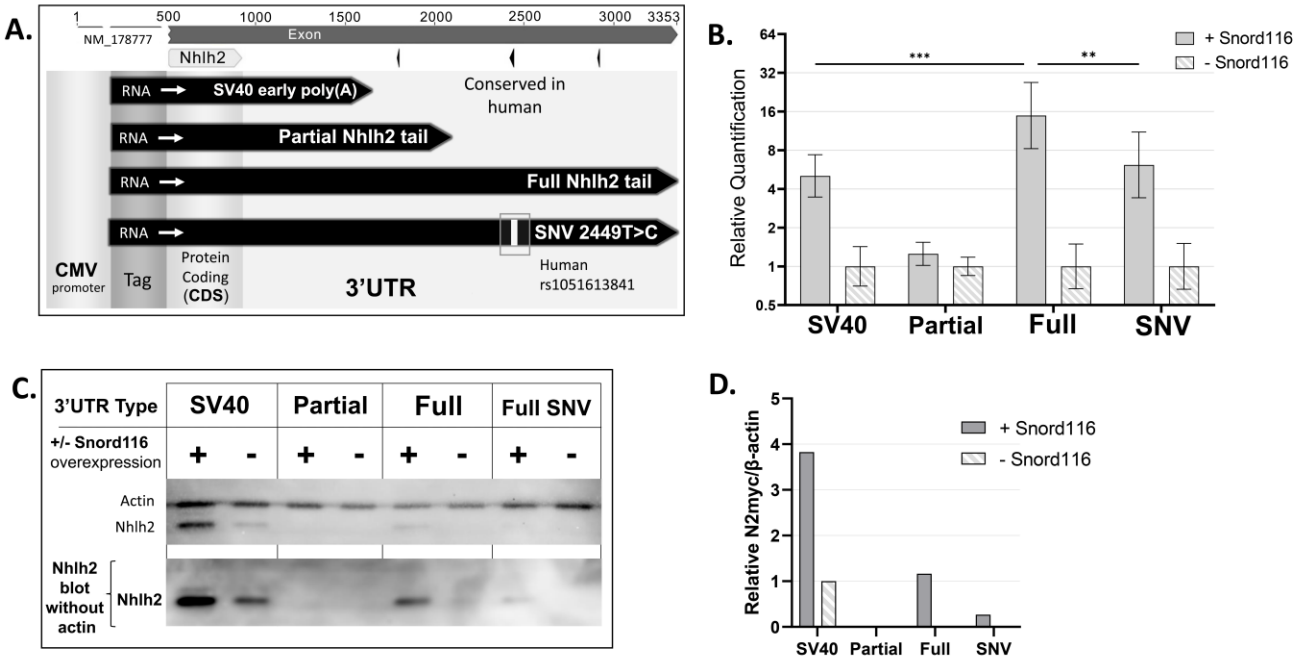

Figure 3: Post-transcriptional Regulation of Nhlh2 by Snord116 is reduced by a SNV in the predicted interaction region within the Nhlh2 3'UTR. A., Reporter plasmids expressing mouse Nhlh2 mRNA. Mouse Nhlh2 mRNA (NM_178777) with annotated exons, coding sequence (CDS), and predicted Snord116 interaction sites. Four different expression vectors for tagged Nhlh2 mRNA with varying 3'UTRs are shown to scale in comparison to Nhlh2 mRNA. The mouse vector was engineered to contain a T>C SNV within the predicted interaction region which is shown by the white bar on that vector. **B.**, Relative expression of tagged Nhlh2 RNA with different 3'UTRs during Snord116 overexpression in N29/2 cells. Nhlh2 SNV at predicted Snord116 interaction site decreases Snord116-induced fold change. For the +Snord116 condition, one-way ANOVA $F(3,29) = 30.992$, $p<0.001$ with Bonferroni correction shows the only 3'UTR types to not be significantly different to each other are SV40 and SNV. All other comparisons are significantly different ($p<0.05$); N= 6 for partial 3'UTR conditions; N= 9 for SV40, Full, and SNV conditions. Error bars indicate ±SD. **$p<0.01$, ***$p<0.001$. Statistical analysis performed on respective ddCT values from which Relative Quantification (RQ) values are derived. **C.**, Representative Western blot shows higher protein translation of the +Snord116 conditions and the SV40 3'UTR construct. Both blots are from the same samples but the bottom blot is with anti-myc tag antibody alone to allow for longer signal development. Note the western blot is normalized across 3'UTR type, unlike Figure 3B. **D.** Optical density of representative Western blot.

(**Figure 3B**). The construct containing the engineered SNV in the consensus motif, led to a smaller, yet still significant increase of ~6-fold in *Nhlh2-myc* mRNA levels, while the partial tail without the predicted interaction site showed no increase in response to *Snord116* overexpression. Interestingly, the construct with the SV-40 3'UTR showed a similar increase of ~5-fold, although the strongest predicted *Snord116* interaction site for this tail was a relatively weak (-5.54 kcal/mol) in the 3'UTR. **Figure 3C** shows that the different 3'UTR constructs lead to different steady-state *Nhlh2* protein levels, consistent with the mRNA levels. Like the protein levels, SV40 3'UTR shows greater baseline RNA expression when normalized across 3'UTR (**Supplemental Figure 2**). Snord116 overexpression ranged from about 100 – 1000-fold higher (**Supplemental Figure 3**). Of note, all constructs were under the control of the CMV promoter and had the identical *Nhlh2-myc* coding region through the *Nhlh2* stop codon. Thus, differences in expression level could only be attributed to differences in the 3'-UTR of the constructs, and the presence/absence of the putative motif. These data suggest that *Snord116* controls expression of *Nhlh2,* post-transcriptionally, through the 3'UTR motif identified by *in silico* binding analysis.

Snord116 **snoRNA stabilizes** ***Nhlh2*** **mRNA**

While post-transcriptional regulation of mRNA can be due to changes in mRNA translation efficiency, the 3'-UTR of an mRNA often directs regulation due to changes in mRNA stability. To test whether *Snord116* levels altered mRNA stability of *Nhlh2*, the same constructs as above and the N29/2 cell line was used in an actinomycin D assay. Actinomycin D (also known as dactinomycin) is an antibiotic and chemotherapeutic that inhibits DNA-dependent RNA synthesis through DNA intercalation and inhibition of RNA polymerase I, II, and III(17, 18). As transcription of new mRNA is blocked when actinomycin D is added to a cell culture, the level of mRNA at times following addition of the chemical can be used to determine mRNA stability. As shown in **Figure 4,** *Snord116* shows general overall stabilization of the SV40, Full, and SNV tails, throughout the 3-hour time course. This is consistent with *Snord116*'s effect on steady-state levels (**Figure 3B**). The stabilization effect size is greater for the Full and SNV tails than SV40 (**Figure 4E**). Additionally, this difference in stabilization effect size seems to be mediated by an early rapid decay of the Full/SNV tails without *Snord116*. About 50% of the RNA from the SNV/Full tails are degraded by 45 minutes, while both the partial/SV40 tails'

levels remain higher ($p<0.05$) and degrade to about 50% between 90 – 180 minutes (**Figure 4A-4D**). This indicates a relative baseline instability for the Full/SNV tails. This high initial decay rate within the first 45 minutes also slows down by the 90min and 180min intervals for Full/SNV tails (**Supplemental Figure 4**). Interestingly, with the addition of *Snord116*, this initially high rate of decay is blunted, indicating that *Snord116* has a protective effect against RNA decay within the first 45 minutes for the Full/SNV tails (**Figure 4G**). Critically, the *Snord116* protective effect at 45 minutes trends to being less effective for the SNV tail when compared to the full tail but does not reach a significance difference between the two ($p=0.10$). Of note, Snord116 RNA does not decay over time (**Supplemental Figure 5**).

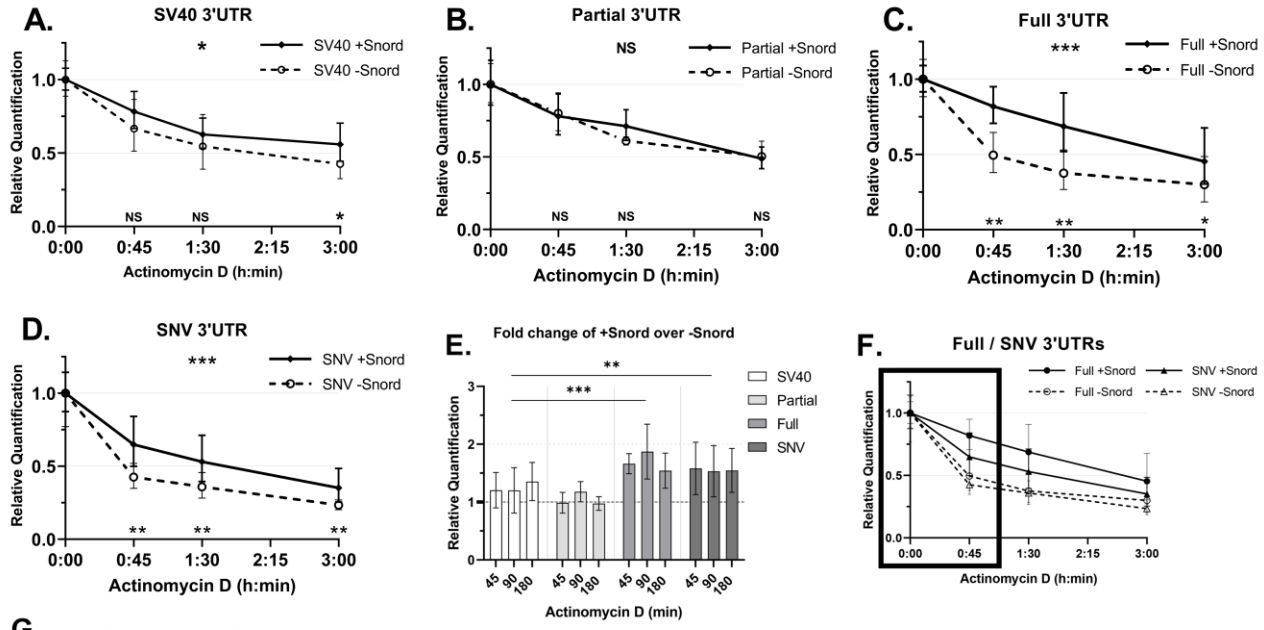

Figure 4: Snord116 stabilizes target RNAs and protects against early rapid decay dependent on 3'UTR. A-D., Relative expression of reporter mRNAs with different 3'UTRs during Snord116 overexpression and actinomycin D treatment. Snord116 overexpression indicated by solid lines, and negative control indicated by dotted lines. Significance indicators for main effect across all time points between +/-Snord116 are shown just below the title of each figure. Significance indicators for individual time points between +/-Snord116 are shown just above the X-axis. **E.**, Fold change of +Snord116 relative to -Snord116 condition for each 3'UTR and time point. **F.**, Relative expression of Full and SNV 3'UTRs modified from Fig.4C-D. Boxed area emphasizing 45-minute time point for the context of Figure 4G. **G.**, Decay rate shown as percent decay for the 45-minute time point for each 3'UTR and Snord116 condition. Significance indicators correspond to differences between +/-Snord116 conditions within a 3'UTR condition. N=6 for partial 3'UTR condition; N=9 for SV40, Full, and SNV conditions. Error bars indicate ±SD. *p<0.05, **p<0.01, ***p<0.001, ^{NS}p>0.05

4.4 Discussion

Snord116 has been previously implicated in changes of gene expression, with proposed molecular mechanisms including alternative splicing and RNA-stability (3, 19-21). The current

study is the first to demonstrate that RNA stability indeed is a molecular mechanism for *Snord116*-dependent changes in gene expression. As this study was done using cell lines and molecular constructs, there are minimal confounds from the *PWS* locus and the *Snord116* host gene (*116HG).* Rather, these results can be directly attributed to a *Snord116* snoRNA and its target gene.

The current study is the first to show evidence for an interaction of *Snord116* RNA with a predicted target. Although RNA interaction prediction for targets of *SNORD116* have been performed previously, there was no experimental validation of these interactions(19, 22). Using the snoTARGET software (22), previous predictions failed to include *NHLH2* as a potential target. Furthermore, the predicted strength of interaction with *NHLH2* is relatively low compared to other predicted target RNAs. The current study suggests that while interaction prediction is a useful tool, as implicated by the predicted effect of the SNV on the 3'UTR:Snord116 interaction, other factors, such as protein or other interactions should be considered.

Using both the data in this paper, and previous work, we predict that high *NHLH2* levels may be present in cells expressing *SNORD116* and/or treated with leptin. *Snord116* expression from wild type mouse hypothalamus increases with refeeding after overnight fasting (3). As both leptin and *Snord116* levels increase during a refeeding period, these two paths appear to converge synergistically on *Nhlh2* upregulation: transcriptional upregulation of *Nhlh2* through leptin signaling (14), and post-transcriptional upregulation of *Nhlh2* through *Snord116.* While some previous studies have not detected changes in the levels of hypothalamic *NHLH2* mRNA in PWS patient post-mortem tissue or PWS model mice (19-21), our data suggest that changes in *Nhlh2* levels may occur with a short temporal window that the other studies failed to capture. Conversely, another study has demonstrated that growing lymphoblastoid cells derived from PWS patients show a -1.5 fold expression of *NHLH2* mRNA compared to normal lymphoblastoid cells (23). It may be questioned if the current study is relevant to the biological levels of the genes in question. In our approximation, when compared to mouse hypothalamus tissue by RT-QPCR, the current study's *Snord116* levels are greatly under-expressed, and *Nhlh2* levels range from equal expression to slight under-expression (data not shown). Part of the rationale for using the N29/2 cell line is that *Snord116* levels are

low, replicating a PWS-like condition, and allowing specific overexpression of exogenous *Snord116*.

The current study shows that high expression of *Snord116* leads to higher stability of *Nhlh2* mRNA and subsequently, higher levels of translated protein. At steady-state levels, the SNV 3'UTR seems to disrupt *Snord116*-dependent upregulation when compared to the full wildtype 3'UTR, implying that the predicted interaction site is playing a role in *Snord116* interaction (Figure 3B). However, this disruption from the SNV is not seen in the RNA decay experiment (Figure 4). The *Snord116* protective effect at 45 minutes only trends to being less effective for the SNV tail when compared to the full tail ($p=0.10$). This may be due to some differences between steady-state and RNA decay experiments. The steady-state experiment may be sensitive to the accrual of RNA over a 24-hour period post-transfection and any RNA stability differences may lead to a cumulative effect. The RNA decay experiment is sensitive to a smaller timeframe, and highlights that the initial 45 minutes may be critical for stabilization effects between the Full and SNV 3'UTRs. Therefore, small differences in stability that do not show statistical significance at 45 minutes may be amplified when these small differences accumulate over time and show differences at steady-state levels. Additionally, it is possible that a more disruptive SNV may show stronger effects than the one used in the current study. Furthermore, the steady-state experiment did not include a media refresh prior to cell lysis, while the RNA decay experiment refreshed the media with the addition of Actinomycin D at the 0-minute timepoint, which could add a serum or media factor that affects expression levels.

While the current study implies *Snord116* stabilizes target RNAs, it is possible that results from steady state experiments are influenced by differences in transcription (Figure 3B). However, the consistent pattern of effect size between steady-state and RNA decay studies implies that RNA stability is playing a major role. Future work will have to examine possible effects on transcription.

The use of the *Snord116* expression construct minimizes confounds associated with the PWS genomic locus, as there are many species of ncRNAs and host genes expressed from the locus (24-26). Use of the N29/2 neuronal cell line, which has endogenously low levels of *Snord116* lends confidence that the results shown are due to an overexpression of *Snord116* rather than changes in the many host genes and ncRNAs found at the PWS genomic locus that are often associated with a genomic deletion. It is worth noting that the construct used

contains *Snord116* within its natural intron, as this is necessary for proper snoRNA maturation and processing (20). The natural genomic processing of the *Snord116* host gene (*116HG*) results in a much longer ncRNA with many exons that are not within the construct used (24, 27). There is no way to completely exclude a requirement for the endogenous host gene or other genes within the PWS locus which are present in N29/2 cells. Expression levels of *116HG* were not tested in the present study, while *Snord116* snoRNA levels were tested by RT-QPCR to validate overexpression (**Supplemental Figures 3 and 5**).

Use of the SNV-containing construct appears to confirm that the interaction motif is within the predicted regions on both *Nhlh2* and *Snord116*. Based on this, a model was created that predicts the secondary structure and interaction between *NHLH2* and *SNORD116-3* (**Figure 5**). As shown in the prediction, interaction with *SNORD116-3* occurs within a stem-loop structure on the *NHLH2* 3'UTR. In examining the structure, the stem-loop may be either stabilized or disrupted by *SNORD116-3* interactions, which likely depends on RNA-binding protein interactions within that region. Of interest, hnRNP-U has previously been shown to stabilize *NHLH2* mRNA, although the position of that interaction is not known (28). Thus, while the most well-established mechanism of non-methylating SNORDs is through pre-mRNA splicing (20), enhancement of mRNA stability by SNORDs remain a tantalizing mechanism. It remains to be seen whether the mRNA stability observed in the current study is through the canonical SNORD mechanism of 2'-O methylation or non-canonical mechanisms.

In examining the *NHLH2* RNA sequence around the putative *SNORD116* interaction motif using RegRNA 2.0 (29), there are no overlaps of known motifs within the putative *SNORD116* interaction motif. However, a poly(A) signal is about 100bp downstream of the predicted interaction site for both mouse and human. The mouse transcript has a splice variant that ends at this poly(A) signal (XM_006501112), while the one used in the current study is the splice variant with the longest 3'UTR (NM_178777) (**Figure 1D**). *Snord116* may be mediating it's RNA stability effect through poly(A) signal pathways, as the partial 3'UTR RNA used in the current study does not contain a strong poly(A) signal, while the SV40 3'UTR does. Additionally, in mouse *Nhlh2,* but not human, there is a 60-72nt (depending on strain) trinucleotide repeat region of GAA about 20nt upstream of the predicted *Snord116* interaction region. This region is predicted to be an exon splicing enhancer, although there is little evidence of any splice variants using this exon splice site. Furthermore, just five base pairs

upstream from the interaction site is a putative microRNA interaction site, predicted using TargetScanHuman (30). Both the *SNORD116* and miR-9-5p sites lie within the predicted stem-loop structure on the *NHLH2* mRNA 3'UTR (**Figure 5**). *MiR-9-5p* is a neuronally-expressed microRNA whose dysregulation has been implicated in several neurodegenerative diseases (31). Interestingly, interaction with *miR-9-5p* has been shown to decrease target mRNA stability (32, 33). Experiments to examine if *SNORD116* disrupts the *NHLH2* stem-loop structure are out of the scope of this study, but would allow one to determine if *miR-9-5p* directly binds to and increases the stability of *NHLH2* mRNA. In either scenario, the possible interaction with *miR-9-5p* or other secondary factors, including proteins may explain why the SNV had a weaker effect overall on *Nhlh2* stability levels than we had predicted using *in silico* tools, and suggest that a second region mediating additional mRNA stability control for *NHLH2* may occur outside of the predicted *NHLH2*:*SNORD116* interaction motif. The entire region shown in Figure 5 has high homology in vertebrates (data not shown). Phylogenetic conservation of small motifs in untranslated regions suggest a functional conservation (34, 35) that can be used to predict and test functional interactions, as was done herein. This longer region within the *NHLH2* 3'UTR can be used to identify other possible *SNORD116-3* targets that may also contain this motif in their 3'-UTR. Likewise, as all of the *SNORD116* snoRNAs within group 1 are highly conserved but still have some nucleotide-based substitutions between them (16), we can use this information to determine if all group 1 snoRNAs can interact with similar targets or whether each has a specific set of targets with highly conserved/high energy interaction. Indeed, as shown by our work, a single SNV on the target mRNA can reduce the ability of overexpressed *Snord116* RNA to stabilize the target

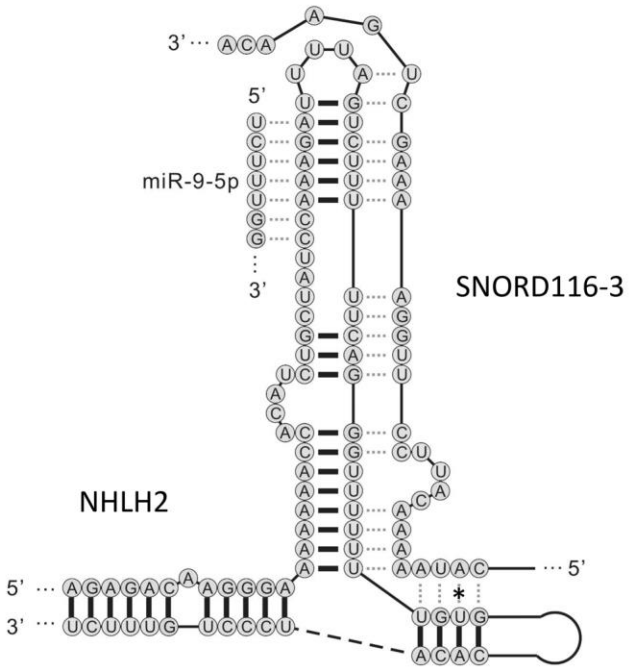

Figure 5: Predicted model of SNORD116:NHLH2 interaction. The ViennaRNA package software was used to predict the folding structure for NHLH2 3'UTR, and then the interaction with SNORD116. The miR-9-5p interaction site was identified using TargetScan. Both interactions were added to the overall structure for viewing of their relative positions on the NHLH2 3'UTR only, not to indicate whether one or both simultaneously interaction with the stem-loop structure. * indicates the site of the NHLH2 SNV used in the current study

mRNA. It is possible that the reverse is true as well—with SNVs within the *SNORD116* locus possibly leading to PWS-like phenotypes.

While we do not find an exact match to the *NHLH2:SNORD116* motif in the *PCSK1* mRNA or other RNA-seq identified RNAs to date (3), it is possible that a similar motif, and different *SNORD116* cluster snoRNAs contribute to these downregulations in PWS models. It is also possible that downregulation of *PCSK1* and other mRNAs in neuronally-induced PWS stem cells simply results from the loss of direct, leptin-induced transcriptional regulation by *NHLH2, as* we have previously shown for *Pcsk1* (10). Additionally, there is a convincing mechanism for *PCSK1* downregulation through *MAGEL2* loss in PWS patients with a large deletion of the genomic locus (36). However, these findings do not explain the low levels of *PCSK1* mRNA and protein found in a PWS microdeletion model of neuronally differentiated iPSCs containing a genomic deletion of only *SNORD109A, SNORD116* cluster, and *IPW* (3). Additionally, PWS mouse models with intact *Magel2* and loss of the paternal *Snord116* cluster have lower levels of *Pcsk1* mRNA and protein in islet cells and stomach (3, 36). These data suggest that loss of *Snord116* may lead to downregulation of *Nhlh2*-dependent *Pcsk1* in addition to the *MAGEL2* mechanism. This may add to the ongoing explanation of why PWS patients with large genomic deletions show stronger phenotypes.

NHLH2 is a basic-helix-loop-helix transcription factor, with multiple known and putative targets (9-11, 37-39). Many of these targets (i.e. *PCSK1, MC4R*) are involved in neuronal control of body weight, and may provide an explanation for some of the phenotypes of PWS. *SNORD116*-mediated post-transcriptional regulation of *NHLH2* could result in hundreds of downstream regulatory changes. For PWS patients, these data now suggest why PWS patients, and the *Nhlh2* knockout mouse share many of the same phenotypes (3, 9), and may open further analyses into therapeutic interventions that can increase levels of *NHLH2* or one of its transcriptional targets, even in individuals with impaired *SNORD116*.

4.5 Methods

Nucleotide Alignments

Nucleotide alignment and annotation performed using Geneious Prime 2020.1.2 (https://www.geneious.com, Biomatters, New Zealand). The “Geneious alignment” algorithm

on default settings was used for pairwise nucleotide alignment of human and mouse sequences with annotations. Phylogenetic nucleotide alignment of *SNORD116* was based on original alignments from Kocher and Good (16).

RNA-RNA Interaction Prediction

IntaRNA (40-43) was used to predict the interaction structures between SNORD116 and its targets. Specifically, the entire mRNA sequence of NHLH2 (Gene ID: 4808) was input for analysis.. IntaRNA is an algorithm that computes an interaction structure with minimum free energy from two input sequences using dynamic programming routine. The prediction considers only the energy contribution of the interaction structures, while the potential secondary structures both RNA strands are not considered. All secondary structures of single stranded RNA are predicted by ViennaRNA 2.0 (44).

Generation of Constructs

The *Nhlh2*-myc tagged construct with SV40 p(A) tail was a generous gift from Dr. Thomas Braun, Max Planck Institute, Bad Nauheim, Germany. This construct contained in the pCS2-MT backbone was used to generate the *Nhlh2*-myc tag with a partial 3'UTR used in a previous study (13). The partial 3'UTR construct was then used for generating the full 3'UTR and the full 3'UTR containing the rs1051613841 SNV. Specifically, a separate vector containing the 1145bp of extra 3'UTR cDNA was cloned using PCR amplification with PstI sites on the 5' and 3' ends of the PCR product, and subsequently cloned into a PstI site at the end of the partial 3'UTR. This vector containing the full 3'UTR was then used to create the SNV construct by site-directed mutagenesis using the Phusion Site-Directed Mutagenesis Kit (ThermoFisher # F541), and mutagenesis primers (**Supplementary Table 1**). The myc-tags on these constructs allow for QPCR analysis of tagged RNA separate from endogenous RNA and allow for primary antibody detection for Western blotting.

The mouse *Snord116* expression vector was a generous gift from Dr. Stefan Stamm, University of Kentucky, Lexington, USA (20). This construct was used to generate a negative control vector for *Snord116* expression by excising the *Snord116* insert using MssI digestion (2722bp), and ligation of the blunt ended fragment of interest (5035bp). This left a backbone

nearly identical to the pCDNA5/FRT/TO vector, but missing 102bp of the multiple cloning site in between the CMV promoter and bGH p(A) terminator.

All constructs were sequenced and subjected to restriction enzyme digests followed by agarose gel electrophoresis for validation of cloning procedures.

Cell Culture and Transfections

The mouse hypothalamus neuron cell line, N29/2 (15), was maintained in T25 flasks in DMEM (4.5g/L glucose, with 110mg/L sodium pyruvate) (ThermoFisher # 11995065) and 10% fetal bovine serum (GE Healthcare #SH30396.03HI) with penicillin (50 units/mL) /streptomycin (50ug/mL) (Thermo # 15070063) at 4-6% CO2 and 37°C. Cells were detached from flasks using trypsin-EDTA (ThermoFisher # 25300054) and 6-well plates were seeded with 2 x 10^4 - 10^5 cells per well. Transfections were done 2-4 days post seeding using Opti-MEM® media (ThermoFisher # 31985070) and Lipofectamine® 3000 (ThermoFisher #L3000008) according to manufacturer's instructions at 60-90% cell confluence. All transfections were performed between 3pm and 6pm. 200ng of each plasmid DNA was transfected for Leptin receptor, *Stat3*, +/-*Snord116*, *Nhlh2*-myctag for a total of 800ng DNA per well of a 6-well plate. Leptin receptor and *Stat3* expression vectors were included to ensure the expression of these key regulatory components of *Nhlh2* and for consistency with previous studies of *Nhlh2* (10, 11, 13, 14).

RNA Purification

24 hours post transfection, cell culture media was removed, and cells were lysed with 1mL of TRIzol® Reagent (ThermoFisher #15596018) directly in 6-well culture plates. TRIzol samples were frozen at -20°C in microfuge tubes until purified (1-14 days) using the TRIzol+Purelink RNA minikit (ThermoFisher #12183025) following manufacturer's instructions for the TRIzol® Plus Total Transcriptome Isolation protocol. Purified RNA was then DNAse treated using TURBO DNA-free™ Kit (ThermoFisher #AM1907) according to manufacturer's instructions, diluted to 60ng/□L in nuclease-free water, and stored at -80°C.

Reverse-Transcriptase Quantitative PCR

For RT-QPCR, Power SYBR® Green RNA-to-CT™ 1-Step Kit (ThermoFisher #4389986) was used according to manufacturer's instructions. 10uL reactions were performed using 150nM final primer concentration. Primers were assessed for efficiency using a dilution series and fell within 90%-110% efficiency. 90ng RNA was used per 10uL reaction. Two technical replicates were performed. Control reactions for each sample (No reverse-transcriptase and no-template controls) were used for quality control. 384-well plates were run on the ViiA 7 Real-Time PCR System (ThermoFisher) according to RT-QPCR mix instructions and thermocycling conditions were not modified from suggested protocol (1-step annealing/extension at 60°C). Quality control measures including melt-curve analysis, technical replicate analysis, etc. were analyzed by thermocycler software and by operator; any major errors were excluded from analysis when appropriate, and/or new samples and plates were run when appropriate. Candidate reference genes for ddCT analysis were analyzed for appropriate reference controls. Mouse beta-actin was used as reference gene control for steady-state experiments. Potential reference genes were evaluated for the Actinomycin D experiments, but none were satisfactory and thus no reference gene was used for RNA decay experiments. The CT values used reflect molarity of the target RNA, as total RNA remained the same for each reaction (90ng). Relative change in molarity over the RNA decay time course is thereby relative to the average decay of total RNA (e.g. If a target gene's relative quantification stays at 1.0 throughout the 180 minutes of Actinomycin D treatment, it decays at the same rate as the total RNA average decay rate).

Western Blot

Constructs were transfected into N29/2 cells, and 24 hours following transfection, cells were washed, lysed in RIPA buffer, scraped from the tissue culture plates, and processed for Western analysis using standard methods. Equal amounts of protein (7 □g/lane), as determined using Bradford Reagent (AMRESCO #E530-1L) were separated on a 12% SDS polyacrylamide gel and transferred to PVDF membrane. Western blotting was performed using rabbit anti-myctag polyclonal primary antibody (Proteintech #16286-1-AP) with goat anti-rabbit horseradish peroxidase-linked antibody as a secondary antibody. Chemiluminescent signal was detected using the SuperSignal™ West Femto Maximum Sensitivity Substrate (ThermoFisher #34095).

RNA stability assay

24 hours post-transfection, cell culture media was refreshed with 5 □g/ ml Actinomycin D (Sigma #SBR00013-1ML) for 45, 90, and 180 minutes before lysis with Trizol directly in 6-well plates. The 0-minute timepoints were refreshed with media containing no Actinomycin D for 50 minutes before lysis. Plates with Actinomycin D were concealed from light during the duration of Actinomycin D incubation. The full time-course experiment was replicated 3 independent times with 3 separate vials of frozen N29/2 cells.

Statistical Analysis

All RT-QPCR data were analyzed using Microsoft Excel 16 for Microsoft 365, IBM SPSS Statistics 26 for Windows, and GraphPad Prism 9.0.0. N=6 for partial 3'UTR conditions; N= 9 for SV40, Full, and Full SNV conditions. Error bars indicate ±SD. The 2^{ddCT} method of relative quantification was used. Statistical significance tests performed on respective ddCT values from which Relative Quantification values are derived. Significance is expressed at *p<0.05, **p<0.01, ***p<0.001, ^{NS}p>0.05.

For steady-state experiments, a two-way ANOVA with Bonferroni correction was used for relative expression of tagged RNA normalized within 3'UTR type. CT and dCT values used are provided in Supplemental File 1.

For RNA decay analysis, CT values were normalized to the average CT of the 0-minute time point within a transfection, within 3'UTR condition, and within Snord116 condition [CT(0.minute.average)-CT(individual.value)]. 0-minute-normalized CT values (0dCT) were then pooled across transfection trial and assessed for normality. For **Figure 4A-D**, 2-Way ANOVAs with Šídák's multiple comparisons test within timepoints were run on each 3'UTR excluding the 0-min timepoints. 2^{0dCT} are displayed in Figure 4A-D. For figure 4E, +Snord116 CTs were normalized to average -Snord116 CTs within transfection trial, 3'UTR, and timepoints. [CT(-Snord116.average(TransfectionTrial'x'.Timepoint'y'.3'UTR'z'))-CT(individual.value(TransfectionTrial'x'.Timepoint'y'.3'UTR'z'))] These -Snord116 normalized CT values were analyzed using 2-Way ANOVA with Šídák's multiple comparisons test excluding 0-minute timepoints. $2^{(-snord116.normalized.CTs)}$ are graphed. For decay rate, 0-minute-normalized CT values were used to calculate CT differences between one timepoint and the

next successive timepoint and adjusted for 45-minute intervals. Individual CT values were normalized to the average CT value of the previous timepoint within a condition. These values were used to perform 2-Way ANOVAs with Šídák's multiple comparisons test within 3'UTR, shown in **Figure 4G** and within 3'UTR/Snord116 for **Supplemental Figure 1**. Normalized CT values were adjusted to percentage values for graphs $[(1-(2^{(decay.rate.normalized.CT)}))*100]$. CT values used are provided in Supplemental File 2.

Acknowledgements

We would like to thank Joe Grieco (Virginia Tech) for his assistance in Western Blots and Dr. Stefan Stamm (University of Kentucky), for the gift of the mouse Snord116 expression vector. The work was funded by a grant (#532939) from the Foundation for Prader-Willi Research (FPWR) to D.J.G., an internal grant to the Adaptive Brain and Behavior Destination Area at Virginia Tech to D.J.G, and a student research award from Sigma Xi to M.A.K.

Author Contributions

Matthew A. Kocher conceived of, designed, and performed the experiments, the analysis of the data and the writing of the manuscript. Deborah J. Good conceived of and designed the experiments and performed the writing of the manuscript. Fenix W. Huang performed RNA-RNA interaction predictions and edited the manuscript. Erin Le generated reporter constructs and edited the manuscript.

Conflict of Interest Statement

D.J.G. receives funding from the BASF Chemical Company, Berkeley, CA for a PWS-related project, but none of these funds were used for the project reported herein.

4.6 References

1 Butler, M.G., Miller, J.L. and Forster, J.L. (2019) Prader-Willi Syndrome - Clinical Genetics, Diagnosis and Treatment Approaches: An Update. Curr. Pediatr. Rev., 15, 207-244.

2 Tan, Q., Potter, K.J., Burnett, L.C., Orsso, C.E., Inman, M., Ryman, D.C. and Haqq, A.M. (2020) Prader-Willi-Like Phenotype Caused by an Atypical 15q11.2 Microdeletion. Genes (Basel), 11.
3 Burnett, L.C., LeDuc, C.A., Sulsona, C.R., Paull, D., Rausch, R., Eddiry, S., Carli, J.F., Morabito, M.V., Skowronski, A.A., Hubner, G. et al. (2017) Deficiency in prohormone convertase PC1 impairs prohormone processing in Prader-Willi syndrome. J. Clin. Invest., 127, 293-305.
4 Coyle, C.A., Jing, E., Hosmer, T., Powers, J.B., Wade, G. and Good, D.J. (2002) Reduced voluntary activity precedes adult-onset obesity in Nhlh2 knockout mice. Physiol. Behav., 77, 387-402.
5 Cogliati, T., Delgado-Romero, P., Norwitz, E.R., Guduric-Fuchs, J., Kaiser, U.B., Wray, S. and Kirsch, I.R. (2007) Pubertal impairment in Nhlh2 null mice is associated with hypothalamic and pituitary deficiencies. Mol. Endocrinol., 21, 3013-3027.
6 Good, D.J., Porter, F.D., Mahon, K.A., Parlow, A.F., Westphal, H. and Kirsch, I.R. (1997) Hypogonadism and obesity in mice with a targeted deletion of the Nhlh2 gene. Nat. Genet., 15, 397-401.
7 Morales, J.S., Valenzuela, P.L., Pareja-Galeano, H., Rincon-Castanedo, C., Rubin, D.A. and Lucia, A. (2019) Physical exercise and Prader-Willi syndrome: A systematic review. Clin. Endocrinol. (Oxf), 90, 649-661.
8 Bekx, M.T., Carrel, A.L., Shriver, T.C., Li, Z. and Allen, D.B. (2003) Decreased energy expenditure is caused by abnormal body composition in infants with Prader-Willi Syndrome. J. Pediatr., 143, 372-376.
9 Good, D.J. and Braun, T. (2013) NHLH2: at the intersection of obesity and fertility. Trends Endocrinol. Metab., 24, 385-390.
10 Fox, D.L. and Good, D.J. (2008) Nescient helix-loop-helix 2 interacts with signal transducer and activator of transcription 3 to regulate transcription of prohormone convertase 1/3. Mol. Endocrinol., 22, 1438-1448.
11 Wankhade, U.D. and Good, D.J. (2011) Melanocortin 4 receptor is a transcriptional target of nescient helix-loop-helix-2. Mol. Cell. Endocrinol., 341, 39-47.
12 Kruger, M., Ruschke, K. and Braun, T. (2004) NSCL-1 and NSCL-2 synergistically determine the fate of GnRH-1 neurons and control necdin gene expression. EMBO J, 23, 4353-4364.
13 Al Rayyan, N., Wankhade, U.D., Bush, K. and Good, D.J. (2013) Two single nucleotide polymorphisms in the human nescient helix-loop-helix 2 (NHLH2) gene reduce mRNA stability and DNA binding. Gene, 512, 134-142.
14 Al Rayyan, N., Zhang, J., Burnside, A.S. and Good, D.J. (2014) Leptin signaling regulates hypothalamic expression of nescient helix-loop-helix 2 (Nhlh2) through signal transducer and activator 3 (Stat3). Mol. Cell. Endocrinol., 384, 134-142.
15 Belsham, D.D., Cai, F., Cui, H., Smukler, S.R., Salapatek, A.M. and Shkreta, L. (2004) Generation of a phenotypic array of hypothalamic neuronal cell models to study complex neuroendocrine disorders. Endocrinology, 145, 393-400.
16 Good, D.J. and Kocher, M.A. (2017) Phylogenetic Analysis of the SNORD116 Locus. Genes (Basel), 8.
17 Sobell, H.M. (1985) Actinomycin and DNA transcription. Proc. Natl. Acad. Sci. U S A, 82, 5328-5331.

18 Sobell, H.M., Jain, S.C., Sakore, T.D. and Nordman, C.E. (1971) Stereochemistry of actinomycin--DNA binding. Nat. New. Biol., 231, 200-205.
19 Bochukova, E.G., Lawler, K., Croizier, S., Keogh, J.M., Patel, N., Strohbehn, G., Lo, K.K., Humphrey, J., Hokken-Koelega, A., Damen, L. et al. (2018) A Transcriptomic Signature of the Hypothalamic Response to Fasting and BDNF Deficiency in Prader-Willi Syndrome. Cell Rep., 22, 3401-3408.
20 Falaleeva, M., Surface, J., Shen, M., de la Grange, P. and Stamm, S. (2015) SNORD116 and SNORD115 change expression of multiple genes and modify each other's activity. Gene, 572, 266-273.
21 Polex-Wolf, J., Lam, B.Y., Larder, R., Tadross, J., Rimmington, D., Bosch, F., Cenzano, V.J., Ayuso, E., Ma, M.K., Rainbow, K. et al. (2018) Hypothalamic loss of Snord116 recapitulates the hyperphagia of Prader-Willi syndrome. J. Clin. Invest., 128, 960-969.
22 Bazeley, P.S., Shepelev, V., Talebizadeh, Z., Butler, M.G., Fedorova, L., Filatov, V. and Fedorov, A. (2008) snoTARGET shows that human orphan snoRNA targets locate close to alternative splice junctions. Gene, 408, 172-179.
23 Bittel, D.C., Kibiryeva, N., McNulty, S.G., Driscoll, D.J., Butler, M.G. and White, R.A. (2007) Whole genome microarray analysis of gene expression in an imprinting center deletion mouse model of Prader-Willi syndrome. Am. J. Med. Genet. A., 143A, 422-429.
24 Coulson, R.L., Powell, W.T., Yasui, D.H., Dileep, G., Resnick, J. and LaSalle, J.M. (2018) Prader-Willi locus Snord116 RNA processing requires an active endogenous allele and neuron-specific splicing by Rbfox3/NeuN. Hum. Mol. Genet., 27, 4051-4060.
25 Wu, H., Yin, Q.F., Luo, Z., Yao, R.W., Zheng, C.C., Zhang, J., Xiang, J.F., Yang, L. and Chen, L.L. (2016) Unusual Processing Generates SPA LncRNAs that Sequester Multiple RNA Binding Proteins. Mol. Cell, 64, 534-548.
26 Yin, Q.F., Yang, L., Zhang, Y., Xiang, J.F., Wu, Y.W., Carmichael, G.G. and Chen, L.L. (2012) Long noncoding RNAs with snoRNA ends. Mol. Cell, 48, 219-230.
27 Powell, W.T., Coulson, R.L., Crary, F.K., Wong, S.S., Ach, R.A., Tsang, P., Alice Yamada, N., Yasui, D.H. and Lasalle, J.M. (2013) A Prader-Willi locus lncRNA cloud modulates diurnal genes and energy expenditure. Hum. Mol. Genet., 22, 4318-4328.
28 Yugami, M., Kabe, Y., Yamaguchi, Y., Wada, T. and Handa, H. (2007) hnRNP-U enhances the expression of specific genes by stabilizing mRNA. FEBS Lett., 581, 1-7.
29 Chang, T.H., Huang, H.Y., Hsu, J.B., Weng, S.L., Horng, J.T. and Huang, H.D. (2013) An enhanced computational platform for investigating the roles of regulatory RNA and for identifying functional RNA motifs. BMC Bioinformatics, 14 Suppl 2, S4.
30 Agarwal, V., Bell, G.W., Nam, J.W. and Bartel, D.P. (2015) Predicting effective microRNA target sites in mammalian mRNAs. Elife, 4.
31 Juzwik, C.A., S, S.D., Zhang, Y., Paradis-Isler, N., Sylvester, A., Amar-Zifkin, A., Douglas, C., Morquette, B., Moore, C.S. and Fournier, A.E. (2019) microRNA dysregulation in neurodegenerative diseases: A systematic review. Prog. Neurobiol., 182, 101664.
32 Wu, J., He, J., Tian, X., Luo, Y., Zhong, J., Zhang, H., Li, H., Cen, B., Jiang, T. and Sun, X. (2020) microRNA-9-5p alleviates blood-brain barrier damage and neuroinflammation after traumatic brain injury. J. Neurochem., 153, 710-726.
33 Hawley, Z.C.E., Campos-Melo, D. and Strong, M.J. (2019) MiR-105 and miR-9 regulate the mRNA stability of neuronal intermediate filaments. Implications for the pathogenesis of amyotrophic lateral sclerosis (ALS). Brain. Res., 1706, 93-100.

34 Plass, M., Rasmussen, S.H. and Krogh, A. (2017) Highly accessible AU-rich regions in 3' untranslated regions are hotspots for binding of regulatory factors. PLoS Comput. Biol., 13, e1005460.
35 Zuccotti, P., Peroni, D., Potrich, V., Quattrone, A. and Dassi, E. (2020) Hyperconserved Elements in Human 5'UTRs Shape Essential Post-transcriptional Regulatory Networks. Front. Mol. Biosci., 7, 220.
36 Chen, H., Victor, A.K., Klein, J., Tacer, K.F., Tai, D.J., de Esch, C., Nuttle, A., Temirov, J., Burnett, L.C., Rosenbaum, M. et al. (2020) Loss of MAGEL2 in Prader-Willi syndrome leads to decreased secretory granule and neuropeptide production. JCI Insight, 5.
37 Good, D.J., Li, M. and Deater-Deckard, K. (2015) A Genetic Basis for Motivated Exercise. Exerc. Sport. Sci. Rev., 43, 231-237.
38 Jiang, H. and Good, D.J. (2016) A molecular conundrum involving hypothalamic responses to and roles of long non-coding RNAs following food deprivation. Mol. Cell. Endocrinol., 438, 52-60.
39 Jiang, H., Modise, T., Helm, R., Jensen, R.V. and Good, D.J. (2015) Characterization of the hypothalamic transcriptome in response to food deprivation reveals global changes in long noncoding RNA, and cell cycle response genes. Genes Nutr., 10, 48.
40 Busch, A., Richter, A.S. and Backofen, R. (2008) IntaRNA: efficient prediction of bacterial sRNA targets incorporating target site accessibility and seed regions. Bioinformatics, 24, 2849-2856.
41 Mann, M., Wright, P.R. and Backofen, R. (2017) IntaRNA 2.0: enhanced and customizable prediction of RNA-RNA interactions. Nucleic Acids Res., 45, W435-W439.
42 Raden, M., Ali, S.M., Alkhnbashi, O.S., Busch, A., Costa, F., Davis, J.A., Eggenhofer, F., Gelhausen, R., Georg, J., Heyne, S. et al. (2018) Freiburg RNA tools: a central online resource for RNA-focused research and teaching. Nucleic Acids Res., 46, W25-W29.
43 Wright, P.R., Georg, J., Mann, M., Sorescu, D.A., Richter, A.S., Lott, S., Kleinkauf, R., Hess, W.R. and Backofen, R. (2014) CopraRNA and IntaRNA: predicting small RNA targets, networks and interaction domains. Nucleic Acids Res., 42, W119-123.
44 Lorenz, R., Bernhart, S.H., Höner zu Siederdissen, C., Tafer, H., Flamm, C., Stadler, P.F. and Hofacker, I.L. (2011) ViennaRNA Package 2.0. Algorithms for Molecular Biology, 6, doi:10.1186/1748-7188-1186-1126.

4.7 Supplemental Figures

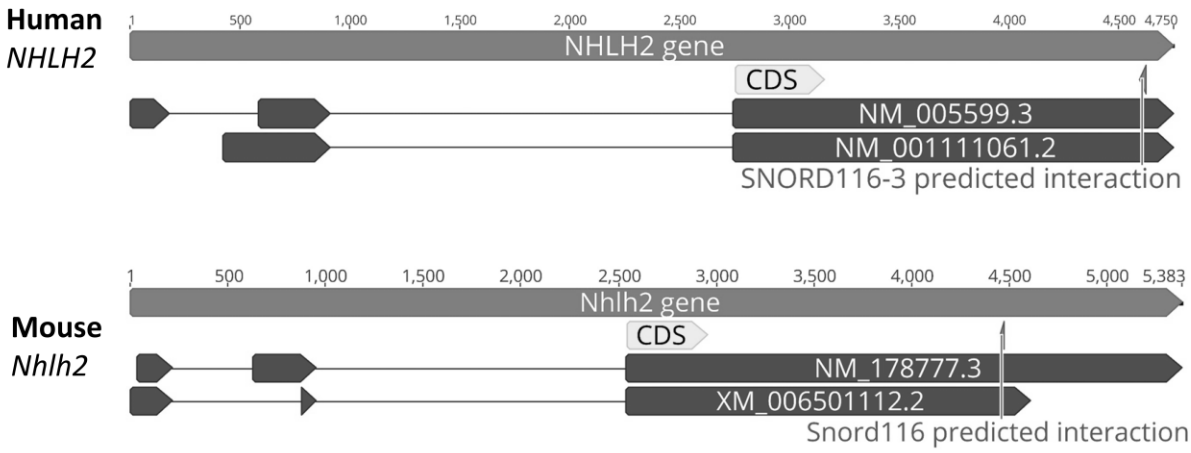

Supplemental Figure 1: All Splice Variants of NHLH2 contain predicted SNORD116 interaction site. Splice variants for human and mouse NHLH2/Nhlh2. NCBI sequence accession numbers given within the third exon of the cartoon for the splice variant. The coding region is indicated by the light grey box, CDS (cDNA sequence). The SNORD116 predicted interaction site is shown by the grey line on all splice variants.

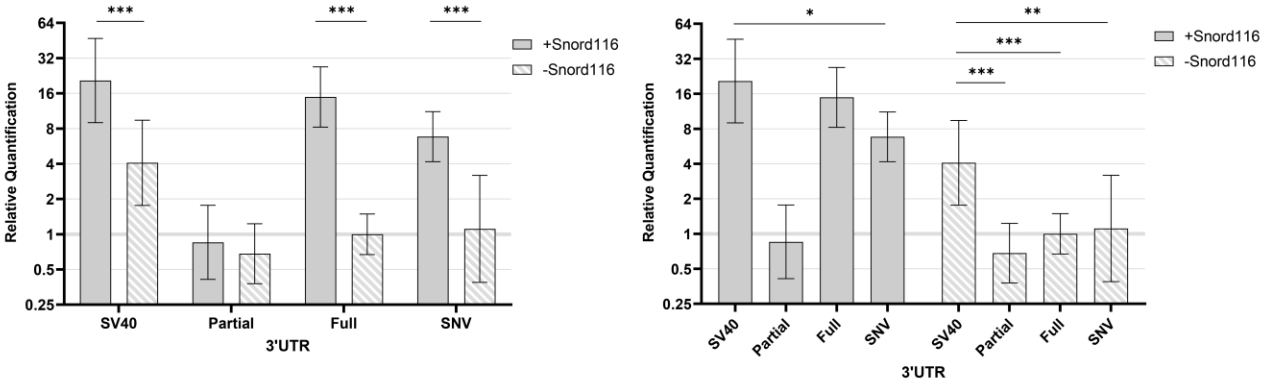

Supplemental Figure 2: Steady State N2myc RNA levels normalized between 3'UTR. Both graphs represent the same data but visually organized differently. N=6 for partial 3'UTR condition; N=9 for SV40, Full, and SNV conditions. Error bars indicate ±SD. *p<0.05, **p<0.01, ***p<0.001.

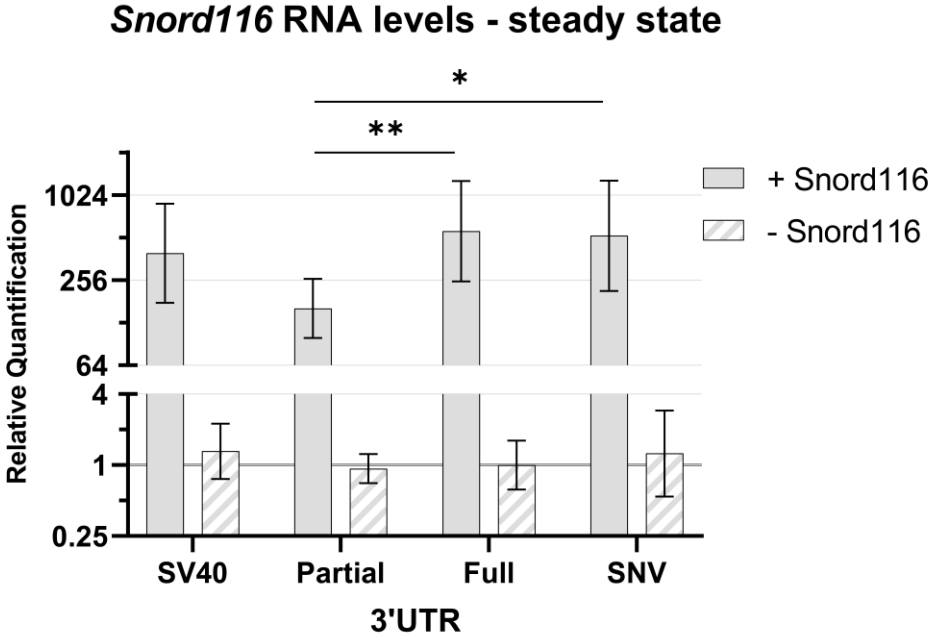

Supplemental Figure 3: Snord116 RNA levels during steady state overexpression. N=6 for partial 3'UTR condition; N=9 for SV40, Full, and SNV conditions. Error bars indicate ±SD. *p<0.05, **p<0.01, ***p<0.001.

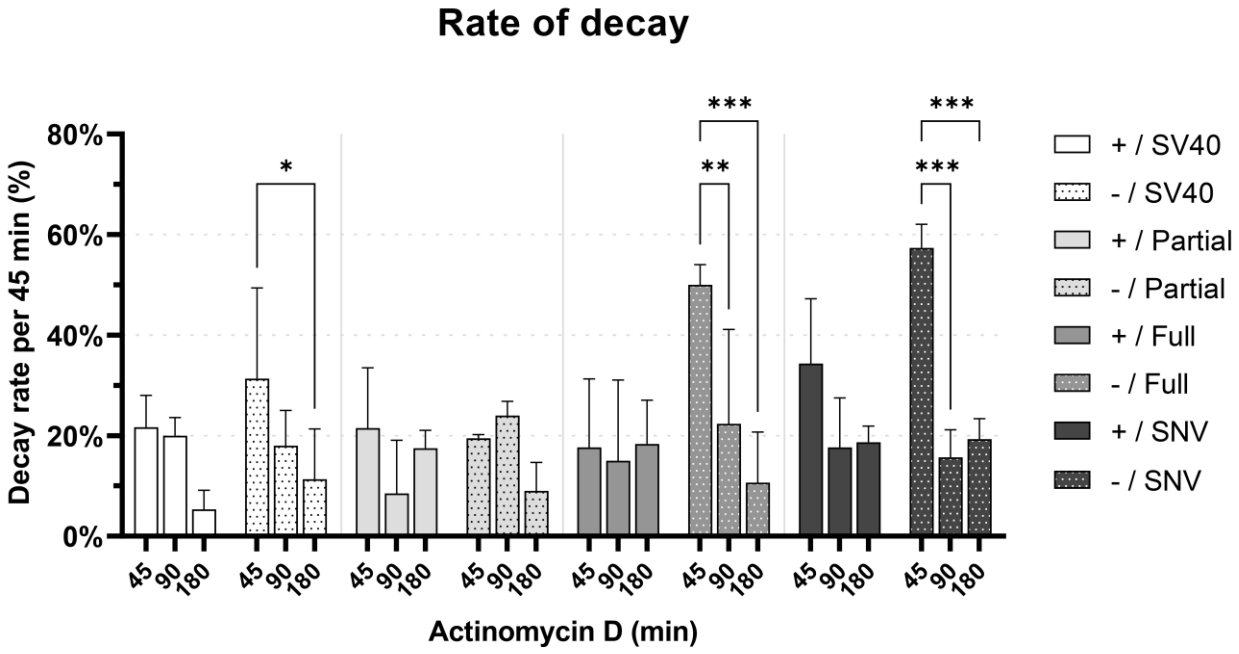

Supplemental Figure 4: Rapid initial decay rate without Snord116 slows over time. Decay rate corresponding to data shown in Figure 4A-D. Decay rate shown as percent decay for each time point, 3'UTR, and Snord116 condition. N=6 for partial 3'UTR condition; N=9 for SV40, Full, and SNV conditions. Error bars indicate +SD. *p<0.05, **p<0.01, ***p<0.001

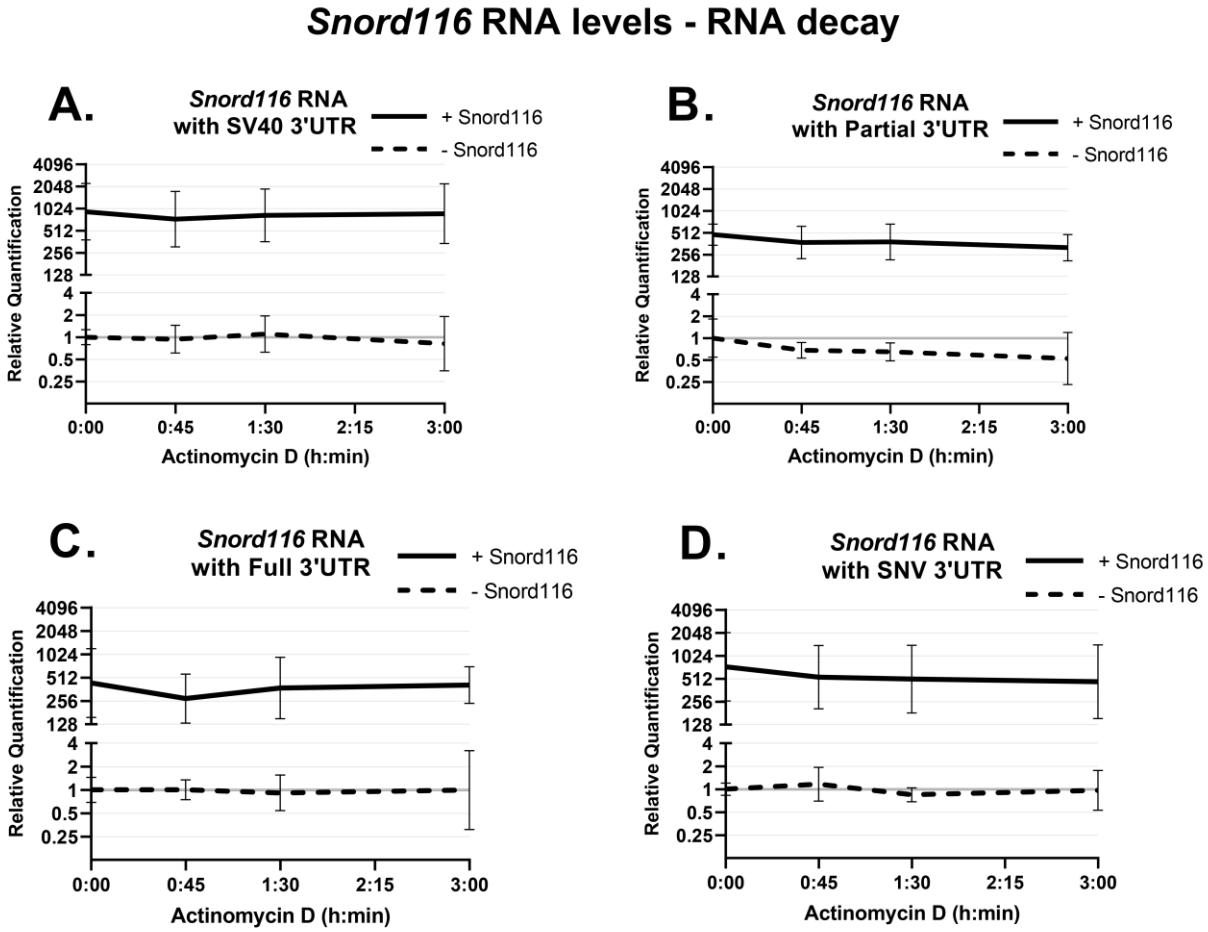

Supplemental Figure 5: Snord116 RNA does not decay during Actinomycin D treatment. A., Snord116 levels co-expressed with SV40 3'UTR. **B.**, Snord116 levels co-expressed with Partial 3'UTR. **C.**, Snord116 levels co-expressed with Full 3'UTR. **D.**, Snord116 levels co-expressed with SNV 3'UTR. N=6 for partial 3'UTR condition; N=9 for SV40, Full, and SNV conditions. Error bars indicate ±SD

A.

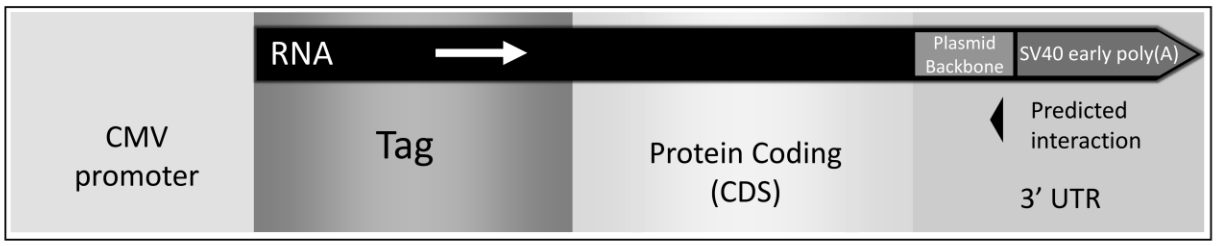

B.

```
SV40 3'UTR
            81       89
             |       |
5'-GGA...AUUA         AGAC...AAC-3'
            CGUAGAUCC
            |:|||||||
            GUAUCUAGG
3'-CCU...AGUA         -5'
            |       |
            9       1
Mouse Snord116-1

interaction energy = -5.53504 kcal/mol
```

Supplemental Figure 6: Location and strength of predicted Snord116 interaction with SV40 3'UTR. A., Model of SV40 reporter with location of predicted interaction site. **B.**, INTA-RNA predicted structure of the displayed site.

Supplemental Table 1. Primers used in the study.

Primer	Function	Sequence
Nhlh2 primer, forward	SNV Mutagenesis	5'-CAGGGTTTTTTTGCGTCTCTGTTGCTT-3'
Nhlh2 primer, reverse	SNV Mutagenesis	5'-AAAAAGACTAAAATCTTTGGATAGCAGATGTGG-3'
Mouse b-Actin, forward	QPCR	5'-GGAATCCTGTGGCATCCAT-3'
Mouse b-Actin, reverse	QPCR	5'-GGAGGAGCAATGATCTTGATCT-3'
Nhlh2, myc-tag, forward	QPCR	5'-ATGGAGAGCTTGGGCGACCTCA-3'
Nhlh2, myc-tag, reverse	QPCR	5'- TTGGTCCGGACTCAGCATCATCGAAT-3'
Mouse Snord116, forward	QPCR	5'- TGGATCTATGATGATTCCCAG-3'
Mouse Snord116, reverse	QPCR	5'- TGGACCTCAGTTCCGATGAG-3'

Chapter 5. *Snord116* knockdown and paternal knockout models have no effect on *Nhlh2* or *Pcsk1* RNA levels

5.1 Abstract

In PWS mouse models, loss of the *Snord116* gene cluster may decrease RNA and protein expression of the *Nhlh2* and *Pcsk1* genes. However, some studies find no difference in these genes of interest. Some of the inconsistency may lie in age of the mice, feeding conditions, methods used, etc. The current study shows that general dissection of PWS mouse model hypothalamus shows no difference in these genes of interest within sex or fed state. Additionally, *Snord116* knockdown in the Neuro2A mouse neuroblastoma cell line has no effect on *Nhlh2* or *Pcsk1* mRNA levels. These data are summarized in the context of recent studies showing various findings.

5.2 Introduction

Recent studies of PWS mouse models have shown that deletion of the gene *Snord116* may lower the levels of *Nhlh2* and *Pcsk1* RNA and protein.[1] However, subsequent studies using RNAseq in specific mouse hypothalamic nuclei have found no difference for either of these genes.[2] Additionally, *Nhlh2* mRNA may be post-transcriptionally stabilized by *Snord116* (Chapter 4, Kocher et al. 2021 under review). Because of the varying results from different studies, we chose to examine Prader-Willi Syndrome (PWS) model mice to potentially resolve a debated topic in the field. Do PWS mice models have low *Nhlh2* or *Pcsk1* gene expression? This topic is critical to the field of PWS research, as dysregulated *Nhlh2* and *Pcsk1* may explain the disease state of PWS. Differing contexts between the various studies surrounding the mouse model may explain the difference in findings. For example, age of mice, fed state of mice, temperature of home cage, subsection of hypothalamus, cell types, etc. may show

different findings.[1–4] Here, we attempt to replicate the setting in which the original finding of differential *Nhlh2* was first found.[1]

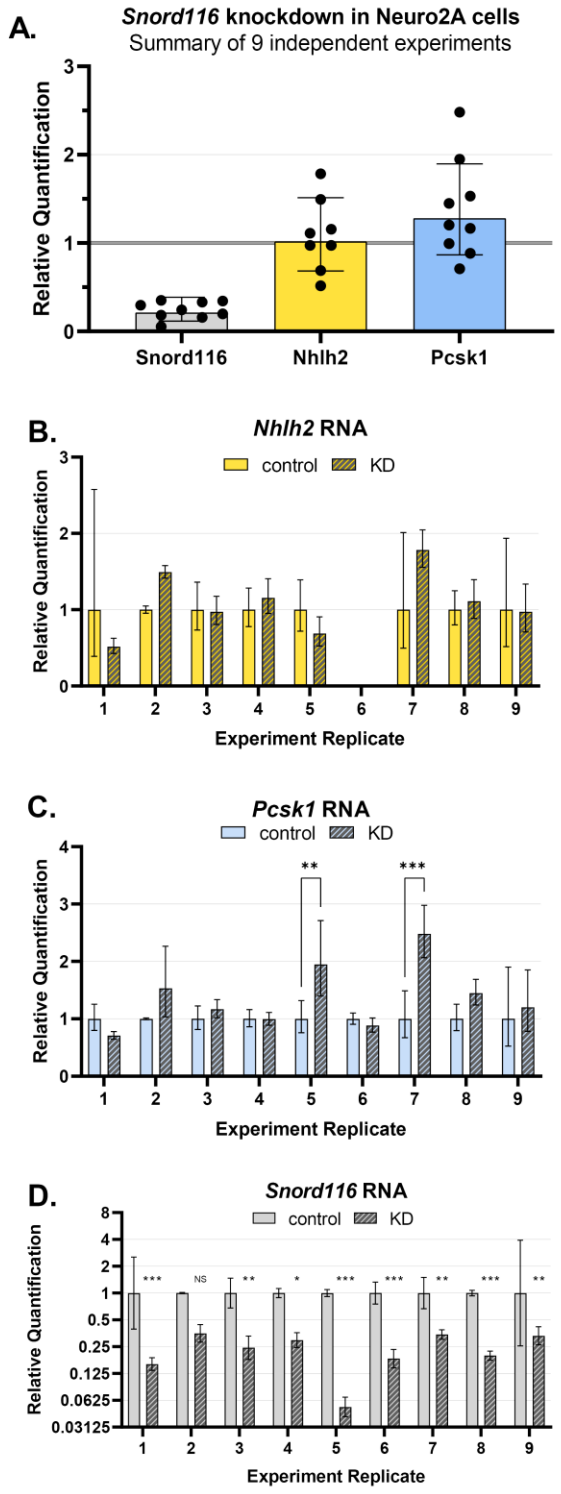

Figure 1. Snord116 in Neuro2A cells has no effect on Nhlh2 or Pcsk1 RNA. A. Summary of 9 independent experiments. **B.** Nhlh2 RNA levels. Experiment 6 did not pass quality control measures. **C.** Pcsk1 RNA levels. 2 out of 9 experiments showed an increase. **D.** Snord116 RNA levels. Experimental replicate 2's sample size was only N=2 after quality control. N=2-6 per condition (x9 experiments). Error bars show SD.

Additionally, to further model PWS, we examined the neuroblastoma cell line Neuro2A (N2A) under *Snord116* knockdown conditions. N2A cells have high levels of endogenous *Snord116* and express endogenous *Nhlh2* and *Pcsk1* RNA, making them a good *in vitro* model to examine the effects of *Snord116* knockdown on the two genes of interest. Anti-sense oligonucleotides (ASOs) designed to target snoRNAs for degradation by RNAse H mechanisms were transfected in N2A cells. ASOs with specific molecular modifications and design are used to target nucleolar RNAs such as snoRNAs because the more commonly used small interfering RNA (siRNA) does not function in the nucleus, as siRNAs make use of the endogenous RNA-induced silencing complex (RISC) that carries out its function in the cytoplasm.[5–8]

5.3 Results

Snord116 knockdown in a mouse neuroblastoma cell line has no effect on *Nhlh2* or *Pcsk1* RNA levels.

Transfection of N2A cells with ASOs led to successful knockdown of *Snord116* RNA as measured by reverse-transcriptase quantitative polymerase chain reaction (RT-QPCR).

Knockdown levels ranged from 5% to 40% of the levels of control conditions (**Figure 1A, 1D**). However, *Nhlh2* and *Pcsk1* RNA levels showed no change in response to *Snord116* knockdown (**Figure 1A-C**).

PWS mouse model hypothalamus shows no effect on *Nhlh2* or *Pcsk1* RNA levels.

As measured by RT-QPCR, whole hypothalamic brain tissue shows no difference between genotype for *Nhlh2* or *Pcsk1* RNA levels (**Figure 2**). Specifically, Male ad-lib fed mice (**Figure 2A**), Male 5-hour refed mice (**Figure 2B**), Female ad-lib fed diestrus mice (**Figure 2C**), and Female 5-hour refed diestrus mice (**Figure 2D**) showed no difference in the genes of interest, although *Snord116* knockout is observed.

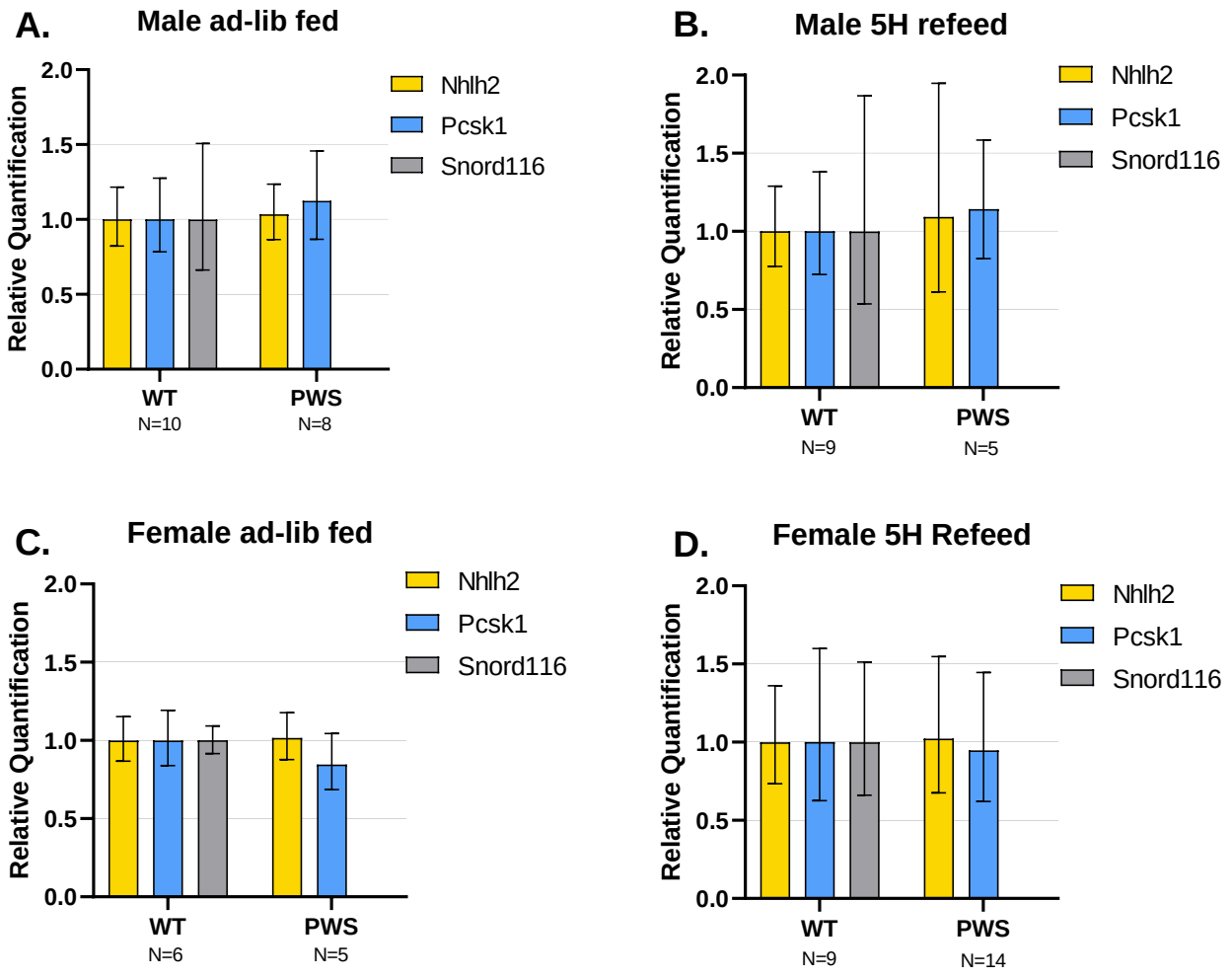

Figure 2. PWS Mouse model hypothalamus shows no difference between *Nhlh2* or *Pcsk1* RNA. A. Male ad-lib fed. **B.** Male 5-hour refed mice. **C.** Female ad-libitum fed. **D.** Female 5-hour refed mice. Sample size is

indicated under X-axis labels. PWS indicates paternal *Snord116* deletion mice. WT indicates wildtype mice. Error bars indicate SD.

5.4 Discussion

The current study does not support the role of mouse *Snord116* in regulating *Nhlh2* or *Pcsk1*. However, there are many caveats to consider when examining the results and synthesizing it with previous findings in the field.

Snord116 knockdown in a mouse neuroblastoma cell line

For the N2A cell line experiments, there are a few contrasting points with Chapter 4 (Kocher et al. 2021, under review). A comparison of key differences between these two studies is displayed in **Table 1**. One of the major differences between the two studies is the cell line used. The current study used Neuro2A cells, a neuroblastoma cell line that can differentiate into neurons.[9,10] Neuroblasts are neural progenitor cells that may have relevance to PWS, as nervous system development may be impaired and PWS can be detected prenatally.[11–14] This differs from the study in Chapter 4, that used N29/2 cells, a mouse hypothalamic neuron cell line.[15] Although both cell lines are immortalized, the two cell lines are at two ends of the spectrum of neuronal differentiation. However, as with many cell lines, it may be argued that an immortalized neuron cell line does not represent the biological system well, as mature differentiated neurons do not typically divide and neurogenesis is limited to specialized areas of the brain such as the olfactory system, the subventricular zone of the lateral ventricles, and the hippocampus. However, there is evidence that neurogenesis also takes place in the adult mouse hypothalamus with implicated roles in the energy balance system.[16,17] Additionally, *Nhlh2* may play a role in the developing nervous system in the ventral telencephalon and the hypothalamus as well as neuroblastoma itself and the energy balance system and gonadotropic system in the mature brain.[18–30] Therefore both of these cell lines may be useful models for examining *Nhlh2* but it is possible the molecular relationships between *Snord116* and *Nhlh2* are divergent. Additionally, some snoRNAs and SNORDs have been implicated in carcinogenesis, although there is no evidence *Snord116* plays a role in cancer.[31–33] It is worth noting that many studies characterizing the molecular role of *Nhlh2* and its regulation have

been performed in N29/2 cells.[24,34–36] However, because N29/2 has such low levels of *Snord116*, the current knockdown approach was more appropriate in the N2A cell line. Further study and consideration may be needed to evaluate the appropriateness for these two cell lines in studies involving *Nhlh2* and *Snord116*.

TABLE 1	**Chapter 4** ***Snord116* overexpression**	**Chapter 5** ***Snord116* knockdown**
Cell type	N29/2 - mouse hypothalamic neuron cell line Low *Snord116, Nhlh2, Pcsk1*	Neuro2A – mouse neuroblastoma cell line Higher *Snord116, Nhlh2, Pcsk1*
***Snord116* manipulation**	*Snord116 e*xpression plasmid with minimal host genes	Knockdown ASO - may have non-specific effects on host gene or other ncRNAs from the genomic locus
***Snord116* levels**	100 – 1000-fold higher than control	2.5 – 20-fold lower than control
Dependent variable	Exogenous Nhlh2 reporter RNA	Endogenous Nhlh2 RNA
Co-transfection	Leptin receptor and Stat3	none
Media	4.5g/mL glucose	1g/mL glucose

Another key difference between the studies from Chapter 4 and the current study of Chapter 5 is the method of *Snord116* RNA manipulation. In N29/2 cells, overexpression was achieved by transfection of a plasmid expressing *Snord116* with minimal host genes involving the PWS genomic locus. This approach may be a more precise approach compared to the current study's *Snord116* knockdown using ASOs. Because of the nature of the genomic locus, detection of *Snord116* by RT-QPCR is not able to differentiate between the mature *Snord116* snoRNP/snoRNA and the many ncRNAs and host genes involved at the PWS genomic locus. Because of this problem, the knockdown experiments cannot be completely confident that only *Snord116* is knocked down, or what the ratio of non-specific effects may be. One approach to examine this specificity is to perform a Northern blot to detect the many species of ncRNAs and host-genes and possible changes that come with the ASO knockdown. The current knockdown study is comparatively less precise than the Chapter 4 study in its *Snord116* manipulation specificity. Additionally, ASOs may trigger toxicity phenotypes although chemical modifications on ASOs are designed to overcome this and use of a control ASO is critical in accounting for this. These various differences between overexpression and

knockdown methodology may contribute to inconsistency in findings between studies and the knockdown approach appears to have more negative points when compared to the overexpression approach.

Related to the *Snord116* manipulation method, the knockdown effect size (2.5 – 20-fold lower than control) was much weaker than the overexpression approach (100 – 1000-fold higher than control). This may also contribute to inconsistency between findings. Genomic deletion of the highly expressed *Snord116* cluster results in a much larger effect size than even 100 – 1000-fold and thus the knockdown approach may be a relatively weak effect size in the grand system.

Additionally, although both Chapter 4 and Chapter 5 studies examined *Nhlh2* RNA level as the dependent variable, the overexpression approach used co-transfected exogenous reporter constructs which allowed observation of key differences dependent on *Nhlh2* 3'UTR. The current study's knockdown approach measured the endogenous levels of *Nhlh2* at the coding sequence, which does not allow observations of splice variant specific effects that may be possible as the results from Chapter 4 would imply. Examining *Nhlh2* splice variants may be achieved using splice-variant specific primers for RT-QPCR. Additionally, with immortalized cell lines the transcripts of some RNAs may drift and the biologically relevant form of the transcript may be lost. Therefore, it is possible that endogenous *Nhlh2* RNA transcripts may be differently transcribed and use of an exogenous reporter RNA may lend more confidence that the RNA in question is truly the one expressed, although there are caveats that come with transfection of an exogenous reporter that must be considered.

Previous studies examining *Nhlh2* including Chapter 4 co-transfected Leptin receptor (LepR) and *Stat3* expression vectors, two genes that are key regulatory components of *Nhlh2.*[34–36] The current knockdown study did not replicate this, and these may be important regulatory components that are not present. Although *Stat3* RNA is expressed in N2A cells, LepR RNA may be at a very low level or not expressed (data not shown). This uncertainty or variability in expression of these genes could be reduced with co-transfection of their expression constructs. It is possible that the regulatory effect *Snord116* has on *Nhlh2* is dependent on these components. Although the logistics and possibility of co-transfecting large 5 – 8kb plasmids with 20nt ASOs may be questioned, it is likely to be possible.

The last major difference between Chapter 4 and Chapter 5 studies is the culture media. The current study used 1g/mL glucose Dulbecco's modified eagle medium (DMEM) while the overexpression study used 4.5g/mL glucose DMEM. The 1g/mL glucose DMEM is often referred to as "low glucose" media although 1g/mL is a "normal" glucose level *in vivo* while the 4.5g/mL glucose DMEM is commonly referred to as "high glucose" and is above diabetic levels *in vivo*.[37] The 4.5g/mL glucose seems to be closer to the more commonly used glucose levels in many *in vitro* experiments, including previous studies of *Nhlh2*, although glucose concentration is not always reported.[35,36]

PWS mouse model hypothalamus

For the *Snord116*del mouse model experiments, main differences between key studies are summarized in **Table 2**. These key studies all observed hypothalamus RNA samples from the same PWS mouse model of whole-body paternal deletion of *Snord116.* These studies also detected *Nhlh2* mRNA with targeted RT-QPCR methods or global RNA approaches via microarray or RNAseq. These key studies include the original finding of differential *Nhlh2* expression in *Snord116* paternal deletion mouse hypothalamus, RNAseq studies examining hypothalamic nuclei that failed to find differences in *Nhlh2*, and a microarray study that found little overall differences between mouse genotypes.[1,2,38] All studies included analysis of whole hypothalamus RNA, while one study also performed RNAseq on hypothalamic nuclei including the paraventricular nucleus (PVN), arcuate nucleus (ARC), ventromedial nucleus of the hypothalamus (VMH), and the dorsomedial nucleus of the hypothalamus (DMH).[2]

Each study had a large variation in age of mice observed, from 5 day old or 13 day old in the microarray study, 8-12 weeks old in the current study, 16-19 weeks old in the RNAseq study, non-specified "adult" mice, and 7 – 11 month old mice. This presents a major problem in comparing these studies, as developmental timepoint is a major influence on gene expression. The study comparing 5 day old mice to 13 day old mice touches upon major differential gene expression between these conditions. The developmental timeline is important to consider in PWS studies, as PWS patients show multiphasic developmental symptoms.[11]

The time of tissue collection can be a major factor in gene expression studies, with some PWS mouse models showing aberrant patterns of circadian related genes and circadian-dependent neurological activity and behavior.[39–42] This is in agreement with reports of PWS

patients that have sleep related symptoms.[11] These findings imply that time of day should be

TABLE 2	Ding et al. 2010 [38]	Burnett et al. 2016 [1]	Polex-Wolf et al. 2018 [2]	Current Study
Method	Microarray whole hypothalamus Whole brain stored in RNAlater overnight and then dissected Lysed in guanidinum thiocyanate reagent	RT-QPCR whole hypothalamus fresh homogenization in guanidinum thiocyanate reagent Same day RNA purification	RNAseq: 4 nuclei, PVN, ARC, VMH, DMH RT-QPCR: whole hypothalamus Whole brain fresh-frozen, cryosection dissection, lysed in guanidinum thiocyanate reagent	RT-QPCR whole hypothalamus fresh homogenization in guanidinum thiocyanate reagent Stored at -20°C before RNA purification
Mouse Age	5 days 13 days	"Adult"	RNAseq: 16-19 weeks QPCR: 7-11 months	8-12 weeks
Fed state	6-hour fasted (5 day old mice only) Ad-lib fed	16-hour overnight fasted 16-hour overnight fasted +5-hour refeed	24-hour fasted Ad-lib fed	Ad-lib fed 16-hour overnight fasted +5-hour refeed
Time of tissue collection	3pm – 4pm	Fasted – 9am 5-hour refed – 2pm	None described	12pm - 2pm
Sex	Male and Female	Male	Male	Male and Female
Sample size	N=1-5 mice per pooled RNA sample (median 4) N=2-4 pooled RNA samples	N = 11-15 per condtion	RNAseq: N=4-6 QPCR: N=3-6	N=5-14 (median 8.5)
Difference between genotypes?	No	*Nhlh2* – yes, refed and fasted *Pcsk1* – no, p=0.09 for fasted	No (*Nhlh2, Pcsk1, Pomc, Npy,Lepr, Agrp*)	No

considered when collecting samples. There is some slight variation in sample collection time

between the studies examined, although some differences are unavoidable due to what was prioritized for some studies. Unfortunately, the RNAseq study of Polex-Wolf et al. did not report time of sample collection.[2] Additionally, the Burnett et al. study contained both fasted and refed animals, and due to the logistical nature of this experiment it was prioritized to keep the total overnight fasting times consistent between these cohorts, so a comparison between fasted and refed states here may possibly contain some circadian effects (personal communication). However, genotype differences within fed state still showed differences for *Nhlh2* in both fed states and times of day.[1] Because the current study of Chapter 5 attempted to replicate this study, which found differences in *Nhlh2* between PWS and WT mice, we chose to replicate the 5-hour refeed and include an ad-lib fed condition rather than a fasted condition. These conditions may be more relevant for observing changes with *Nhlh2* RNA as its levels are low during fasted states and increases upon feeding and potentially peaks in expression levels around 2-hours of leptin stimulation and/or refeeding.[36,43] This design also allows the current study to minimize any circadian effects by collecting samples at the same time of day. Of note, the Burnett et al. study reports that WT *Snord116* increases with refeeding, however this may in part be a circadian effect, as expression of the *Snord116* host-gene transcriptional unit is affected by time of day, showing increased signal during light hours.[1,40] However, these potential effects due to fed state and circadian timing seem to be irrelevant for *Nhlh2* expression differences between PWS and WT mice, as changes in *Nhlh2* were observed in both conditions.[1] In summary, the current study should partially replicate the circadian conditions of Burnett et al. that found *Nhlh2* differences in PWS mouse models.

The fed state of mice also shows variation between studies. There is a combination of ad-libitum fed, fasted, and 5-hour refed across the studies. Fed state is worth noting due to the interest in hyperphagia, obesity, energy expenditure, hypothalamic energy signaling, hormonal changes, etc. surrounding PWS and the mouse model. Aberrant patterns of POMC-NPY feeding balance signals are observed in genetic obesity, diet induced obesity, and in *Snord116* bi-allelic deletion mouse models. Additionally bi-allelic deletion of *Snord116* in only the NPY neurons recapitulates nearly all of the same phenotypes as whole body congenital deletions.[1,3,4,44–46] Additionally, *Nhlh2* responds to fed state, as it shows low expression during fasting and increases with refeeding and leptin stimulation, potentially peaking at 2-hours postprandial time.[36,43] Therefore, it may be more likely to observe differences in *Snord116*-

dependent *Nhlh2* RNA levels during periods of *Nhlh2* increase, where effect sizes are potentially larger. Additionally, because *Nhlh2* responds to leptin signals, the temporal pattern of this transcription factor may be an important component that is regulated by *Snord116.* The current study replicated a fed condition that observed differences in *Nhlh2* in Burnett et al.

In summary, the current study replicated favorable conditions in which *Nhlh2* differences were observed between PWS paternal deletion mice and WT mice. However, there are differences in age (e.g. “adult mice”, and 8-12 week old mice) which cannot be overlooked. Additionally, there are implicit details that may be divergent between studies, such as the precise area dissected of the hypothalamus. It is possible the current study did not include the exact same portion of hypothalamus as Burnett et al.; however, RNA-seq studies examining specific hypothalamic nuclei did not find differences either, suggesting it may not be an issue of brain subregion. Additionally, all these studies used brain tissue without cell sorting to examine specific cell types such as neurons, and neuron sub-populations. *Nhlh2* and *Snord116* are mainly neuronally expressed genes so there may be some reduction of observable effect size when brain tissue with all cell types is used. Furthermore, *Nhlh2* may only be expressed in a relatively small subpopulation of hypothalamic neurons, such as a high proportion of *Kiss1* neurons or only about a third of rostral arcuate *POMC* neurons.[23,47] This cell-type specificity may be important and could be missed when brain tissue RNA is used. High diversity of neuron cell types in the brain and its subregions make single-cell RNA sequencing techniques an attractive approach for future directions, as well as RNA *in situ* hybridization techniques that may identify cell types and subregions with co-expression of our genes of interest. Approaches with the spatial resolution to detect RNA transcripts within cellular compartments may also reveal co-localization effects.

As mentioned, the data in Chapter 4 shows that *Snord116* stabilizes *Nhlh2* mRNA, protecting it from RNA degradation at the 45-minute timepoint. This suggests that the timing of *Nhlh2* transcriptional activity should be examined with higher precision in PWS mouse models. A potential improvement on the current study may be to leptin stimulate the mice and take hypothalamus samples at the key 45-minute post-leptin timepoint, as well as other timepoints if possible. It is also possible the data from the current study was subject to less than perfect dissection methods, RNA purification methods, or RT-QPCR methods that limited any potential

findings. However, the high variability observed between studies of PWS mouse models is not uncommon, as discussed in the literature review in Chapter 2.

In conclusion, both knockdown of *Snord116* in Neuro2A cells and paternal deletion of *Snord116* in mice failed to recapitulate findings that *Nhlh2* RNA levels are reduced with loss of *Snord116*. Nuances to these studies and context of other findings suggest there are improvements that could be made in the current study's approach regarding consideration of *Nhlh2* RNA splice variants, leptin signaling, and cell type specificity.

5.5 Methods

Mouse care and tissue collection

All animal protocols were approved by local Institutional Animal Care and Use Committee at Virginia Polytechnic Institute and State University. All mice were on a C57BL/6J background with *Snord116* paternal deletion mice (B6[Cg]-Snord116tm1.1Uta/J Stock No: 008149 | 1-loxp (KO), Snord116del) obtained from Jackson Laboratories. Genotyping was performed as reported.[48] Mice were housed at room temperature at about 22°C with 12-hour light/dark cycles at 7am and 7pm and ad-libitum access to food (4.5% crude fat) and water. Mice were weaned at 3 weeks old and housed with littermates of the same sex. For tissue dissection, mice were euthanized between 8 and 12 weeks old by CO2 asphyxiation and decapitated between 12pm and 2pm. Brains were then dissected using a brain block and surgical tools, and whole hypothalamus tissue was lysed in TRIzol using a rotor stator homogenizer. TRIzol samples were stored at -20°C until RNA purification (1 week – 1 year). Fresh/autoclaved rotor stator homogenizers were used between samples.

For ad-lib fed conditions, mice were euthanized in home cages or separated from littermates if needed before euthanization.

For 5-hour refeed conditions, between 5pm – 6pm mice were separated from home cages and singly housed in cages without food or bedding (to prevent mice from eating bedding). The following day, food was reintroduced at 9am until mice were euthanized at 2pm and tissue was collected. The weight of food and mice were measured before food deprivation, before food reintroduction, and at euthanization.

Female mice estrous cycles were checked between 8am – 11am using PBS washes and observed under a microscope. Animals observed to be in diestrus were then euthanized for tissue collection at 1pm for ad-lib fed conditions. For 5-hour refeed conditions, female mice observed to be in diestrus were selected for overnight fasting and then refed for 5 hours and euthanized for tissue collection the following day.

Cell Culture and Transfections

The mouse neuroblastoma cell line, Neuro2A, was maintained in T25 flasks in DMEM (1g/L glucose) and 10% fetal bovine serum (GE Healthcare #SH30396.03HI) with penicillin (50 units/mL) /streptomycin (50mg/mL) (Thermo # 15070063) at 4-6% CO2 and 37°C. Cells were detached from flasks using trypsin-EDTA (ThermoFisher # 25300054) and 6-well plates were seeded with 2 x 10^4 - 10^5 cells per well. Transfections were done 2-4 days post seeding using Opti-MEM® media (ThermoFisher # 31985070) and Lipofectamine® 3000 (ThermoFisher #L3000008) according to manufacturer's instructions at 60-90% cell confluence.

Anti-sense oligos (ASO) were 20nt 5nt-10nt-5nt RNA/DNA/RNA with phosphorothioate backbone and methylated RNA.[5–8] Snord116-targetting ASOs and control ASOs targeting nothing were transfected to a final concentration of 100nM, as optimized for *Snord116* knockdown.

RNA Purification

For cell culture, 24 hours post transfection, cell culture media was removed, and cells were lysed with 1mL of TRIzol® Reagent (ThermoFisher #15596018) directly in 6-well culture plates. For mouse hypothalamus, tissue was lysed in TRIzol using a rotor stator homogenizer. TRIzol samples were frozen at -20°C in microfuge tubes until purified (1-14 days for cell culture / 1 week to 1 year for mouse hypothalamus). Thawed TRIzol samples were purified using the TRIzol+Purelink RNA minikit (ThermoFisher #12183025) following manufacturer's instructions for the TRIzol® Plus Total Transcriptome Isolation protocol. Purified RNA was then DNAse treated using TURBO DNA-free™ Kit (ThermoFisher #AM1907) according to manufacturer's instructions, diluted to 60ng/uL in nuclease-free water, and stored at -80°C.

Reverse-Transcriptase Quantitative PCR

For RT-QPCR, Power SYBR® Green RNA-to-CT™ 1-Step Kit (ThermoFisher #4389986) was used according to manufacturer's instructions. 10uL reactions were performed using 150nM final primer concentration. Primers were assessed for efficiency using a dilution series and fell within 90%-110% efficiency. 90ng RNA was used per 10uL reaction. Two to three technical replicates were performed. Control reactions for each sample (No reverse-transcriptase and no-template controls) were used for quality control. 384-well plates were run on the ViiA 7 Real-Time PCR System (ThermoFisher) according to RT-QPCR mix instructions and thermocycling conditions were not modified from suggested protocol (1-step annealing/extension at 60°C). Quality control measures including melt-curve analysis, technical replicate analysis, etc. were analyzed by thermocycler software and by operator; any major errors were excluded from analysis when appropriate, and/or new samples and plates were run when appropriate. Candidate reference genes for ddCT analysis were analyzed for appropriate reference controls. Mouse beta-actin was used as reference gene control for all experiments.

Statistical Analysis

All RT-QPCR data were analyzed using Microsoft Excel 16 for Microsoft 365, IBM SPSS Statistics 26 for Windows, and GraphPad Prism 9.0.0. Number of samples in statistical tests are described in respective figures. Error bars indicate ±SD. The 2^{ddCT} method of relative quantification was used. Statistical significance tests performed on respective ddCT values from which Relative Quantification values are derived. Significance is expressed at *$p<0.05$, **$p<0.01$, ***$p<0.001$.

A two-way ANOVA with Bonferroni correction was used for relative expression of RNA normalized to WT or control conditions.

5.6 References

1. Burnett LC, LeDuc CA, Sulsona CR, et al. Deficiency in prohormone convertase PC1 impairs prohormone processing in Prader-Willi syndrome. *J Clin Invest*. 2016;127(1):293-305. doi:10.1172/JCI88648

2. Polex-Wolf J, Lam BYH, Larder R, et al. Hypothalamic loss of Snord116 recapitulates the hyperphagia of Prader-Willi syndrome. *J Clin Invest*. 2018;128(3):960-969. doi:10.1172/JCI97007
3. Qi Y, Purtell L, Fu M, et al. Ambient temperature modulates the effects of the Prader-Willi syndrome candidate gene Snord116 on energy homeostasis. *Neuropeptides*. 2017;61:87-93. doi:10.1016/j.npep.2016.10.006
4. Qi Y, Purtell L, Fu M, et al. Hypothalamus Specific Re-Introduction of SNORD116 into Otherwise Snord116 Deficient Mice Increased Energy Expenditure. *J Neuroendocrinol*. 2017;29(10):e12457. doi:https://doi.org/10.1111/jne.12457
5. Liang X-H, Sun H, Nichols JG, Crooke ST. RNase H1-Dependent Antisense Oligonucleotides Are Robustly Active in Directing RNA Cleavage in Both the Cytoplasm and the Nucleus. *Mol Ther*. 2017;25(9):2075-2092. doi:10.1016/j.ymthe.2017.06.002
6. Watts JK, Corey DR. Gene silencing by siRNAs and antisense oligonucleotides in the laboratory and the clinic. *J Pathol*. 2012;226(2):365-379. doi:10.1002/path.2993
7. Liang X, Vickers TA, Guo S, Crooke ST. Efficient and specific knockdown of small non-coding RNAs in mammalian cells and in mice. *Nucleic Acids Res*. 2011;39(3):e13. doi:10.1093/nar/gkq1121
8. Ideue T, Hino K, Kitao S, Yokoi T, Hirose T. Efficient oligonucleotide-mediated degradation of nuclear noncoding RNAs in mammalian cultured cells. *RNA*. 2009;15(8):1578-1587. doi:10.1261/rna.1657609
9. Mao AJ, Bechberger J, Lidington D, Galipeau J, Laird DW, Naus CCG. Neuronal Differentiation and Growth Control of Neuro-2a Cells After Retroviral Gene Delivery of Connexin43 *. *J Biol Chem*. 2000;275(44):34407-34414. doi:10.1074/jbc.M003917200
10. Neuro-2a ATCC ® CCL-131™ Mus musculus brain neuroblastoma. Accessed February 24, 2021. https://www.atcc.org/products/all/CCL-131.aspx/#generalinformation
11. Butler MG, Miller JL, Forster JL. Prader-Willi Syndrome - Clinical Genetics, Diagnosis and Treatment Approaches: An Update. *Curr Pediatr Rev*. 2019;15(4):207-244. doi:10.2174/1573396315666190716120925
12. Butler MG, Sturich J, Myers SE, Gold J-A, Kimonis V, Driscoll DJ. Is gestation in Prader-Willi syndrome affected by the genetic subtype? *J Assist Reprod Genet*. 2009;26(8):461-466. doi:10.1007/s10815-009-9341-7
13. Gross N, Rabinowitz R, Gross-Tsur V, Hirsch HJ, Eldar-Geva T. Prader–Willi syndrome can be diagnosed prenatally. *Am J Med Genet A*. 2015;167(1):80-85. doi:https://doi.org/10.1002/ajmg.a.36812
14. Miller JL, Lynn CH, Driscoll DC, et al. Nutritional Phases in Prader–Willi Syndrome. *Am J Med Genet A*. 2011;155A(5):1040-1049. doi:10.1002/ajmg.a.33951
15. Belsham DD, Cai F, Cui H, Smukler SR, Salapatek AMF, Shkreta L. Generation of a Phenotypic Array of Hypothalamic Neuronal Cell Models to Study Complex Neuroendocrine Disorders. *Endocrinology*. 2004;145(1):393-400. doi:10.1210/en.2003-0946
16. Cheng M-F. Hypothalamic neurogenesis in the adult brain. *Front Neuroendocrinol*. 2013;34(3):167-178. doi:10.1016/j.yfrne.2013.05.001
17. Recabal A, Caprile T, García-Robles M de los A. Hypothalamic Neurogenesis as an Adaptive Metabolic Mechanism. *Front Neurosci*. 2017;11. doi:10.3389/fnins.2017.00190
18. Pelling M, Anthwal N, McNay D, et al. Differential requirements for neurogenin 3 in the development of POMC and NPY neurons in the hypothalamus. *Dev Biol*. 2011;349(2):406-416. doi:10.1016/j.ydbio.2010.11.007

19. Gobel V, Lipkowitz S, Kozak CA, Kirsch IR. NSCL-2: a basic domain helix-loop-helix gene expressed in early neurogenesis. *Cell Growth Differ*. 1992;3(3):143.
20. Itoh F, Nakane T, Chiba S. Gene expression of MASH-1, MATH-1, neuroD and NSCL-2, basic helix-loop-helix proteins, during neural differentiation in P19 embryonal carcinoma cells. *Tohoku J Exp Med*. 1997;182(4):327-336. doi:10.1620/tjem.182.327
21. Krüger M, Ruschke K, Braun T. NSCL-1 and NSCL-2 synergistically determine the fate of GnRH-1 neurons and control necdin gene expression. *EMBO J*. 2004;23(21):4353-4364. doi:10.1038/sj.emboj.7600431
22. McNay DEG, Pelling M, Claxton S, Guillemot F, Ang S-L. Mash1 Is Required for Generic and Subtype Differentiation of Hypothalamic Neuroendocrine Cells. *Mol Endocrinol*. 2006;20(7):1623-1632. doi:10.1210/me.2005-0518
23. Jing E, Nillni EA, Sanchez VC, Stuart RC, Good DJ. Deletion of the Nhlh2 Transcription Factor Decreases the Levels of the Anorexigenic Peptides α Melanocyte-Stimulating Hormone and Thyrotropin-Releasing Hormone and Implicates Prohormone Convertases I and II in Obesity. *Endocrinology*. 2004;145(4):1503-1513. doi:10.1210/en.2003-0834
24. Fox DL, Good DJ. Nescient Helix-Loop-Helix 2 Interacts with Signal Transducer and Activator of Transcription 3 to Regulate Transcription of Prohormone Convertase 1/3. *Mol Endocrinol*. 2008;22(6):1438-1448. doi:10.1210/me.2008-0010
25. Brown L, Espinosa R, Le Beau MM, Siciliano MJ, Baer R. HEN1 and HEN2: a subgroup of basic helix-loop-helix genes that are coexpressed in a human neuroblastoma. *Proc Natl Acad Sci U S A*. 1992;89(18):8492-8496.
26. Giwa A, Fatai A, Gamieldien J, Christoffels A, Bendou H. Identification of novel prognostic markers of survival time in high-risk neuroblastoma using gene expression profiles. *Oncotarget*. 2020;11(46):4293-4305. doi:10.18632/oncotarget.27808
27. Haire MF, Chiaramello A. Transient expression of the basic helix-loop-helix protein NSCL-2 in the mouse cerebellum during postnatal development. *Mol Brain Res*. 1996;36(1):174-178. doi:10.1016/0169-328X(95)00282-W
28. Schmid T, Günther S, Mendler L, Braun T. Loss of NSCL-2 in Gonadotropin Releasing Hormone Neurons Leads to Reduction of Pro-Opiomelanocortin Neurons in Specific Hypothalamic Nuclei and Causes Visceral Obesity. *J Neurosci*. 2013;33(25):10459-10470. doi:10.1523/JNEUROSCI.5287-12.2013
29. Suzuki Y, Tsuruga E, Yajima T, Takeda M. Expression of bHLH Transcription Factors NSCL1 and NSCL2 in the Mouse Olfactory System. *Chem Senses*. 2003;28(7):603-608. doi:10.1093/chemse/bjg051
30. Aoyama M, Ozaki T, Inuzuka H, et al. LMO3 Interacts with Neuronal Transcription Factor, HEN2, and Acts as an Oncogene in Neuroblastoma. *Cancer Res*. 2005;65(11):4587-4597. doi:10.1158/0008-5472.CAN-04-4630
31. Jorjani H, Kehr S, Jedlinski DJ, et al. An updated human snoRNAome. *Nucleic Acids Res*. 2016;44(11):5068-5082. doi:10.1093/nar/gkw386
32. Castle JC, Armour CD, Löwer M, et al. Digital Genome-Wide ncRNA Expression, Including SnoRNAs, across 11 Human Tissues Using PolyA-Neutral Amplification. *PLoS ONE*. 2010;5(7). doi:10.1371/journal.pone.0011779
33. Mannoor K, Liao J, Jiang F. Small nucleolar RNAs in cancer. *Biochim Biophys Acta*. 2012;1826(1). doi:10.1016/j.bbcan.2012.03.005

34. Wankhade UD, Good DJ. Melanocortin 4 Receptor is a Transcriptional Target of Nescient Helix-Loop-Helix-2. *Mol Cell Endocrinol*. 2011;341(1-2):39-47. doi:10.1016/j.mce.2011.05.022
35. AL_Rayyan N, Wankhade U, Bush K, Good DJ. Two Single Nucleotide Polymorphisms in the Human Nescient Helix Loop Helix 2 (NHLH2) Gene Reduce mRNA Stability and DNA Binding. *Gene*. 2013;512(1):134-142. doi:10.1016/j.gene.2012.09.068
36. Rayyan NA, Zhang J, Burnside AS, Good DJ. Leptin Signaling Regulates Hypothalamic Expression of Nescient helix-loop-helix 2 (Nhlh2) Through Signal Transducer and Activator 3 (Stat3). *Mol Cell Endocrinol*. 2014;384(0):134-142. doi:10.1016/j.mce.2014.01.017
37. Glucose in Cell Culture. Sigma-Aldrich. Accessed February 24, 2021. https://www.sigmaaldrich.com/life-science/cell-culture/learning-center/media-expert/glucose.html
38. Ding F, Li HH, Li J, Myers RM, Francke U. Neonatal Maternal Deprivation Response and Developmental Changes in Gene Expression Revealed by Hypothalamic Gene Expression Profiling in Mice. *PLoS ONE*. 2010;5(2). doi:10.1371/journal.pone.0009402
39. Coulson RL, Yasui DH, Dunaway KW, et al. Snord116-dependent diurnal rhythm of DNA methylation in mouse cortex. *Nat Commun*. 2018;9. doi:10.1038/s41467-018-03676-0
40. Powell WT, Coulson RL, Crary FK, et al. A Prader–Willi locus lncRNA cloud modulates diurnal genes and energy expenditure. *Hum Mol Genet*. 2013;22(21):4318-4328. doi:10.1093/hmg/ddt281
41. Pace M, Falappa M, Freschi A, et al. Loss of Snord116 impacts lateral hypothalamus, sleep, and food-related behaviors. *JCI Insight*. 2020;5(12). doi:10.1172/jci.insight.137495
42. Lassi G, Priano L, Maggi S, et al. Deletion of the Snord116/SNORD116 Alters Sleep in Mice and Patients with Prader-Willi Syndrome. *Sleep*. 2016;39(3):637-644. doi:10.5665/sleep.5542
43. Vella KR, Burnside AS, Brennan KM, Good DJ. Expression of the Hypothalamic Transcription Factor Nhlh2 is Dependent on Energy Availability. *J Neuroendocrinol*. 2007;19(7):499-510. doi:10.1111/j.1365-2826.2007.01556.x
44. Qi Y, Purtell L, Fu M, et al. Snord116 is critical in the regulation of food intake and body weight. *Sci Rep*. 2016;6. doi:10.1038/srep18614
45. Purtell L, Qi Y, Campbell L, Sainsbury A, Herzog H. Adult-onset deletion of the Prader-Willi syndrome susceptibility gene Snord116 in mice results in reduced feeding and increased fat mass. *Transl Pediatr*. 2017;6(2):88-97-97.
46. Khor E-C, Fanshawe B, Qi Y, et al. Prader-Willi Critical Region, a Non-Translated, Imprinted Central Regulator of Bone Mass: Possible Role in Skeletal Abnormalities in Prader-Willi Syndrome. *PLoS ONE*. 2016;11(1). doi:10.1371/journal.pone.0148155
47. Mickelsen LE, Flynn WF, Springer K, et al. Cellular taxonomy and spatial organization of the murine ventral posterior hypothalamus. *eLife*. 2020;9. doi:10.7554/eLife.58901
48. Ding F, Li HH, Zhang S, et al. SnoRNA Snord116 (Pwcr1/MBII-85) Deletion Causes Growth Deficiency and Hyperphagia in Mice. *PLOS ONE*. 2008;3(3):e1709. doi:10.1371/journal.pone.0001709

5.7 Supplemental Figures

Supplemental Table 1.

Oligo	Function	Sequence
Mouse b-actin, forward	QPCR	5' GGAATCCTGTGGCATCCAT
Mouse b-actin, reverse	QPCR	5' GGAGGAGCAATGATCTTGATCT
Nhlh2 primer, forward	QPCR	5' CCGAGCTCCGCAAACTACTA
Nhlh2 primer, reverse	QPCR	5' ATGGCCAAGCGCAGAATCTC
Pcsk1 primer, forward	QPCR	5' CATGAAGCAGCCTCGTGTGTA
Pcsk1 primer, reverse	QPCR	5' TTGCCATTCAGGCTCTTTTGTG
Snord116 primer, forward	QPCR	5' TGGATCTATGATGATTCCCAG
Snord116 primer, reverse	QPCR	5' TGGACCTCAGTTCCGATGAG
Snord116 antisense oligo	*In vitro* Knockdown	5' *CUUUU*CCAAGGAATG*UUUGA*
Snord116-scramble antisense oligo	*In vitro* Knockdown control	5' *AGAGA*TTCGTCTTAT*GUAUC*
oIMR7958 WT primer	Mouse genotyping	5’ AATCCCCAACCTACTTCAAACAGTC
oIMR7959 Common primer	Mouse genotyping	5’ TGGATCTCTCCTTGCTTGTTTTCTC
oIMR7960 KO primer	Mouse genotyping	5’ TTTACGGTACATGACAGCACTCAAG

Chapter 6. Gene Expression Profile of Hypothalamus from *Snord116*$^{m+/p-}$ Mice with Dietary Nutraceutical Supplementation

6.1 Abstract

The Prader-Willi syndrome mouse model with paternally inherited deletion of the *Snord116* gene shares many phenotypes with the *Nhlh2* knockout mouse. Homozygous deletion of *Nhlh2* in mice recapitulates many phenotypes of Prader-Willi Syndrome, including obesity, hypogonadism, and developmental delay. A known intervention in *Nhlh2* knockout mouse involving dietary supplementation of conjugated linoleic acid reduces obesity and increases voluntary physical activity in these mice. Because of potential reduction in obesity, the same dietary intervention was tested in *Snord116* paternal deletion mice to test the applicability for translation in to human Prader-Willi Syndrome patients. This chapter focuses on hypothalamus mRNA sequencing results from this study in which we find mild differences between genotypes and diets. These results are discussed in the context of other gene expression studies for PWS mouse model hypothalamus which show variation between studies.

6.2 Introduction

Prader-Willi Syndrome (PWS) patients currently have only one treatment approved by the Food and Drug Administration (FDA), which is growth hormone (GH) supplementation. Currently, there are a handful of experimental therapies in clinical trials to test the reduction of hyperphagia and obesity in PWS, as there is still an unmet need for treating these symptoms in PWS patients.[1] One dietary supplement that may hold promise is conjugated linoleic acid (CLA). Dietary supplementation of CLA in WT mice prevents body weight gain and fat accumulation.[2–5] Furthermore, dietary CLA supplementation also shows benefits for *Nhlh2* knockout mice, a model that shares many phenotypes of PWS patients including obesity, hypogonadism, and developmental delay.[2–11] This mouse model has a reduction in obesity,

reduction in body fat, increase in voluntary physical activity, and an increase in skeletal muscle mass with dietary supplementation of CLA.[2–5]

CLAs are polyunsaturated fatty acids that are structural and geometric isomers of linoleic acid, fatty acids with 18 carbon atoms and 2 double bonds (18:2) both in the *cis* configuration. Conjugated linoleic acids are isomers of linoleic acids where the 2 double bonds are “conjugated”, meaning they don’t have a methylene group separating them.[12,13] The most common CLAs have double bonds in the cis-9, trans-11 structure (CLA-9,11) or trans-10, cis-12 structure (CLA-10,12). The CLA-9,11 isomer is naturally found in ruminant animal food products and is also known as rumenic acid.[12,13] Because of the double bond in the *trans* configuration, CLA is technically a trans fatty acid, however, the associations with trans-fat consumption and negative health outcomes is largely between industrially produced trans-fat consumption, while ruminant-derived trans fats lack these negative health associations.[13] In humans, CLA has shown efficacy against cancer, obesity, and atherosclerosis and is currently “generally recognized as safe” (GRAS) by the FDA.[13] CLA products are commonly marketed as dietary supplements for weight loss in humans.

While CLA has been tested extensively in many mouse models, there is no study examining the effects of CLA in PWS mouse models. The positive benefits seen in *Nhlh2* knockout mice with CLA dietary supplementation are expected to translate to the PWS mouse model and hopefully PWS patients. Furthermore, the mechanisms behind CLA’s effects have been characterized in skeletal muscle, adipose tissue, and other organ systems, but there is little data on potential hypothalamic effects.[13] Understanding this gap in knowledge is valuable, as hypothalamic defects in PWS patients and mouse models are considered the main cause of symptoms.[14,15] *Nhlh2* knockout mice phenotypes are also largely attributed to hypothalamic disturbances, yet the effectiveness of CLA supplementation has not been investigated in the hypothalamus of this mouse model.[2–5,9,10]

The present study focuses on the hypothalamic mRNA expression of mice with paternally inherited deletions of the *Snord116* gene cluster (*Snord116*$^{m+/p-}$), a mouse model for PWS. Wildtype (WT) and *Snord116*$^{m+/p-}$ mice were fed high-fat diets with or without supplementation of CLA (0.33% w/w) from 6-10 weeks old to 25-29 weeks old at brain tissue collection.

6.3 Results

mRNA sequencing of whole hypothalamus shows strongest differences across diet

Whole hypothalamus RNA underwent poly(A) selection, high throughput massively parallel RNA sequencing, alignment to a mouse reference genome, and quantified to gene and RNA annotations. Differential expression analysis was made across genotypes and diets using the DESeq2 plugin for Geneious Prime.[16]

6 comparisons were made between conditions. 3 comparisons were across genotype (PWS/WT) for all diets, within control diet, and within CLA diet. 3 comparisons were across diet (CLA/control) for all genotypes, within WT, and within PWS. **Figure 1** shows a summary of the comparisons made. The effect sizes for all comparisons are relatively weak, with only 6 out of 524 total differentially expressed genes (DEGs) above an absolute Log2 fold change of 0.5 and 4 out 6 of these genes being related to the genomic deletion at the *Snord116* cluster.

Figure 1 Differentially Expressed Genes (DEGs)

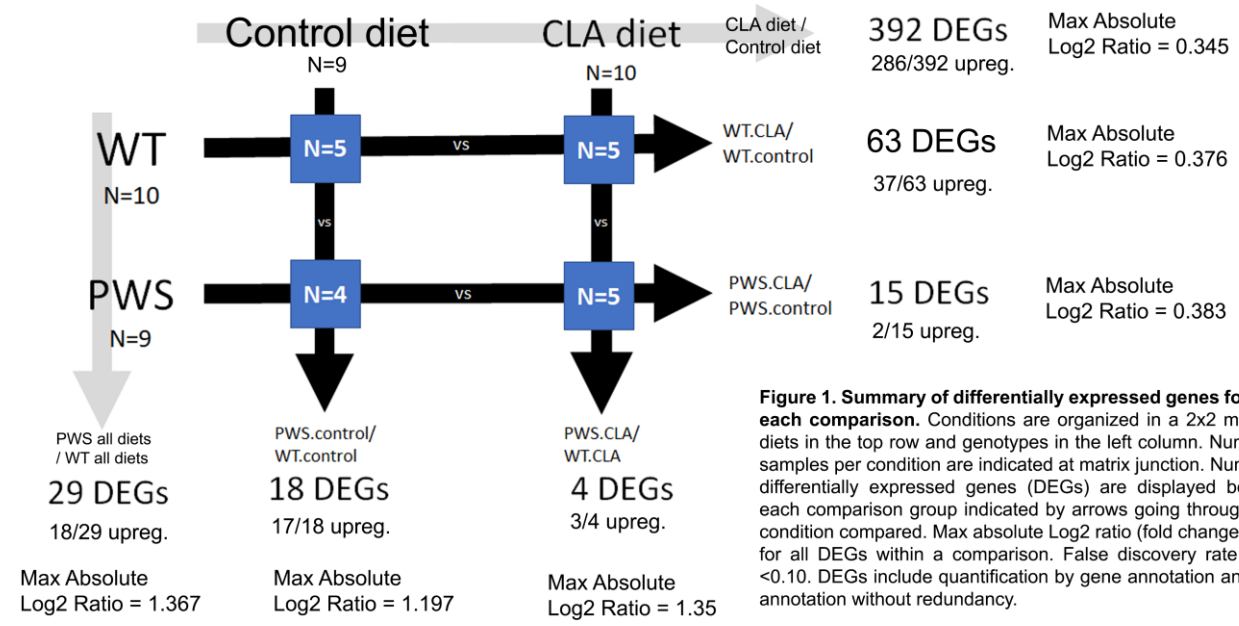

Figure 1. Summary of differentially expressed genes found in each comparison. Conditions are organized in a 2x2 matrix of diets in the top row and genotypes in the left column. Number of samples per condition are indicated at matrix junction. Number of differentially expressed genes (DEGs) are displayed between each comparison group indicated by arrows going through each condition compared. Max absolute Log2 ratio (fold change) found for all DEGs within a comparison. False discovery rate (FDR) <0.10. DEGs include quantification by gene annotation and RNA annotation without redundancy.

5 out of 6 of the comparisons have a majority of DEGs upregulated when compared to the control condition (WT or control diet). Generally, the PWS control diet condition had the least amount of variance between samples, as displayed by the principal component analysis (PCA) plot of **Figure 2**.

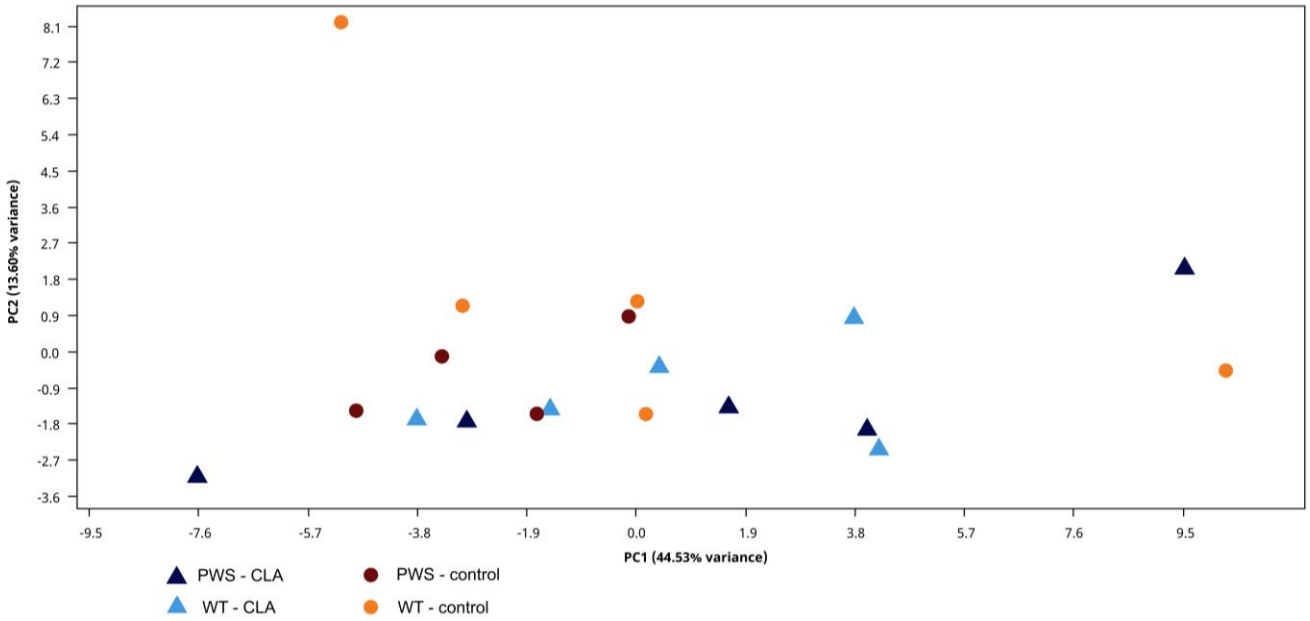

Figure 2. Principal Component Analysis (PCA) plot of all samples. PC1 on the X-axis represents a group of genes that explains 44.53% of the variance across samples. PC2 on the Y-axis represents a group of genes that explains 13.6% of the variance across samples. The closer individual samples are to each other, the less variance there is between them in these two dimensions. Strong evidence for differences between experimental conditions would be displayed by high spatial separation between conditions (high variance across conditions), and low spatial distance within a condition (low variance within a condition).

RT-QPCR validation of select DEGs

A select number of DEGs were chosen to validate by reverse transcriptase quantitative polymerase chain reaction (RT-QPCR). The DEGs listed in **Table 1** were selected for RT-QPCR targets based on high absolute effect size between conditions, high expression levels, highest confidence in differential expression, reproducibility between multiple algorithms, and biological role.

TABLE 1.

Gene	Comparison	Fold change	Gene name
Gria4	WT / PWS (both diets + CLA diet)	1.23 (both diets) 1.27 (CLA diet)	glutamate receptor, ionotropic, AMPA4 subunit
Gabrg2	WT / PWS (both diets)	1.16	gamma-aminobutyric acid (GABA) A receptor, subunit gamma 2
Chmp1b	Control / CLA diets (both genotypes + WT only)	1.27 (both genotypes) 1.29 (WT only)	charged multivesicular body protein 1B
Retreg2	Control / CLA diets (both genotypes + PWS only)	0.89 (both genotypes) 0.85 (PWS only)	reticulophagy regulator family member 2

Of the 7 comparisons among 4 DEGs tested via RT-QPCR, only 2 out of 7 replicated significant differences found by Rna-seq (**Figure 3**).

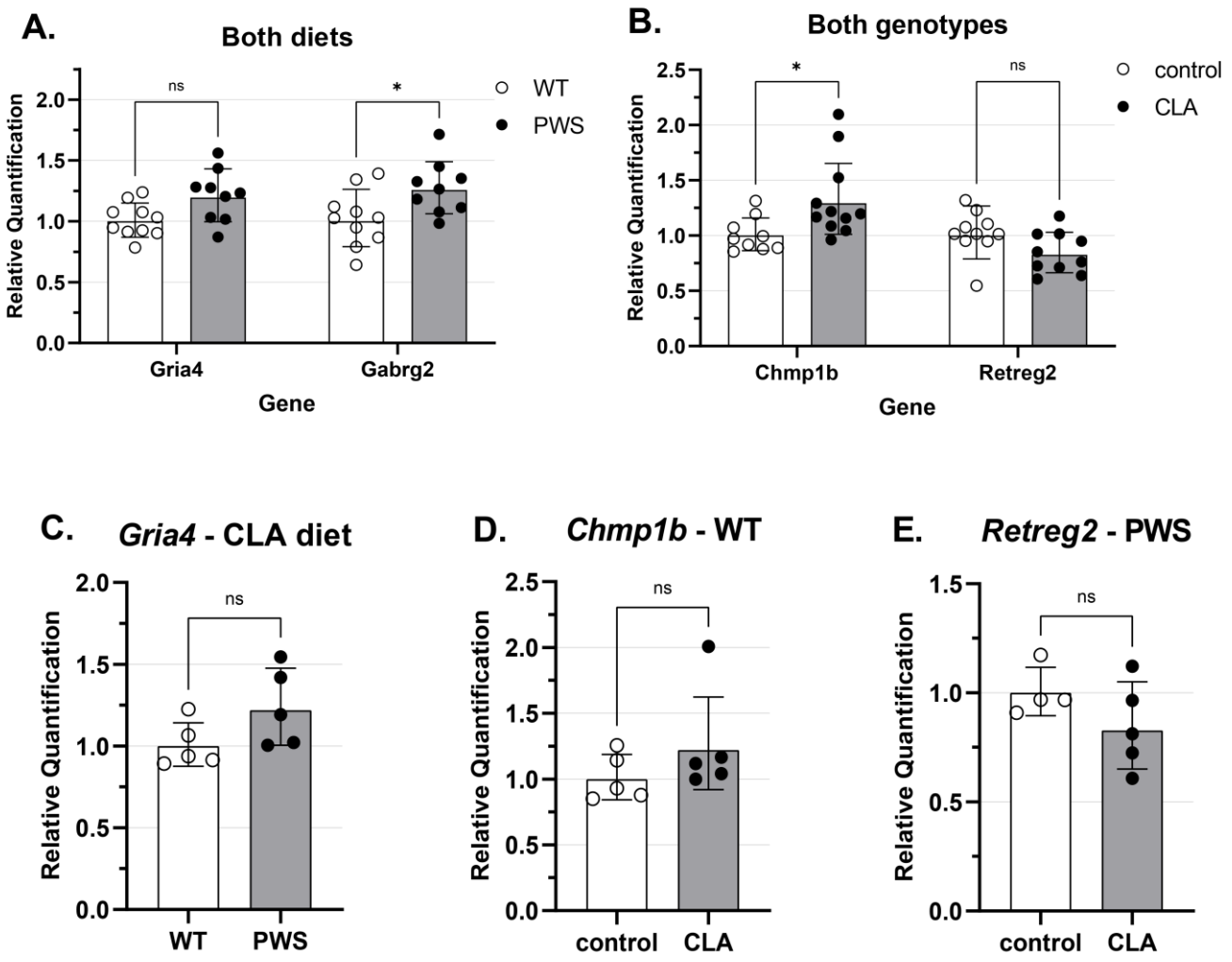

Figure 3. RT-QPCR validation of DEGs found in RNAseq. A. Two DEGs found between genotype regardless of diet. **B.** Two DEGs found between diet regardless of genotype. **C.** DEG between genotypes within CLA diet. **D.** DEG between diets within WT mice. **E.** DEG between diets within PWS mice. Error bars show SD.

6.4 Discussion

Overall, the RNA-seq study found relatively little difference in RNA expression across all conditions examined. The largest effect size for DEGs was only about 2-fold and it was from

IPW, a gene related to the *Snord116* cluster that is partially deleted in the PWS mouse model used. The next highest effect size ranged from 1.36 – 1.56-fold from *Ndn*, another gene that is related to PWS that is often deleted in PWS type 1 large deletions. Interestingly *Ndn* was upregulated in PWS mouse models for all diet conditions but has not yet been verified by RT-QPCR. The weak effect size for all DEGs in the current RNA-seq study also leads to difficulty in validation of DEGs, as RT-QPCR is limited by the sample size in the current study and their natural variability.

The RNA expression of PWS mouse models has been explored before, as discussed in Chapter 5. One study using microarray of neonatal mice hypothalamus also failed to find major differences between WT mice and *Snord116*$^{m+/p-}$ mice.[17] However, this study had pooled samples and a low N between comparisons group, although it could detect strong changes between developmental timepoints. Another microarray study of RNA expression, this time in *Snord116*$^{m-/p-}$ mice, shows increases in many neuropeptide genes including *Pomc*, *Npy*, *Hcrt*, *Pmch*, and *Ghrh*.[18] Magnitude of increases range from 2.2-fold increase in GhRH mRNA to 1.13-fold increase in *Pmch* mRNA, as validated by *in situ* hybridization (ISH).[18] Additionally, another study in *Snord116*$^{m-/p-}$ mice shows increased *Pomc* and *Npy* mRNA via ISH,[19] and another study in *Snord116*$^{m+/p-}$ mice finds increased *Agrp* and *Npy* mRNA with RT-QPCR only during 5-hour refeeding conditions.[20]

For RNA-seq studies, there are two studies done in *Snord116*$^{m+/p-}$ mice. One study examined whole hypothalamus poly(A) RNA, finding nearly 9000 DEGs with an absolute fold change greater than 2.[21] These DEGs include *Nhlh2* (down)*, Pcsk1* (down), *Gria4* (down, opposite of current study), *Gabrg2* (down, opposite of current study), *Retreg2* (down, not a DEG across genotype in current study).[21] There are nearly 50,000 annotated genes in the mouse genome and not all are poly(A) encoding genes, meaning about 18% are differentially expressed in the study described which had a sample size of 3 mice per genotype taken at the beginning of the light period at Zeitgeber time 0.

The other RNA-seq study in *Snord116*$^{m+/p-}$ mouse hypothalamus examined hypothalamic nuclei including the paraventricular nucleus (PVN), arcuate nucleus (ARC), ventromedial hypothalamus (VMH), and dorsomedial hypothalamus (DMH).[22] Unlike previous studies, this study fails to find differences in expression of *Pomc, Npy, Lepr, or Agrp* in the arcuate nucleus that mediates appetite regulation.[22] Even after adult deletion of *Snord116* in

the mediobasal hypothalamus which led to obesity in some mice, obese mice show no difference in these key genes or *Nhlh2* and *Pcsk1*.[22] The only DEG reported in the obese mice is suppressor of cytokine signalling 3 (*Socs3*), which increases in obese mice.[22] This gene is a negative regulator of leptin signaling which may mediate central leptin resistance.[23] Mice with increased *Socs3* in POMC neurons show increased body weight and adiposity.[24] These summary of these gene expression studies shows that there is high variability across all studies investigating PWS mouse model hypothalamus, with some reporting almost no differences and some reporting a high number of DEGs. The central melanocortin system of POMC-NPY/AGRP genes is also variable between studies.

Possible explanations for no major differences observed in the current study could be due to testing the whole hypothalamus rather than hypothalamic nuclei or specific cell types. However, a study that isolates hypothalamic nuclei also reports no major differences in appetite homeostasis genes of interest, suggesting that nuclei isolation may lead to similar outcomes.[22] As of yet, there are no single cell genomics studies in PWS mouse hypothalamus. The single-cell sequencing (scSeq) approach may be an interesting path forward, as the diversity of function and molecular signature is high in brain tissue and hypothalamus, and use of scSeq has helped spatially and functionally map discrete regions.[25] It is possible that changes in gene expression are truly mild in magnitude and below the detection limits of the current study. As discussed in Chapter 5, the developmental timepoint, circadian timepoint, and fed state may influence outcomes in this study. Furthermore, changes in gene expression could be of greater magnitude in other brain regions, such as the pituitary, or other hypothalamic neuron efferent targets such as the hindbrain.

The only DEG between genotypes validated in the current study is *Gabrg2*, gamma-aminobutyric acid (GABA) A receptor, subunit gamma 2. This is a ligand-gated ion channel receptor subunit for the inhibitory neurotransmitter GABA. The mature GABA receptor contains 5 subunits, with about 20 different possible subunits from 8 different isoform classes. The gamma subunit isoform has 3 total genes and contains a benzodiazepine binding site. Mutations in this gene have been linked to epilepsy and anxiety-like behavior in mice.[26–28] In the PVN of the hypothalamus, *Gabrg2* has been implicated in diurnal rhythmicity in metabolism and diet-induced obesity through upstream regulation by the circadian gene *Bmal1*.[29] Loss of *Gabrg2* in the PVN leads to obesity and loss of diurnal rhythm of energy expenditure and food

intake.[29] Additionally, *Gabrg2* is diurnally regulated in the suprachiasmatic nucleus (SCN) of hamster and mice.[30] The current study shows that PWS mice have an increase in *Gabrg2* expression across all diets. There is little known about how upregulation of this gene may affect this behavior, although it may suggest a normal diurnal rhythm of metabolism. Data collected from the main study may want to examine the diurnal activity of PWS mouse models, with the additional consideration that PWS mouse models show disrupted circadian-related behavior.[21,31–33]

Regarding the CLA diet, this is the first RNA-seq study examining the hypothalamus in mice with a CLA supplemented diet to the author's knowledge. CLA diet mice generally show higher variability in RNA-seq results than control diet mice (**Figure 2**). Additionally, **Figure 2** shows that samples grouped by diet have the most segregation of clusters between any comparisons, which is also displayed by the highest number of DEGs out of all comparisons (**Figure 1**). This suggests that diet is a stronger factor for differential gene expression than genotype. This further suggests that PWS mouse models show little difference in overall hypothalamic RNA expression. However, while diet may be important for differential gene expression, the magnitude of differences is still very weak at maximum absolute Log2 fold change of 0.345, or 1.27-fold. It is questionable how many of these DEGs can be validated by RT-QPCR due to limitations of low effect size. Gene ontology analysis for this set of 392 genes is shown in **Table 2** analyzed using MouseMine by mouse genomics informatics.[34] Many of the enriched pathways are implicated in metabolic processes. Furthermore, the effects of CLA diet have been explored at the molecular level in muscle, adipose tissue, liver, and other organ systems outside the brain. Indications are that some mechanisms for reduction of weight and fat mass are likely due to increased fatty acid oxidation and browning of white adipose tissue likely independent of the nervous system, and therefore it is possible that the CLA diet has little direct impact on hypothalamic gene expression.[13] However, diet can influence hypothalamus molecular signatures, with studies showing increased inflammation influenced by diet, and intracerebroventricular administration of CLA may decrease appetite in mice through reduction of NPY and AgRP signalling.[35–37] The only DEG confirmed via RT-QPCR with CLA diet is charged multivesicular body protein 1b (*Chmp1b*), a gene involved in the endosomal sorting complexes required for transport (ESCRT) that may be involved in the multi vesicular body (MVB), a specialized endosome.[38–40] *Chmp1b* has been implicated to support lipid-droplet to

peroxisome fatty acid trafficking.[41] This gene is increased with CLA diet, which supports the idea that CLA promotes increased fatty acid oxidation, as *Chmp1b* is implicated to support this as well, among many other functions. In the context of the brain, peroxisome breakdown of fatty acids is essential for the building blocks of the myelin sheath that coats axons.[42] This pathway is an interesting target, and further investigation on this dataset may investigate the intersection of fatty acid oxidation and myelin pathways.

Table 2. Gene ontology for differentially expressed genes across diets including all genotypes.

Biological Process - Gene ontology enrichment	**Adjusted p-value** (Holm-Bonferroni)
cellular metabolic process	3.94E-05
phosphate-containing compound metabolic process	0.00036
phosphorus metabolic process	0.000535
organophosphate metabolic process	0.002057
organonitrogen compound metabolic process	0.002665
primary metabolic process	0.004663
generation of precursor metabolites and energy	0.011009
cellular protein metabolic process	0.012829
rRNA processing	0.025972
rRNA metabolic process	0.046374

In terms of methodology, there are improvements that could be made. First, the mRNA-seq library prep used in the current study retains “stranded” info, allowing mapping to the forward or negative strand of the mouse reference sequence. However, the quantification methods used here are unable to use the stranded directionality info and instead treat the mapped reads as if strandedness is unknown. Therefore, a more effective quantification method can be used to quantify the stranded reads more accurately to annotations with directionality. The human reference genome Gencode release 19 has an estimated 19% of overlapping genes transcribed from opposite strands.[43] The percentage of ambiguous reads in human blood-derived cells is about 6% with non-stranded RNA-seq and drops to about 3% with stranded RNA-seq.[43] While using stranded info more effectively would be an improvement on the current method, it likely does not account for the majority of why such weak differences are seen between conditions. Additionally, it cannot be ruled out that sample collection and

preparation could potentially be flawed, and improvements in sample collection may increase accuracy and confidence in findings.

There are many algorithms for use in RNA-seq for all stages of the pipeline. In terms of quantification algorithms and differential expression analysis, it has been suggested that the one used in the current study, DESeq2, may perform better when there are a high number of differentially expressed genes.[44,45] Both RNA-seq studies described in comparison to the current one used different algorithms. The study on whole hypothalamus finding about 9000 DEGs also used DESeq2 for quantification, but different read assembly methods. The study examining hypothalamic nuclei used different highly cited methods for both read assembly and quantification of DEGs. The diversity of algorithms and methodology is a persistent problem (or blessing) for bioinformatics in which standardization throughout the field is still changing rapidly, and while awareness of limitations and uses of certain approaches is essential, it is unavoidable that studies will diverge in approaches. There are reviews evaluating the reproducibility between RNA-seq algorithms and validation through RT-QPCR, and for the most part, most approaches are adequately consistent between each other and can be validated.[44–51]

Future work with this dataset may want to integrate other variables besides diet and genotype. For example, the main study recorded many measures such as body weight, body fat, glucose tolerance test, anxiety-like behavior, etc. which are not detailed in the current work. Integration of this data, as well as genetic background (e.g., litter, parents, siblings, etc.) may guide further findings in this dataset but are outside the scope of the current report. Other DEGs found in the current report also need to be validated by RT-QPCR (e.g., *Ipw*, *Ndn*).

6.5 Methods

Mouse care and tissue collection

All animal protocols were approved by local Institutional Animal Care and Use Committee at Virginia Polytechnic Institute and State University. All mice were on a C57BL/6J background with *Snord116* paternal deletion mice (B6[Cg]-Snord116tm1.1Uta/J Stock No: 008149 | 1-loxp (KO), Snord116del) obtained from Jackson Laboratories. Genotyping was performed as reported.[52] Mice were housed at room temperature at about 22°C with 12-hour

light/dark cycles at 7am and 7pm and ad-libitum access to food (20% fat w/w) and water. Mice were weaned at 3 weeks old and housed with littermates of the same sex. Mice were singly housed at 6 – 10 weeks old until the endpoint of the study. Standard measurements such as body weight, body fat percentage, etc. were taken throughout the study and assays including treadmill running, glucose tolerance test, etc. were performed before and after 12 weeks of dietary condition. For tissue dissection, mice were euthanized between 25 and 29 weeks old by CO2 asphyxiation and decapitated between 12pm and 2pm. Brains were then dissected using a brain block and surgical tools, and whole hypothalamus tissue was lysed in TRIzol using a rotor stator homogenizer. TRIzol samples were stored at -20°C until RNA purification (2 weeks – 5 months). Fresh/autoclaved rotor stator homogenizers were used between samples.

RNA Purification

Fresh hypothalamus tissue was lysed in TRIzol using a rotor stator homogenizer. TRIzol samples were frozen at -20°C in microfuge tubes until purified (2 weeks to 5 months). Thawed TRIzol samples were purified using the TRIzol+Purelink RNA minikit (ThermoFisher #12183025) following manufacturer's instructions for the TRIzol® Plus Total Transcriptome Isolation protocol. Purified RNA was then DNAse treated using TURBO DNA-free™ Kit (ThermoFisher #AM1907) according to manufacturer's instructions, diluted to 60ng/uL in nuclease-free water, and stored at -80°C.

RNA sequencing

RNA sequencing and library preparation was performed by Virginia Tech's Genomics Sequencing Center facility at the Fralin Life Sciences Institute. Total RNA with RIN ≥ 8.0, was converted into a strand-specific library using Illumina's TruSeq Stranded mRNA HT Sample Prep Kit (Illumina, RS-122-2103), for subsequent cluster generation and sequencing on Illumina's NextSeq. The library was enriched by 14 cycles of PCR, validated using Agilent TapeStation and quantitated by qPCR. Individually indexed cDNA libraries were pooled and sequenced on NextSeq 75 SR.

The Illumina NextSeq Control Software v2.1.0.32 with Real Time Analysis RTA v2.4.11.0 was used to provide the management and execution of the NextSeq 500 and to

generate BCL files. The BCL files were converted to FASTQ files, adapters trimmed and demultiplexed using bcl2fastq Conversion Software v2.20.

FastQ files were aligned to mouse genome GRCm38.p6 using the Geneious RNA assembler 2020.1.2 from Geneious Prime with map quality 30 (99.9% confidence). Alignments were quantified to gene and RNA annotations and comparisons across experimental conditions were performed using the DESeq2 plugin in Geneious Prime.[16,53,54] False discovery rate (FDR) was calculated using the Benjamini-Hochberg procedure.

Reverse-Transcriptase Quantitative PCR

For RT-QPCR, Power SYBR® Green RNA-to-CT™ 1-Step Kit (ThermoFisher #4389986) was used according to manufacturer's instructions. 10uL reactions were performed using 150nM final primer concentration. Primers were assessed for efficiency using a dilution series and fell within 90%-110% efficiency. 90ng RNA was used per 10uL reaction. Two to three technical replicates were performed. Control reactions for each sample (No reverse-transcriptase and no-template controls) were used for quality control. 384-well plates were run on the ViiA 7 Real-Time PCR System (ThermoFisher) according to RT-QPCR mix instructions and thermocycling conditions were not modified from suggested protocol (1-step annealing/extension at 60°C). Quality control measures including melt-curve analysis, technical replicate analysis, etc. were analyzed by thermocycler software and by operator; any major errors were excluded from analysis when appropriate, and/or new samples and plates were run when appropriate. Candidate reference genes for ddCT analysis were analyzed for appropriate reference controls. Mouse beta-actin was used as reference gene control for all experiments.

Statistical Analysis

All RT-QPCR data were analyzed using Microsoft Excel 16 for Microsoft 365, IBM SPSS Statistics 26 for Windows, and GraphPad Prism 9.0.0. Number of samples in statistical tests are described in respective figures. Error bars indicate ±SD. The 2^{ddCT} method of relative quantification was used. Statistical significance tests performed on respective ddCT values from which Relative Quantification values are derived. Significance is expressed at *$p<0.05$, **$p<0.01$, ***$p<0.001$, $^{NS}p>0.05$.

A two-way ANOVA with Bonferroni correction was used for relative expression of RNA normalized to WT or control conditions (**Figure 3A, B**). Unpaired t-test was used for select pairwise comparisons (**Figure 3D,E,F**).

6.6 References

1. FPWR. PWS Clinical Trials. Accessed February 27, 2021. https://www.fpwr.org/pws-clinical-trials
2. Hur S, Whitcomb F, Rhee S, Park Y, Good DJ, Park Y. Effects of trans-10,cis-12 Conjugated Linoleic Acid on Body Composition in Genetically Obese Mice. *J Med Food*. 2009;12(1):56-63. doi:10.1089/jmf.2008.0110
3. Kim JH, Gilliard D, Good DJ, Park Y. Preventive effects of conjugated linoleic acid on obesity by improved physical activity in nescient basic helix-loop-helix 2 knockout mice during growth period. *Food Funct*. 2012;3(12):1280-1285. doi:10.1039/C2FO30103B
4. Kim Y, Kim D, Good D, Park Y. Effects of Post-Weaning Administration of Conjugated Linoleic Acid on Development of Obesity in Nescient Basic Helix-Loop-Helix 2 Knockout Mice. *J Agric Food Chem*. 2015;63. doi:10.1021/acs.jafc.5b00840
5. Kim Y, Kim D, Good D, Park Y. Conjugated linoleic acid (CLA) influences muscle metabolism via stimulating mitochondrial biogenesis signaling in adult-onset inactivity induced obese mice. *Eur J Lipid Sci Technol*. 2016;118:1305-1316. doi:10.1002/ejlt.201500220
6. Good DJ, Porter FD, Mahon KA, Parlow AF, Westphal H, Kirsch IR. Hypogonadism and obesity in mice with a targeted deletion of the Nhlh2 gene. *Nat Genet*. 1997;15(4):397-401. doi:10.1038/ng0497-397
7. Coyle CA, Jing E, Hosmer T, Powers JB, Wade G, Good DJ. Reduced voluntary activity precedes adult-onset obesity in Nhlh2 knockout mice. *Physiol Behav*. 2002;77(2):387-402. doi:10.1016/S0031-9384(02)00885-5
8. Jing E, Nillni EA, Sanchez VC, Stuart RC, Good DJ. Deletion of the Nhlh2 Transcription Factor Decreases the Levels of the Anorexigenic Peptides α Melanocyte-Stimulating Hormone and Thyrotropin-Releasing Hormone and Implicates Prohormone Convertases I and II in Obesity. *Endocrinology*. 2004;145(4):1503-1513. doi:10.1210/en.2003-0834
9. Vella KR, Burnside AS, Brennan KM, Good DJ. Expression of the Hypothalamic Transcription Factor Nhlh2 is Dependent on Energy Availability. *J Neuroendocrinol*. 2007;19(7):499-510. doi:10.1111/j.1365-2826.2007.01556.x
10. Good DJ, Coyle CA, Fox DL. Nhlh2: A Basic Helix-Loop-Helix Transcription Factor Controlling Physical Activity. *Exerc Sport Sci Rev*. 2008;36(4):187-192. doi:10.1097/JES.0b013e31818782dd
11. Fox DL, Good DJ. Nescient Helix-Loop-Helix 2 Interacts with Signal Transducer and Activator of Transcription 3 to Regulate Transcription of Prohormone Convertase 1/3. *Mol Endocrinol*. 2008;22(6):1438-1448. doi:10.1210/me.2008-0010
12. Churruca I, Fernández-Quintela A, Portillo MP. Conjugated linoleic acid isomers: Differences in metabolism and biological effects. *BioFactors*. 2009;35(1):105-111. doi:https://doi.org/10.1002/biof.13

13. den Hartigh LJ. Conjugated Linoleic Acid Effects on Cancer, Obesity, and Atherosclerosis: A Review of Pre-Clinical and Human Trials with Current Perspectives. *Nutrients*. 2019;11(2). doi:10.3390/nu11020370
14. Butler MG, Miller JL, Forster JL. Prader-Willi Syndrome - Clinical Genetics, Diagnosis and Treatment Approaches: An Update. *Curr Pediatr Rev*. 2019;15(4):207-244. doi:10.2174/1573396315666190716120925
15. Chung MS, Langouët M, Chamberlain SJ, Carmichael GG. Prader-Willi syndrome: reflections on seminal studies and future therapies. *Open Biol*. 2020;10(9):200195. doi:10.1098/rsob.200195
16. Love MI, Huber W, Anders S. Moderated estimation of fold change and dispersion for RNA-seq data with DESeq2. *Genome Biol*. 2014;15(12). doi:10.1186/s13059-014-0550-8
17. Ding F, Li HH, Li J, Myers RM, Francke U. Neonatal Maternal Deprivation Response and Developmental Changes in Gene Expression Revealed by Hypothalamic Gene Expression Profiling in Mice. *PLoS ONE*. 2010;5(2). doi:10.1371/journal.pone.0009402
18. Qi Y, Purtell L, Fu M, et al. Snord116 is critical in the regulation of food intake and body weight. *Sci Rep*. 2016;6. doi:10.1038/srep18614
19. Khor E-C, Fanshawe B, Qi Y, et al. Prader-Willi Critical Region, a Non-Translated, Imprinted Central Regulator of Bone Mass: Possible Role in Skeletal Abnormalities in Prader-Willi Syndrome. *PLoS ONE*. 2016;11(1). doi:10.1371/journal.pone.0148155
20. Burnett LC, LeDuc CA, Sulsona CR, et al. Deficiency in prohormone convertase PC1 impairs prohormone processing in Prader-Willi syndrome. *J Clin Invest*. 2016;127(1):293-305. doi:10.1172/JCI88648
21. Pace M, Falappa M, Freschi A, et al. Loss of Snord116 impacts lateral hypothalamus, sleep, and food-related behaviors. *JCI Insight*. 2020;5(12). doi:10.1172/jci.insight.137495
22. Polex-Wolf J, Lam BYH, Larder R, et al. Hypothalamic loss of Snord116 recapitulates the hyperphagia of Prader-Willi syndrome. *J Clin Invest*. 2018;128(3):960-969. doi:10.1172/JCI97007
23. Wunderlich CM, Hövelmeyer N, Wunderlich FT. Mechanisms of chronic JAK-STAT3-SOCS3 signaling in obesity. *JAK-STAT*. 2013;2(2). doi:10.4161/jkst.23878
24. Reed AS, Unger EK, Olofsson LE, Piper ML, Myers MG, Xu AW. Functional Role of Suppressor of Cytokine Signaling 3 Upregulation in Hypothalamic Leptin Resistance and Long-Term Energy Homeostasis. *Diabetes*. 2010;59(4):894-906. doi:10.2337/db09-1024
25. Mickelsen LE, Flynn WF, Springer K, et al. Cellular taxonomy and spatial organization of the murine ventral posterior hypothalamus. *eLife*. 2020;9. doi:10.7554/eLife.58901
26. Haerian BS, Baum L. GABRG2 rs211037 polymorphism and epilepsy: A systematic review and meta-analysis. *Seizure - Eur J Epilepsy*. 2013;22(1):53-58. doi:10.1016/j.seizure.2012.10.007
27. Kang J-Q, Macdonald RL. GABRG2 Mutations Associated with a spectrum of epilepsy syndromes from Generalized Absence Epilepsy to Dravet syndrome. *JAMA Neurol*. 2016;73(8):1009-1016. doi:10.1001/jamaneurol.2016.0449
28. Warner TA, Shen W, Huang X, Liu Z, Macdonald RL, Kang J-Q. Differential molecular and behavioural alterations in mouse models of GABRG2 haploinsufficiency versus dominant negative mutations associated with human epilepsy. *Hum Mol Genet*. 2016;25(15):3192-3207. doi:10.1093/hmg/ddw168
29. Kim ER, Xu Y, Cassidy RM, et al. Paraventricular hypothalamus mediates diurnal rhythm of metabolism. *Nat Commun*. 2020;11. doi:10.1038/s41467-020-17578-7

30. Walton JC, McNeill JK, Oliver KA, Albers HE. Temporal Regulation of GABAA Receptor Subunit Expression: Role in Synaptic and Extrasynaptic Communication in the Suprachiasmatic Nucleus. *eNeuro*. 2017;4(2). doi:10.1523/ENEURO.0352-16.2017
31. Lassi G, Priano L, Maggi S, et al. Deletion of the Snord116/SNORD116 Alters Sleep in Mice and Patients with Prader-Willi Syndrome. *Sleep*. 2016;39(3):637-644. doi:10.5665/sleep.5542
32. Coulson RL, Yasui DH, Dunaway KW, et al. Snord116-dependent diurnal rhythm of DNA methylation in mouse cortex. *Nat Commun*. 2018;9. doi:10.1038/s41467-018-03676-0
33. Powell WT, Coulson RL, Crary FK, et al. A Prader–Willi locus lncRNA cloud modulates diurnal genes and energy expenditure. *Hum Mol Genet*. 2013;22(21):4318-4328. doi:10.1093/hmg/ddt281
34. Motenko H, Neuhauser SB, O'Keefe M, Richardson JE. MouseMine: a new data warehouse for MGI. *Mamm Genome*. 2015;26(7-8):325-330. doi:10.1007/s00335-015-9573-z
35. Samodien E, Johnson R, Pheiffer C, et al. Diet-induced hypothalamic dysfunction and metabolic disease, and the therapeutic potential of polyphenols. *Mol Metab*. 2019;27:1-10. doi:10.1016/j.molmet.2019.06.022
36. Velloso LA, Schwartz MW. ALTERED HYPOTHALAMIC FUNCTION IN DIET-INDUCED OBESITY. *Int J Obes 2005*. 2011;35(12):1455-1465. doi:10.1038/ijo.2011.56
37. Cao Z-P, Wang F, Xiang X-S, Cao R, Zhang W-B, Gao S-B. Intracerebroventricular administration of conjugated linoleic acid (CLA) inhibits food intake by decreasing gene expression of NPY and AgRP. *Neurosci Lett*. 2007;418(3):217-221. doi:10.1016/j.neulet.2007.03.010
38. Schmidt O, Teis D. The ESCRT machinery. *Curr Biol*. 2012;22(4):R116-R120. doi:10.1016/j.cub.2012.01.028
39. Crespo-Yàñez X, Aguilar-Gurrieri C, Jacomin A-C, et al. CHMP1B is a target of USP8/UBPY regulated by ubiquitin during endocytosis. *PLoS Genet*. 2018;14(6). doi:10.1371/journal.pgen.1007456
40. McCullough J, Clippinger AK, Talledge N, et al. Structure and membrane remodeling activity of ESCRT-III helical polymers. *Science*. 2015;350(6267):1548-1551. doi:10.1126/science.aad8305
41. Chang C-L, Weigel AV, Ioannou MS, et al. Spastin tethers lipid droplets to peroxisomes and directs fatty acid trafficking through ESCRT-III. *J Cell Biol*. 2019;218(8):2583-2599. doi:10.1083/jcb.201902061
42. Alberts B, Johnson A, Lewis J, Raff M, Roberts K, Walter P. Peroxisomes. *Mol Biol Cell 4th Ed*. Published online 2002. Accessed February 28, 2021. https://www.ncbi.nlm.nih.gov/books/NBK26858/
43. Zhao S, Zhang Y, Gordon W, et al. Comparison of stranded and non-stranded RNA-seq transcriptome profiling and investigation of gene overlap. *BMC Genomics*. 2015;16(1):675. doi:10.1186/s12864-015-1876-7
44. Corchete LA, Rojas EA, Alonso-López D, De Las Rivas J, Gutiérrez NC, Burguillo FJ. Systematic comparison and assessment of RNA-seq procedures for gene expression quantitative analysis. *Sci Rep*. 2020;10(1):19737. doi:10.1038/s41598-020-76881-x
45. Khang TF, Lau CY. Getting the most out of RNA-seq data analysis. *PeerJ*. 2015;3. doi:10.7717/peerj.1360

46. Costa-Silva J, Domingues D, Lopes FM. RNA-Seq differential expression analysis: An extended review and a software tool. *PLoS ONE*. 2017;12(12). doi:10.1371/journal.pone.0190152
47. Dillies M-A, Rau A, Aubert J, et al. A comprehensive evaluation of normalization methods for Illumina high-throughput RNA sequencing data analysis. *Brief Bioinform*. 2013;14(6):671-683. doi:10.1093/bib/bbs046
48. Oshlack A, Wakefield MJ. Transcript length bias in RNA-seq data confounds systems biology. *Biol Direct*. 2009;4(1):14. doi:10.1186/1745-6150-4-14
49. Wagner GP, Kin K, Lynch VJ. Measurement of mRNA abundance using RNA-seq data: RPKM measure is inconsistent among samples. *Theory Biosci*. 2012;131(4):281-285. doi:10.1007/s12064-012-0162-3
50. Soneson C, Delorenzi M. A comparison of methods for differential expression analysis of RNA-seq data. *BMC Bioinformatics*. 2013;14(1):91. doi:10.1186/1471-2105-14-91
51. Rapaport F, Khanin R, Liang Y, et al. Comprehensive evaluation of differential gene expression analysis methods for RNA-seq data. *Genome Biol*. 2013;14(9):R95. doi:10.1186/gb-2013-14-9-r95
52. Ding F, Li HH, Zhang S, et al. SnoRNA Snord116 (Pwcr1/MBII-85) Deletion Causes Growth Deficiency and Hyperphagia in Mice. *PLOS ONE*. 2008;3(3):e1709. doi:10.1371/journal.pone.0001709
53. Love M, Anders S, Huber W. Differential analysis of count data – the DESeq2 package - February 4, 2014. Published online 2014:33.
54. Love MI, Huber W, Anders S. Differential analysis of count data – the DESeq2 package - November 30, 2016. *Genome Biol*. 2016;15(12):550. doi:10.1186/s13059-014-0550-8

Chapter 7. Conclusions

The current study sought to better understand the molecular relationship between the non-coding RNA *SNORD116* and the neuroendocrine transcription factor *NHLH2* with implications of Prader-Willi Syndrome etiology.

The hypothesis that *Snord116* positively regulates *Nhlh2* RNA dependent on the 3'UTR is supported by work in Chapter 4. The related hypothesis that deletion of the *Snord116* gene cluster in mouse leads to low *Nhlh2* RNA levels in the hypothalamus is not supported by work in Chapter 5 and 6. The disagreement between these two main results may be explained by many factors, including splice variant specificity, cell type specificity, and leptin signaling.

Prior to Chapter 3 it was unclear how much variation there was between mouse and human in their *Snord116* gene sequences, and this potential variation in sequence could explain the phenotypic variation between the mouse model and human PWS. This study found that there is phylogenetic conservation shared from human through chimp, rabbit, rat, and mouse in key motif regions of the *SNORD116* RNA sequence including the C/C' boxes, the D' box, and critically, the antisense region upstream of the D' box. This implies that these well characterized snoRNA motifs are likely functionally conserved from mouse to human, indicating that the many copies of *SNORD116* may be targeting RNAs through sequence complementarity as predicted. It further established that mouse *Snord116* homologs are highly homologous to each other, and they are most homologous to human *SNORD116-1* through *SNORD116-9*.

Chapter 4 examined a question of debate in the research community. Does *SNORD116* regulate *NHLH2* at the molecular level? The work of Chapter 4 shows that mouse *Snord116* stabilizes *Nhlh2* mRNA reporters dependent on its 3'UTR. *Nhlh2* mRNA is subject to rapid decay within 45 minutes of transcription and *Snord116* protects against this initial rapid decay. Additionally, a SNV in mouse *Nhlh2* at the predicted site of sequence complementarity between human *SNORD116* and *NHLH2* was able to weaken the positive effect mouse *Snord116* has on *Nhlh2* levels. This suggests that *Snord116* may be mediating its effect at the predicted site of interaction, however this direct interaction is not proven. There are many possible reasons for this regulatory effect including competition with destabilizing elements,

recruiting stabilizing factors to *Nhlh2* RNA, methylation of *Nhlh2* RNA, poly(A) signal dependent factors, etc. Future studies may investigate co-immunoprecipitations of *Nhlh2* and *Snord116* to examine possible direct binding and protein complexes. Additionally, signaling factors such as leptin, glucose, serum, or media refreshment *in vitro* may affect *Snord116*'s stabilizing effect on *Nhlh2* and may be of interest for future studies. Furthermore, the study with *Nhlh2* can serve as a model for *Snord116* function and downstream targets. It is unknown whether *Snord116* may have stabilizing effects for some RNA targets and destabilizing effects for others. The current study also needs to be translated to human genes using *SNORD116-3* and human *NHLH2* which have stronger predicted interactions than the mouse sequences used in the current study. The sequence motif found on the human *NHLH2* predicted interaction site may be useful for future searches of possible *SNORD116* targets. Additionally, the predicted interaction region on *NHLH2* is within a highly conserved sequence, showing nearly 100% conservation through 70 vertebrates. It is unclear why this region is so highly conserved, as motif searches in this region yielded no obvious results. The targeted SNV mutation within this region may have disrupted a functional motif that works in synchrony with *Snord116,* and this disruption reduced the positive regulatory effect of *Snord116,* not through disruption of *Snord116*'s sequence complementarity and ability to bind *Nhlh2*, but through disruption of a co-factor that works in tandem with *Snord116* regulation. There are still many questions to answer from this study with future work, however the priority is likely to replicate the work in human constructs and expand the list of candidate target RNAs for *SNORD116*.

Chapter 5 addressed the lack of reproducibility in *Snord116*$^{m+/p-}$ models between studies. Low *Nhlh2* levels were reported in *Snord116*$^{m+/p-}$ mice, and this finding was not replicated in future independent studies. Chapter 5's study sought to reconcile these differences conclusively. Our work shows that these PWS mouse models had no changes in their hypothalamus for RNA levels of the genes of interest, *Nhlh2* and *Pcsk1*. It is unclear why there is disagreement between studies, but many factors of variation seen between studies are the age of mice, the time of day, the fed state, and the precision and method of sample collection. Additionally, transient knockdown of *Snord116* in a mouse neuroblastoma cell line did not change *Nhlh2* or *Pcsk1* RNA levels. This study had many differences in approach when compared to the study of Chapter 4 that found an increase in *Nhlh2* levels with *Snord116*, which may partially explain the inconsistent findings. However, another explanation for the lack

of findings in the studies of Chapter 5 may be due to the importance of the temporal pattern of *Nhlh2,* which decays rapidly after transcription without the protective effect of *Snord116,* as shown in Chapter 4. A future approach may be to stimulate *Nhlh2* transcription *in vivo* with leptin injection and collect samples shortly afterward in WT mice and PWS model mice. *Snord116* knockdowns *in vitro* may also consider using leptin stimulation for initiating *Nhlh2* transcription and collecting samples shortly after around the 45-minute mark.

Chapter 6 expanded on work with the PWS mouse model *Snord116*$^{m+/p-}$*.* Conjugated linoleic acid (CLA) is a dietary supplement currently on the market for reducing body weight and obesity in humans, and CLA is effective in a mouse model that shares many phenotypes of PWS, the *Nhlh2* homozygous deletion mouse (N2KO mouse). The primary outcomes of this study were not described here, but a secondary goal was to characterize the RNA expression profile of mouse hypothalamus under a CLA supplemented diet for both WT and *Snord116*$^{m+/p-}$ mice. Previously, the RNA expression profile of mouse hypothalamus during a CLA-supplemented diet had not been described for WT mice or PWS mouse models. The current study used mRNA-seq to show that there are little drastic changes between mouse genotypes or between diets. The effect size of differentially expressed genes was relatively mild for all comparisons made, but it appears that the type of diet has a larger effect on differential gene expression than genotype. CLA diet may be changing the expression of many genes involved in metabolic processes. Future directions for the genotype differences include validation of differentially expressed genes, use of single-cell sequencing approaches, and *in situ* hybridizations to identify co-localized genes of interest and cell types and quantify changes between genotypes. Future directions for the CLA diet hypothalamus include integrating additional data from the primary study into the RNA-seq analysis, such as body weight, body composition, glucose tolerance test, and other measures.